Petroleum Science 23 (2026) 1773–1803

Contents lists available at ScienceDirect

Petroleum Science

journal homepage: www.keaipublishing.com/en/journals/petroleum-science

Review Paper

Occurrence mechanism of shale oil in laminated shale reservoirs: A review

Qian Sang [a,b,*], Xue-Qiang Guo [a,b], Ming-Zhe Dong [c]

[a] College of Petroleum Engineering, China University of Petroleum (East China), Qingdao, 266580, Shandong, China
[b] State Key Laboratory of Deep Oil and Gas, China University of Petroleum (East China), Qingdao, 266580, Shandong, China
[c] Department of Chemical and Petroleum Engineering, University of Calgary, Calgary, AB, T2N 1N4, Canada

ARTICLE INFO

Article history:
Received 12 June 2025
Received in revised form
31 October 2025
Accepted 16 March 2026
Available online 19 March 2026

Edited by Xiu-Fang Hu

Keywords:
Laminated shale reservoirs
Occurrence states
Occurrence space
Enrichment patterns
Influencing factors
Occurrence mechanism

ABSTRACT

Shale oil is an important unconventional resource. In-depth exploration of the shale oil occurrence mechanism is beneficial for the selection of sweet spots and the innovation of production technologies. Shale oil in laminated reservoirs shows commercial potential, yet systematic reviews on its occurrence mechanism remain scarce. This article provides a comprehensive summary of the occurrence mechanism of shale oil from four aspects. These include occurrence states, occurrence space, influencing factors and enrichment patterns. In addition, the formation, classification, and controlling factors of laminae, and their significance for shale oil enrichment are discussed. Finally, the challenges facing shale oil occurrence mechanism are described, and the next research work is prospected. The formation of laminae in fine-grained sedimentary rocks is associated with processes such as suspension settling, gravity flow, bottom currents, volcanism, hydrothermal activity, and microbial processes. Two-dimensional nuclear magnetic resonance (NMR) offers the advantages of being non-destructive and rapid in characterizing the occurrence state of shale oil, as well as providing information on pore structure and fluid distribution within shale. Due to the influence of sedimentary tectonics and diagenesis, there are significant differences in the occurrence spaces and formation mechanisms of various types of laminated shales. Compared to the massive reservoirs, laminated shale reservoirs have larger macropore volume, better connectivity, and more developed microfractures. Pure shales and organic-rich laminated shales mainly accumulate adsorbed oil within organic matter nanopores, exhibiting high hydrocarbon generation potential. In contrast, rigid laminated shales tend to accumulate free oil in intergranular mineral pores and fractures, demonstrating greater development potential.
© 2026 The Authors. Publishing services by Elsevier B.V. on behalf of KeAi Communications Co. Ltd. This is an open access article under the CC BY-NC-ND license (http://creativecommons.org/licenses/by-nc-nd/4.0/).

1. Introduction

Shale oil has become a hot spot for exploration and development worldwide (Hu et al., 2024; Yu et al., 2022). According to statistics, the global technically recoverable shale oil resources amount to 251.2 × 10^9 t (Zou et al., 2023). Russia and the United States, in particular, hold significant resource reserves advantages. China's shale oil resources are estimated at (80–100) × 10^9 t (Sun et al., 2025b; Yang, 2024). According to statistics from the National Energy Administration, China's shale oil production exceeded 6 × 10^6 t in 2024, representing a year-on-year increase of more than 30% (Sun et al., 2025b). Shale oil has the potential to play a crucial role in alleviating energy crises and promoting economic development (Fu and He, 2024; Shi et al., 2024).

Shale oil reservoirs are rich in organic matter (OM) and clay minerals, with developed micro-to nano-scale pores, exhibiting the characteristic of "self-generation and self-storage" (Wei et al., 2023a, 2023b; Yan et al., 2023). Among them, laminated shale reservoirs have been proven to be favorable lithofacies with the potential for commercial development (Niu et al., 2025). A thin layer with a sandstone thickness of no more than 1 cm is defined as a lamina (Jiang et al., 2023). Currently, research on laminae mainly focuses on analyzing the continuity of the laminae, mineral composition, interface morphology, classification schemes, controlling factors, sedimentary

* Corresponding author.
E-mail address: 20190005@upc.edu.cn (Q. Sang).
Peer review under the responsibility of China University of Petroleum (Beijing).

https://doi.org/10.1016/j.petsci.2026.03.037
1995-8226/© 2026 The Authors. Publishing services by Elsevier B.V. on behalf of KeAi Communications Co. Ltd. This is an open access article under the CC BY-NC-ND license (http://creativecommons.org/licenses/by-nc-nd/4.0/).

environment, and formation mechanisms (Lazar et al., 2015a; Li et al., 2020d; Xie et al., 2024; Yawar and Schieber, 2017; Zhu et al., 2022). Current issues mainly lie in the lack of a unified standard for the classification of laminae. The formation mechanisms of different laminae also present challenges. In addition, the occurrence and migration of shale oil between different laminae remain significant difficulties.

Shale oil exists in different pore spaces in the form of free, adsorbed, and dissolved states (Wang et al., 2019c). Shale oil has a complex composition, with interactions occurring between its molecules (Wang et al., 2025c). There is still a lack of thorough research on quantitatively characterizing the adsorbed and free oil content in shale (Li et al., 2017). Currently popular methods include rock pyrolysis (Li et al., 2024b), solvent extraction (Tian et al., 2024a), molecular dynamics simulation (Fei et al., 2023), and nuclear magnetic resonance (NMR) (Zhang et al., 2024), among others. Due to the unique nature of shale, both OM and inorganic minerals collectively determine the occurrence characteristics of hydrocarbons (Zhao et al., 2023). However, individual methods have their limitations, necessitating further exploration of new approaches to evaluate the states of shale oil. Due to the low porosity and permeability of shale reservoirs, only a small amount (approximately 10%) of free oil can be extracted using natural energy, while adsorbed oil is nearly inaccessible. However, the amount of adsorbed oil is still considerable (Li et al., 2019b). Therefore, the quantitative characterization of both adsorbed oil and free oil content remains significant. Currently, horizontal well volume fracturing has become an important extraction method for shale reservoirs (Liu et al., 2023c). Volume fracturing creates a complex network of fractures that can facilitate the migration of shale oil (Fan et al., 2025; Gao et al., 2020, 2024). Laminated shale reservoirs commonly contains a large number of natural fractures, and the cross-flow between the laminae can enhance the production of free oil (Dong et al., 2019).

Exploring the occurrence spaces of shale oil is valuable for understanding its accumulation, flow, and production (Zhang et al., 2023d). Loucks et al. (2012) found that the main classification criteria include organic pores, intergranular pores (InterP), intragranular pores (IntraP), and microfractures. The formation and development of shale pore space are primarily controlled by diagenetic processes such as calcite recrystallization, carbonate dissolution, mechanical compaction, dehydration shrinkage, and the transformation of clay minerals (Liu et al., 2022). The occurrence spaces in interlaminar zones and at the interface between laminae and massive shale exhibit certain differences. For instance, laminated shale generally outperforms massive shale in terms of pore size distribution, porosity, pore connectivity, and pore structure (Xin et al., 2022b). The current techniques for characterizing micro-scale pores in shale include image analysis, fluid invasion methods, and non-interference methods (Wei et al., 2023b). As shown in Fig. 1, image analysis primarily includes focused ion beam scanning electron microscopy (FIB-SEM), broad ion beam scanning electron microscopy (BIB-SEM), field emission scanning electron microscopy (FE-SEM), atomic force microscopy (AFM), and transmission electron microscopy (TEM) (Rezaeyan et al., 2023; Tian et al., 2024b; Xu et al., 2024; Yasin et al., 2024). The non-interference methods primarily include NMR, nano-CT, micro-CT, small angle neutron scattering (SANS), ultra small angle neutron scattering (USANS), and small angle X-ray scattering (SAXS) (Rezaeyan et al., 2023; Wan et al., 2024). The fluid invasion methods primarily include CO_2 adsorption, N_2 adsorption, and high-pressure mercury intrusion (HPMI) (Rezaeyan et al., 2023). Relying solely on a single experimental technique cannot comprehensively reflect the pore size, morphology, distribution, and connectivity of shale reservoirs (Yan, 2023). Therefore, using multiple methods to characterize pore structure is important.

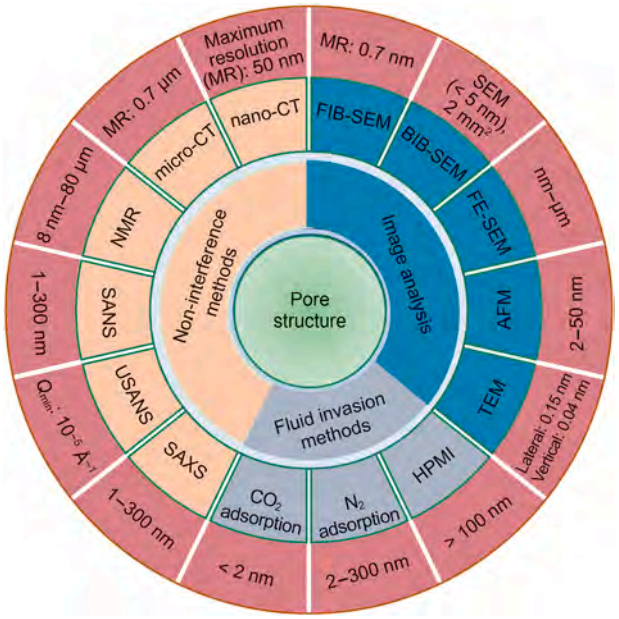

Fig. 1. Characterization methods for pore structure (Klaver et al., 2015; Loucks et al., 2012; Neil et al., 2023; Tian et al., 2024b; Wan et al., 2024; Xu et al., 2024; Yasin et al., 2024).

Till now, many factors influencing the occurrence of shale oil have been identified. These mainly include OM, mineral composition, shale oil components, temperature and pressure, burial history and depth, pore size, and formation water (Fei et al., 2023; He et al., 2025c; Li et al., 2020e; Sun et al., 2024; Wang et al., 2019c, 2025c; Yang et al., 2024). Understanding the mechanisms of influence of various factors is crucial for designing development plans for shale oil. Currently, research on the occurrence mechanisms of shale oil in shale reservoirs mainly includes their states, occurrence spaces, influencing factors, and enrichment patterns (Lv et al., 2025; Wang et al., 2019c; Zhang et al., 2023c, 2023d). NMR has become the most popular method for studying the occurrence mechanisms of shale oil, especially the two-dimensional T_1–T_2 NMR. This is due to the fact that the two-dimensional T_1–T_2 NMR technique can identify different occurrence states of fluids and their distribution in various pore sizes (Zhang et al., 2024). Zhang et al. (2023d) studied the occurrence mechanisms of shale oil in shale nanopores based on two-dimensional NMR and thermogravimetric experiments. The results elucidated the content, distribution, and enrichment patterns of shale oil in different occurrence states. The laminated shale reservoirs exhibit high heterogeneity and a rich system of fractures and pores, making their occurrence mechanisms more complex. However, the occurrence mechanisms of shale oil in laminated shale reservoirs still lack systematic research.

The target of this paper is to clarify the shale oil occurrence mechanism in laminated shale reservoirs, providing theoretical references for sweet spot selection, mobility, and extraction technologies of shale oil. First, the paper briefly summarizes the formation, classification, and controlling factors of laminae, and their significance in shale oil enrichment. Next, it outlines the states of shale oil and the quantitative characterization methods. It elaborates on the occurrence space in laminated shale reservoirs, the characteristics of pore sizes, and the factors influencing shale oil occurrence. Additionally, it summarizes the enrichment models of oil in pure shale and laminated shale reservoirs. Finally, the paper discusses the challenges currently faced by the research on

occurrence mechanisms of shale oil and offers prospects for future research.

2. Formation, controlling factors and classification of laminae

2.1. Formation of laminae

Stratified water bodies are most conducive to the deposition of laminae (Larsen and MacDonald, 1993). Water stratification mainly refers to the chemical stratification (Wang and Mei, 1998) caused by differences in salinity between the surface and bottom waters, and the thermal stratification (Liu et al., 1998) caused by differences in temperature between the surface and bottom. The main depositional mechanisms of laminae include biological processes (Hay et al., 1990), chemical processes (Wang and Zhong, 2004), biogeochemical processes (Thompson et al., 2003), and mechanical processes (Kong et al., 2016). Schieber et al. (2007) used a flume to simulate the formation process of laminae and proposed the flocculation mechanism for laminae formation: clay in the water easily undergoes flocculation with fine detrital particles to form floccules. These floccules continuously envelop detrital particles during transport until reaching the maximum floccule size at mechanical equilibrium. In flume experiments, as hydrodynamics gradually weaken, larger or heavier detrital particles within the floccules are selectively settled first, forming sandy laminated structures. Meanwhile, clay-sized particles and a small amount of fine sand particles continue to be transported, forming flocculent ripple-like structures that move, aggregate, and deposit on the bed to create muddy laminated structures. When the flocculent ripples and sandy particles move simultaneously, they can form laminated structures with alternating mud and sand layers.

The traditional view holds that fine-grained materials generally settle slowly in low-energy, quiet environments, leading to the formation of laminae due to sedimentary interruptions (Schimmelmann et al., 2016). However, flume experiments, observations of marine sedimentation, and detailed examinations of marine mudstones have shown that fine-grained materials can be transported and deposited through various mechanisms, including bottom currents (Yawar and Schieber, 2017), density flow (Wilson and Schieber, 2014), storm flow (Lazar et al., 2015b), and wave-controlled gravity flow (Macquaker et al., 2010a, 2010b), resulting in a diverse range of laminae types (Schieber, 2016). The formation mechanisms mentioned above primarily focus on marine environments. In contrast, the formation of laminae in fine-grained sedimentary rocks is associated with processes such as suspension settling, gravity flow, bottom currents, volcanism, hydrothermal activity, and microbial processes (Hage et al., 2019; Praet et al., 2020; Schieber et al., 2007; Shanmugam, 2008; Xi et al., 2020; Zhu et al., 2019a). Suspension settling can generate seasonal varves and plume flow laminae (Hage et al., 2019; Ojala et al., 2012). Gravity flow can form collapse-type turbidite laminae, density current laminae, and wave-controlled sediment gravity flow laminae (Heard, 2008; Macquaker et al., 2010a; Praet et al., 2020). In lakes, there are three types of bottom currents: wind-driven currents, thermohaline currents, and storm currents. These bottom currents resuspend, transport, and deposit sediments, leading to the formation of laminae (Shanmugam, 2008).

High-quality terrestrial lacustrine source rocks in basins like the Junggar Basin and the Ordos Basin are often associated with volcanic–hydrothermal activities. And volcanic eruptions produce tuffaceous material that settles in deep water, forming tuff or zeolite laminae (Jiang et al., 2022; Lin et al., 2017). When magma or hydrothermal fluids erupt underwater and come into contact with lake water, they generate steam and release energy, producing extremely fine-grained clastic particles. This process leads to the formation of hydrothermal eruption rock laminae (Liu et al., 2018). At the same time, the nutrient elements brought by volcanic eruptions promote algal blooms, resulting in the formation of organic matter laminae (Frogner et al., 2001). In the shallow water environments of the Eocene Green River Formation in North America and the Quaternary lakes of the Qaidam Basin in China, microbial activity produces a large amount of viscous extracellular polymers that capture, aggregate, block, and bind fine-grained materials, leading to the formation of stromatolites or microbial mat laminae (Awramik and Buchheim, 2015; Schieber et al., 2007). Additionally, the settling and burial of calcareous or siliceous biological remains from the surface layer of the lake water can also lead to the formation of bioclastic laminae (Liu and Wang, 2013).

2.2. Controlling factors of laminae

The formation of laminae is primarily controlled by paleoclimate and paleogeography (Anderson and Dean, 1988; Larsen and MacDonald, 1993; Ma et al., 2016). Paleoclimate includes elements such as temperature, precipitation, salinity, and wind field, while paleogeography controls the distribution patterns of laminae through factors like water depth, tectonic features, and material sources (Fig. 2) (Yu, 2023). Temperature affects the continuity, morphology and composition of laminae by controlling waterstratification (Boehrer and Schultze, 2008). Sunlight causes the low-density warm surface water to float on top of the high-density cold water at the bottom, creating thermal stratification in the lake water. This stratification facilitates the suspension and settling of materials to form laminae (Wang and Zhong, 2004). In addition, temperature can also change the composition of laminae by controlling biological activities or evaporation. High temperatures drive water evaporation and enhance biological activity in summer, which can saturate dissolved salts and lead to the formation of carbonate or evaporite laminae. The subsequent death and deposition of organisms in autumn and winter contribute to the formation of OM or clay laminae (Kong et al., 2017).

Humidity and precipitation affect the water medium and the internal and external source material supply, thus controlling the laminar composition. Under a humid climate, denudation is strengthened, terrigenous input is increased, and quartz or clay lamination is formed. Under an arid climate, carbonate and salt laminae are relatively enriched (Ben Dor et al., 2019). In addition, humidity and precipitation affect the laminar type and distribution of gravity flow by controlling lake-level changes (Liu et al., 2020b; Zavala et al., 2021).

Wind field controls the movement of water at different depths, leading to changes in the morphology and grain size of laminae. Plate-like laminae are mostly formed under the conditions of strong-energy underflow or suspended sedimentation. The curved laminae are often related to underflow or waves, where the water body energy is higher. Wavy laminae are often associated with waves, and the current energy is moderate to low (Shi et al., 2018). In terms of particle size, it is easy to deposit clay fine mud laminae (<8 μm) under weak hydrodynamic conditions, to form medium mud laminae dominated by fine silt and carbonate (8–32 μm) under medium to weak hydrodynamic conditions, and to form coarse mud laminae composed of silt and biological debris (32–62.5 μm) under medium to strong hydrodynamic conditions (Lazar et al., 2015a).

Adequate water depth is a favorable condition for resisting wind and waves, maintaining water stratification, and allowing for the slow settling of materials. A greater water depth is more

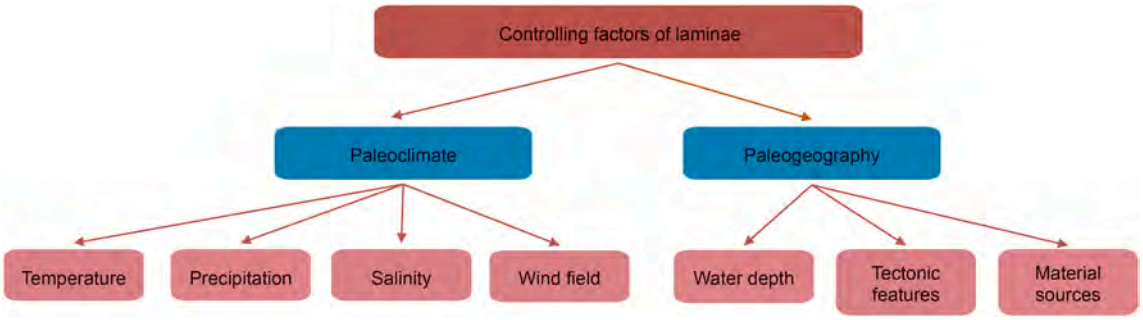

Fig. 2. Controlling factors of laminae (Yu, 2023).

conducive to the formation of laminae (Yu, 2019). Tectonic uplift and subsidence activities control the distribution of source areas and sedimentary zones, thereby influencing the quantity and direction of material supply (Gao et al., 2015; Li et al., 2021). This has a significant impact on the preferential sedimentation patterns of different substances. At the same time, basins with different tectonic types may develop various kinds of laminae. For instance, when density flows advance along the central axis of a rift basin, they can create a stacked sedimentary pattern consisting of thick-bedded sandstone interbedded with laminated sandstone (Irwin, 1965). Regional geological structures can influence the frequency of fluid occurrences in lakes (such as traction flow, bottom flow, and turbidity flow) (Baas et al., 2009; Hampton, 1975; Jiang, 2010; Li et al., 2021; Tylmann and Zolitschka, 2020; Wang et al., 2019d). These fluids can undergo multiple transformations under different conditions, promoting the development of interbedded or layered mixed sedimentary systems.

2.3. Classification of laminae

Identifying and distinguishing the types and genesis mechanisms of shale laminae has always been a focal point and challenge in the analysis of shale sedimentation and reservoir characteristics. The strong heterogeneity of shale has led to the absence of a unified standard for classification schemes (Hua et al., 2021, 2022b). Previous researchers have classified the types of laminae in different blocks based on classification criteria such as lamina thickness (Fu et al., 2022; Li et al., 2020a; Wang et al., 2019a; Zhao et al., 2025), lamina morphology (Liu et al., 2014b; Ma et al., 2024b; Shi et al., 2022; Yawar and Schieber, 2017), sedimentary characteristics (Tang et al., 2019; Wang et al., 2019b; Zeng et al., 2018), lamina composition (Hua et al., 2022a; Liu et al., 2023b; Niu et al., 2025; Xie et al., 2024) and lamina color and brightness (Ma et al., 2017; Sun et al., 2025a). The specific classification can be found in Table 1.

There are certain differences in the formation process of different laminae. During the autumn–winter seasons, the dry climate enhances the physical weathering of source rocks, promoting the input of terrigenous clastic sediments into the lacustrine basin and leading to the development of clastic laminae (Zolitschka et al., 2015). Sandy laminae are related to turbidity current transport and bottom current activity, and are formed in relatively turbulent water bodies with strong clastic input. Terrigenous clay-grade material enters the lake through surface flow, interflow, or bottom current, and subsequently settles slowly to form muddy laminae. In a saline to brackish lacustrine depositional system, the hot and arid conditions of summer, together with elevated lake-water salinity, promote algal blooms that induce carbonate precipitation, resulting in the formation of carbonate laminae (Schieber et al., 2013). The formation of organic-rich laminae depends on biological productivity and preservation conditions under stratified anoxia. The formation of tuffaceous laminae is related to frequent volcanic activity and these laminae

Table 1
Summary of lamina classification criteria.

Basis for classification	References	Classification results
Lamina thickness	Wang et al. (2019a)	Low density–low thickness; low density–high thickness; high density–high thickness.
	Li et al. (2020f)	Thin lamina (<1 mm); thick lamina (>1 mm).
	Fu et al. (2022)	High bedding density (>2000 layers/m); medium bedding density (1000–2000 layers/m); low bedding density (<1000 layers/m).
	Zhao et al. (2025)	Laminated rocks; layered rocks; massive rocks.
Lamina morphology	Liu et al. (2014b)	Wavy laminae; straight laminae.
	Yawar and Schieber (2017)	Low-angle ripple lamination; cross-lamination; parallel laminae.
	Shi et al. (2022)	Thin parallel laminae; thick parallel laminae; wavy laminae; lenticular laminae; weak laminae; sandy laminae.
	Ma et al. (2024b)	Continuous; parallel; plate-like laminae.
Sedimentary characteristics	Zeng et al. (2018)	Finely laminated; widely laminated; discontinuously laminated.
	Wang et al. (2019b)	Horizontal laminae; heterolithic laminae; graded laminae; erosional cross-laminae; wedge-shaped cross-laminae.
	Tang et al. (2019)	Wave to cross bedding; horizontal bedding; weak horizontal bedding; massive structure.
Lamina composition	Hua et al. (2022a)	Clay laminae; calcareous laminae; felsic laminae.
	Liu et al. (2023b)	Mud-rich laminae; carbonate laminae; felsic laminae.
	Xie et al. (2024)	Felsic laminae; graywacke laminae; clay laminae; zeolitic laminae; mixed laminae.
	Niu et al. (2025)	Tuffaceous laminated shale; sandy laminated shale; organic-rich laminated shale.
Color and brightness	Ma et al. (2017)	Yellowish layers of aragonite laminae; grayish layers of aragonite laminae.
	Sun et al. (2025a)	Bright laminae; dark laminae.

often occur interbedded with organic-rich laminae (Niu et al., 2025). The formation mechanism of felsic laminae involves the re-erosion, suspension, and transportation of felsic silt, which subsequently settles to the lake floor together with flocs, resulting in a laminar structure characterized by alternating mud-rich and sand-rich layers (Wang et al., 2023c). Clay laminae develop in relatively high-energy hydrodynamic environments, and their formation mechanism is primarily controlled by the transport processes driven by flocculation of detrital clay particles (Schieber et al., 2007).

Morphologically classified laminae are closely associated with variations in fluid properties, hydrodynamic regimes, and sedimentation processes (Shi et al., 2018, 2022). Planar laminae commonly develop under conditions of relatively strong unidirectional currents or during suspension settling in still water. Curved laminae are often associated with bedload transport under unidirectional currents or with wave oscillation, reflecting relatively high-energy conditions in the water body. Wavy laminae are formed in quiet, reducing water bodies under weak hydrodynamic conditions, and are often related to wave oscillatory flows, which indicate moderate to relatively low energy levels. Thin parallel laminae are formed in quiet, stratified water bodies and exhibit pronounced seasonal variations. Thick parallel laminae are mainly formed in quiet, stratified water bodies with sufficient clastic input. Lenticular laminae are formed under periodic hydrodynamic conditions, where microcrystalline calcite is redeposited due to changes in fluid dynamics.

2.4. Development characteristics of shale laminae in different basins

In China, shale laminae are predominantly developed in several key oil-bearing basins, including the Bohai Bay, Ordos, Junggar, and Songliao basins. Notable differences exist among basins in terms of lamina classification, lamina thickness, and lamina composition. For example, in the Bohai Bay Basin and the Ordos Basin, lamina classification considers factors such as lamina composition, morphology, color, and brightness (Liu et al., 2014b, 2015; Niu et al., 2025; Shi et al., 2022; Sun et al., 2025a; Xin et al., 2022b). In the Songliao Basin and the Junggar Basin, laminae are classified mainly based on composition (He et al., 2025a; Pang, 2023). In the Bohai Bay Basin, the dominant lamina types include felsic laminae, clay laminae, carbonate laminae (calcite laminae and dolomitic laminae), and organic matter laminae. In the Ordos Basin, the dominant lamina types include organic matter laminae, felsic laminae, clay laminae, and tuffaceous laminae. In the Songliao Basin, the dominant lamina types are clay laminae and felsic laminae. In the Junggar Basin, the dominant lamina types consist mainly of combinations of clay laminae, felsic laminae, and carbonate laminae.

The lamina composition in the Bohai Bay Basin mainly consists of clay, OM, dolomite, calcite, feldspar, and quartz (Chen, 2024; Xie et al., 2024). The lamina composition in the Ordos Basin is mainly clay, OM, feldspar, and quartz (Hua, 2023; Xi et al., 2020). The lamina composition in the Songliao Basin is mainly clay, feldspar, and quartz (Chen and Fu, 2025; Yu, 2023). The lamina composition in the Junggar Basin is mainly clay, feldspar, quartz, dolomite, and calcite (Wang, 2022; Xi et al., 2023). The laminae are usually thin (micron-to millimeter-scale) and highly heterogeneous. In the Bohai Bay Basin, the thickness of individual laminae ranges from 20 μm to 1000 μm (Sun et al., 2025a; Xin et al., 2022b). In the Ordos Basin, the thickness of individual laminae ranges from 50 μm to 4000 μm (An, 2023; Hua, 2023). In the Songliao Basin, the thickness of individual laminae ranges from 50 μm to 2000 μm (Hua, 2023; Hua et al., 2022a). In the Junggar Basin, the thickness of individual laminae ranges from 100 μm to 1000 μm (Wu et al., 2022a; Xi et al., 2023). The Ordos Basin exhibits the largest range of lamina thickness, followed by the Songliao Basin, with the Bohai Bay and Junggar basins showing similar ranges.

2.5. The significance of laminae for shale oil enrichment

The significance of laminae development for the enrichment of shale oil mainly lies in its enhancement of storage space. The formation of bedding fractures between laminae is more likely, enhancing the storage capacity of shale oil (Jiang et al., 2013). The laminae composed of specific mineral components have well-developed pores and fractures. For example, laminae composed of carbonate minerals contain more micropores and fractures that have been dissolved by organic acids and formation water (Kong et al., 2016; Wang et al., 2022d). Laminae formed by brittle minerals are more resistant to mechanical compaction and have a better ability to preserve pores during the evolution of pore structure than shale with underdeveloped laminae (Loucks and Ruppel, 2007). Shale with a high brittleness index is more likely to form a network of fractures during the fracturing process, which significantly enhances the production capacity of shale oil (Wang et al., 2015a). For organic-rich laminae, micropores and fractures develop after OM evolution and become the occurrence space for shale oil. The high pressure generated by hydrocarbon generation from OM can also alter the pore structure of adjacent layers (Qiu, 2023). Organic and inorganic pores along laminae enhance the migration and retention capacity of shale oil during the hydrocarbon generation process (Song et al., 2020; Wu et al., 2022a).

3. Occurrence state and characterization methods

3.1. Occurrence state

Currently, there is a consensus in the industry that in-situ shale oil primarily exists in the forms of adsorbed, free, and dissolved states (Shi et al., 2019). Adsorbed oil interacts with OM and inorganic minerals through van der Waals forces and Coulombic forces, resulting in a strong adsorption affinity (Guo et al., 2025). It exists in a "solid-like" form within the pores of OM, inorganic pores, and on the surfaces of microfractures, resulting in low mobility (Li et al., 2016; Ning et al., 2017). Dissolved oil has very low solubility in water and natural gas (Hu et al., 2021). Free oil is lighter and has greater mobility, making it the primary contributor to production in shale reservoirs (Wang et al., 2019c). Song et al. (2024) indicated that in micropores ($r < 2$ nm), shale oil primarily exists in an adsorbed state (Fig. 3(a)). As shown in Fig. 3(b), shale oil exists simultaneously in both adsorbed and free states within pores of sizes ($2\ \text{nm} < r < 100\ \text{nm}$). When $r > 10$ nm (Fig. 3(c)), the flow of oil is no longer affected by pore diameter. Movable oil is primarily found in larger mesopores and macropores.

3.2. Solvent extraction

The characterization techniques for the occurrence state of hydrocarbons are mainly divided into qualitative observation and quantitative characterization methods. Qualitative observation methods include environmental scanning electron microscopy, computed tomography (CT), laser confocal microscopy, energy spectrum identification, FE-SEM, and focused ion beam etching techniques (Gou et al., 2019; Wan et al., 2024; Zhang et al., 2023c). These methods allow for the direct observation of the occurrence state of residual oil, elucidating its morphology, location, and spatial size. Currently, the observation scale has been developed from the micron level to the nanometer level. Quantitative

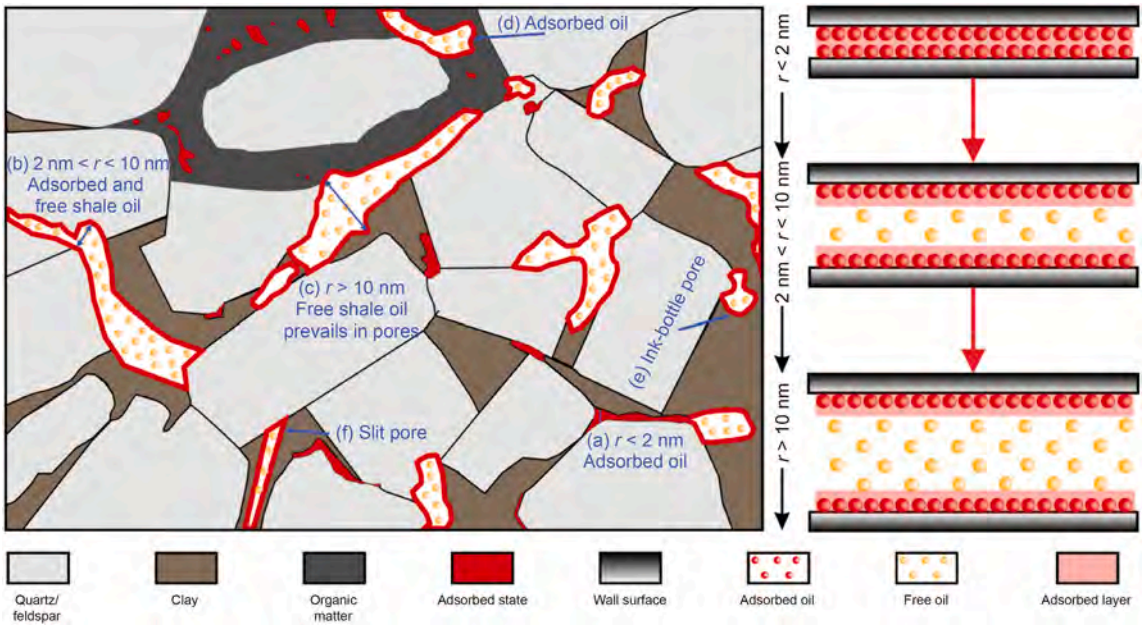

Fig. 3. Occurrence states in different pore types (Song et al., 2024).

characterization methods mainly include solvent extraction, rock pyrolysis, vacuum imbibition, molecular simulation and NMR. This article focuses on the quantitative characterization methods.

The solvent extraction method extracts hydrocarbons in different occurrence states using solvents of varying polarities (Tian et al., 2024a; Zhang et al., 2025). The principle lies in the compositional differences between adsorbed and free hydrocarbons; free hydrocarbons are generally dominated by lighter components, while the adsorbed state primarily consists of larger polar molecules or heteroatom compounds. Table 2 lists the organic solvents used in the extraction of shale oil. Dichloromethane (DCM) is the most commonly used among them. However, DCM extraction can easily remain on the surfaces of OM and inorganic minerals, leading to sample losses (Li et al., 2016). The proportions of solvents vary. The types of extracted hydrocarbons primarily include free and adsorbed hydrocarbons.

Table 2
Summary of solvent extraction cases.

References	Solvent types	Types of extracts
Abourriche et al. (2004)	Toluene/phenol	Maltenes; asphaltenes
Chen and Zhang (2017)	DCM, n-hexane and trichloromethane (TCM)	Free hydrocarbon; adsorbed hydrocarbon
Alharthy et al. (2018)	Chloride/acetone	Produced oil; residual oil
Liu et al. (2021b)	DCM/TCM	Free hydrocarbon; adsorbed hydrocarbon
Hou et al. (2021)	DCM and chloroform	Hydrocarbons of different molecular weights
Amer et al. (2022)	Supercritical propane with tetrahydrofuran	Aliphatic hydrocarbons; ethers; carbonyls and sulfur-oxygen compounds
Sun et al. (2022)	DCM/methanol (93:7); DCM/methanol/acetone (50:25:25)	Free state; adsorbed-miscible state; adsorbed state
Zhang et al. (2022)	Chloroform	Inorganic mineral adsorbed oil amount; inorganic pore free oil amount
Yang et al. (2023)	Ternary organic solvent (38:32:30)	Saturates; aromatics; resins; asphaltenes
Tian et al. (2024a)	DCM	Adsorbed oil
Zhang et al. (2025)	DCM/methanol (93:7)	Free oil; adsorbed oil

3.3. Rock pyrolysis

The basis of rock pyrolysis is the differences in thermal volatilization of the various components of shale oil (Xu et al., 2022). The principle is that free hydrocarbons have smaller molecular weights than adsorbed hydrocarbons, making them more thermally volatile and easier to release (Li et al., 2019c). Currently, pyrolysis methods are divided into the traditional pyrolysis method and the multistep Rock-Eval pyrolysis method (MREPM) (Fig. 4) (Li et al., 2024b). The traditional pyrolysis method involves maintaining the temperature at 300 °C for 3 min to obtain the S_1 peak, which is regarded as the free oil amount (Wang et al., 2025a). Then, the temperature is increased to 600 °C to obtain the S_2 peak, which is considered the kerogen pyrolytic hydrocarbon amount. Due to the adsorption of crude oil onto OM and the restrictions posed by pore spaces, the S_1 value obtained from conventional methods does not fully represent the free oil amount. Additionally, as S_2 contains both free and adsorbed oil, using only S_1 and S_2 cannot accurately characterize the quantities of each state of oil (Jiang et al., 2016b; Li et al., 2019c).

The MREPM has gradually replaced the conventional pyrolysis method. Li et al. (2020b) proposed that the sum of $S_{1\text{-}1}$ and $S_{1\text{-}2}$ represents the free hydrocarbons; $S_{2\text{-}1}$ corresponds to the adsorbed hydrocarbons, and $S_{2\text{-}2}$ represents the kerogen cracking hydrocarbons. Currently, researchers have gradually improved the heating program of Rock-Eval pyrolysis by separating the S_1 and S_2 peaks to quantify the amounts of free oil, adsorbed oil, and total oil content in shale formations. Examples include the Extended Slow Heating method developed in Canada (Li et al., 2022), the Rock-Eval Shale Play method developed in France (Ma et al., 2020), the HAWK Petroleum Assessment Method designed by Wildcat Technology (Li et al., 2020c), and the pyrolysis method developed by Sinopec (He et al., 2025b).

3.4. Vacuum imbibition

Sang et al. (2018) first proposed a vacuum imbibition method to characterize the amounts of oil present in OM and inorganic pores. The principle is based on the differences in wettability between organic and inorganic pores, allowing oil and water to enter

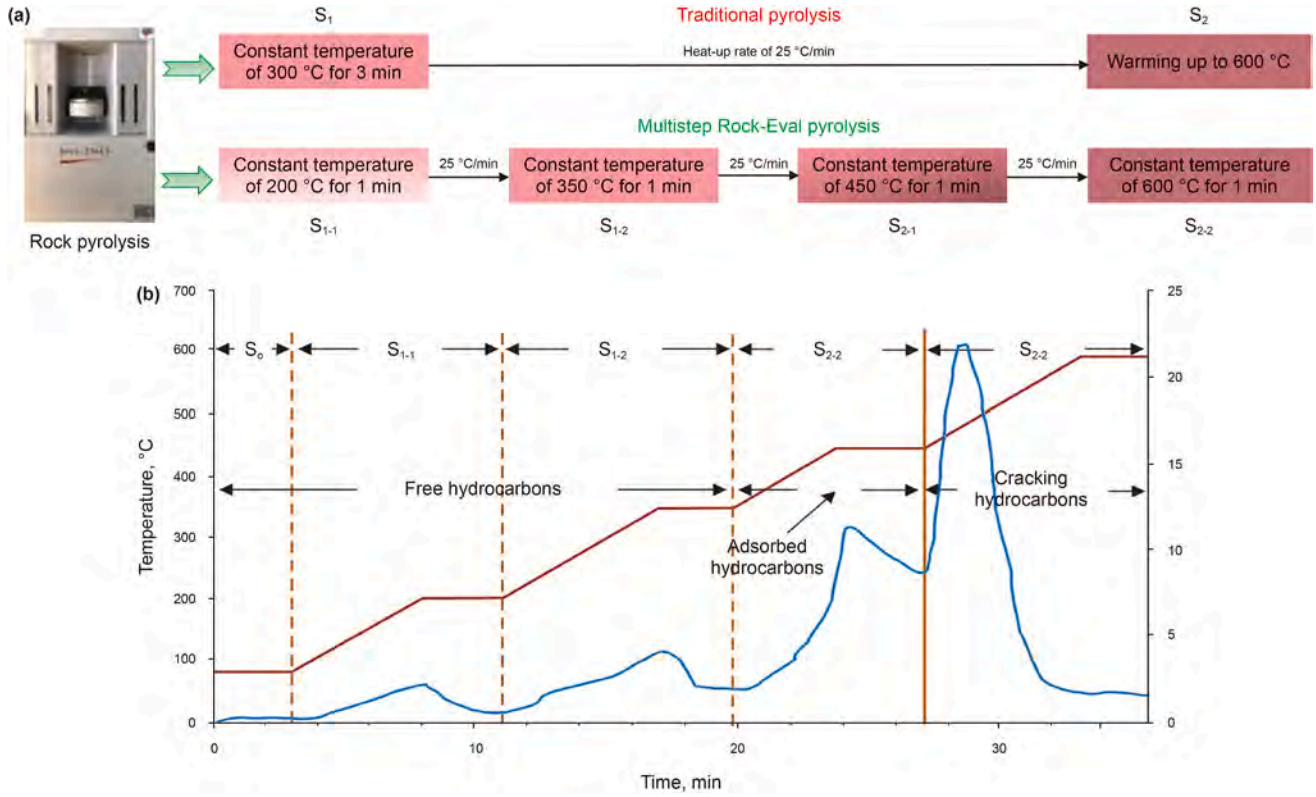

Fig. 4. Rock pyrolysis process (modified from Hu et al., 2021).

different pore spaces. When oil or water is drawn into a hydrophilic capillary, they can be absorbed into the hydrophilic capillary under capillary pressure (Fig. 5(a) and (c)). When oil is absorbed into a hydrophobic capillary, the capillary pressure remains a driving force (Fig. 5(b)). However, when water comes into contact with a hydrophobic capillary, the capillary pressure prevents water from infiltrating the organic pores (Fig. 5(d)). They independently designed a vacuum imbibition experimental device (Fig. 6). Saturation was achieved by performing oil–water vacuum imbibition experiments on equal-mass crushed core samples. They revealed that the oil content in OM ranged from 6% to 55% of the total oil content, with 50% to 90% of the oil content in OM being adsorbed and dissolved by kerogen.

3.5. Molecular simulation

Based on molecular mechanics and molecular dynamics theories, molecular simulation techniques can study the motion laws of molecules or atoms within different systems. Through the density/concentration distribution curve of the adsorbed substance (fluid), the occurrence characteristic of the fluid can be reflected (Chen et al., 2023). Liquid hydrocarbons primarily interact with the pore walls in OM and mineral slits through van der Waals forces and electrostatic forces (Guo et al., 2025). They exist in an adsorbed state on the walls of the slit and in a free state at the center of the slit pore (Jia et al., 2016). Common molecular simulation methods used to research fluid occurrence states

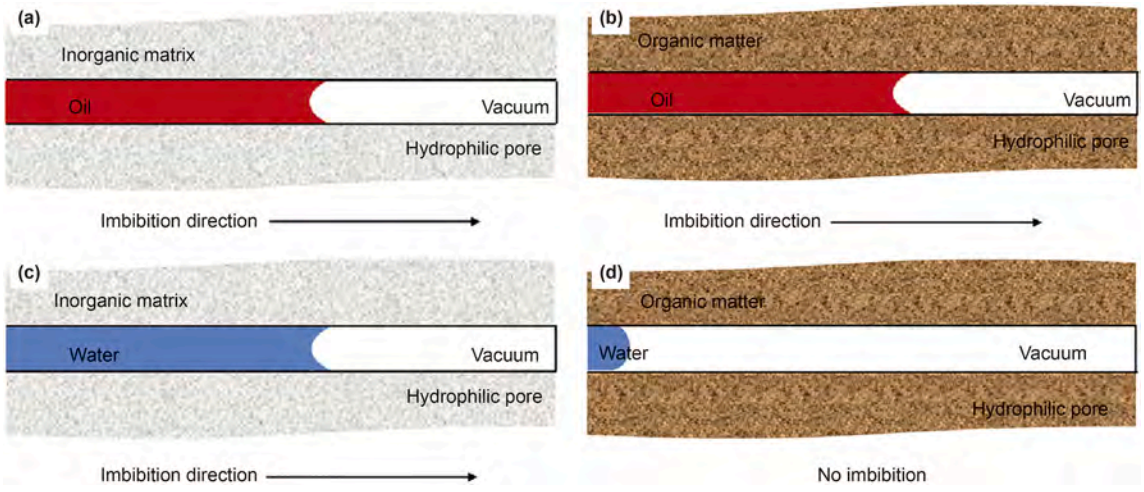

Fig. 5. The oil–water imbibition diagram in capillaries (Sang et al., 2018).

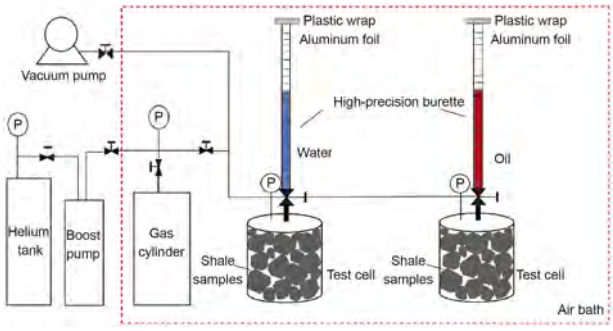

Fig. 6. Schematic diagram of the vacuum imbibition device (Sang et al., 2018).

include Grand Canonical Monte Carlo (GCMC), Molecular Dynamics (MD), and MD-GCMC (Sui and Yao, 2016; Wang and Chang, 2024). Among them, MD is the most common. Table 3 lists the components, pore types, force fields, and characterization methods of the fluid occurrence states. The characterization methods mainly include density distribution, viscosity distribution, self-diffusion coefficient, and adsorption layer molecular orientation, among which the density distribution is the most widely used (Fang et al., 2024; Liu et al., 2019; Wang and Chang, 2024; Wang et al., 2016). In addition, molecular models have gradually evolved from being single-component and single-pore type based to being based on multi-components and multi-pore types.

3.6. NMR technology

NMR technology is an effective method to research the various states of shale oil (Fleury and Romero-Sarmiento, 2016; Liu et al., 2020c). Shale contains kerogen, bitumen, oil, and water (Xu et al., 2022). When using one-dimensional NMR to characterize fluid states, signal overlap can occur, making it difficult to distinguish between different fluids (Mukhametdinova et al., 2021). Two-dimensional NMR technology (including D–T_2 and T_1–T_2) improves the separation of different proton components, allowing for higher resolution (Fleury and Romero-Sarmiento, 2016). In conventional reservoirs, D–T_2 can identify oil and water within the pores (Li et al., 2018; Mukhametdinova et al., 2021). However, in mud shale, the development of micro-nano pore throats results in negligible diffusion of liquid fluids. As a result, the D–T_2 method cannot systematically differentiate the fluid signals in shale reservoirs (Birdwell and Washburn, 2015).

Currently, the two-dimensional T_1–T_2 NMR technique is widely used (Fleury and Romero-Sarmiento, 2016; Li et al., 2018, 2019a). According to the Bloembergen-Purcell-Pound theory, T_1 and T_2 are related to the viscosity and density of fluids (Khatibi et al., 2019). T_1 reflects the mobility of a fluid, and the larger the T_1 value, the poorer the mobility (Bloembergen et al., 1948; Fleury and Romero-Sarmiento, 2016). The first prerequisite of this method is to determine the distribution region of fluids on the T_1–T_2 spectrum (Fig. 7) (Li et al., 2018; Liu et al., 2020c; Nie et al., 2024; Zhang et al., 2023b). Li et al. (2018) found that the T_1/T_2 ratios of oil and asphalt are higher than those of water. The T_1/T_2 ratios of adsorbed or bound state fluids are higher than those of free state fluids. In addition, the T_1/T_2 ratio of kerogen is the highest ($T_1/T_2 > 100$). The higher the NMR frequency, the better the oil–water separation effect (Korb et al., 2014). Therefore, establishing a T_1–T_2 spectrum suitable for the study area is important.

When quantitatively characterizing the oil volume under different states, it is usually necessary to combine other methods for comprehensive characterization. Zhang et al. (2023d) characterized the content of various types of shale oil by combining thermogravimetric experiments with NMR, based on the volatility discrepancies of components in different states. Li et al. (2020b) extracted the T_2 spectrum of organic hydrogen (from OM) from the T_1–T_2 diagram and obtained the T_2 cutoff values for free and adsorbed oil in conjunction with rock pyrolysis experiments. They further calibrated the signal intensity of the T_1–T_2 spectrum using pyrolysis parameters, allowing for a quantitative assessment of the oil content in various states. Zhang et al. (2024) calibrated the oil content of saturated oil shale cores with the signal intensity of the T_1–T_2 spectrum, allowing for the quantitative calculation of the contents of adsorbed oil, free oil, and bound oil (Fig. 8).

AR: as-received; WOR-AR: water and restoration of as-received.

Table 3
Summary of representative content of fluid occurrence states at the nanoscale in shale.

References	Components	Pore types	Force fields	Characterization methods
Severson and Snurr (2007)	C_5/C_{15}	Carbon slit pores	/	Density distribution
Wang et al. (2015b)	*n*-octane	Graphene nanopores	OPLS-AA	Density distribution
Falk et al. (2015)	*n*-alkanes (C_1–C_{12})	Amorphous nanoporous carbons	/	/
Wang et al. (2016)	*n*-octane	Quartz nanopores	CLAYFF, OPLS	Diffusion coefficient and viscosity distribution
Fang et al. (2019)	$C_{10}/C_{12}/C_{16}/C_{20}/C_{30}$	Graphene wall	COMPASS	Adsorption layer molecular orientation
Perez and Devegowda (2019)	Hydrocarbons/water/CO_2/resins asphaltenes	Kerogen Type II-C monomer	Cvff	/
Zhan et al. (2020)	*n*-octane/water	Kaolinite/montmorillonite/illite nanopores	CLAYFF, SPC/E	Density distribution
Xu et al. (2023)	*n*-heptane	Graphene and quartz slit	COMPASS	Density distribution
Tian et al. (2022)	*n*-C_5H_{12}	Kaolinite nanopores	CLAYFF	Density distribution
Fei et al. (2023)	*n*-octane	Kerogen slits	GAFF	Density distribution
Wang and Chang (2024)	Octane	Quartz/calcite/kaolinite/illite/montmorillonite/graphene/kerogen nanopores	COMPASS	Density distribution
Fang et al. (2024)	*n*-octane	Kerogen–illite pores	CLAYFF	Density distribution
Yang et al. (2025)	$C_4/C_8/C_{18}/C_7H_8/C_{33}H_{33}ON/C_{53}H_{58}S/C_{18}H_{36}O_2$	Graphene/quartz/montmorillonite pores	COMPASS	Density distribution

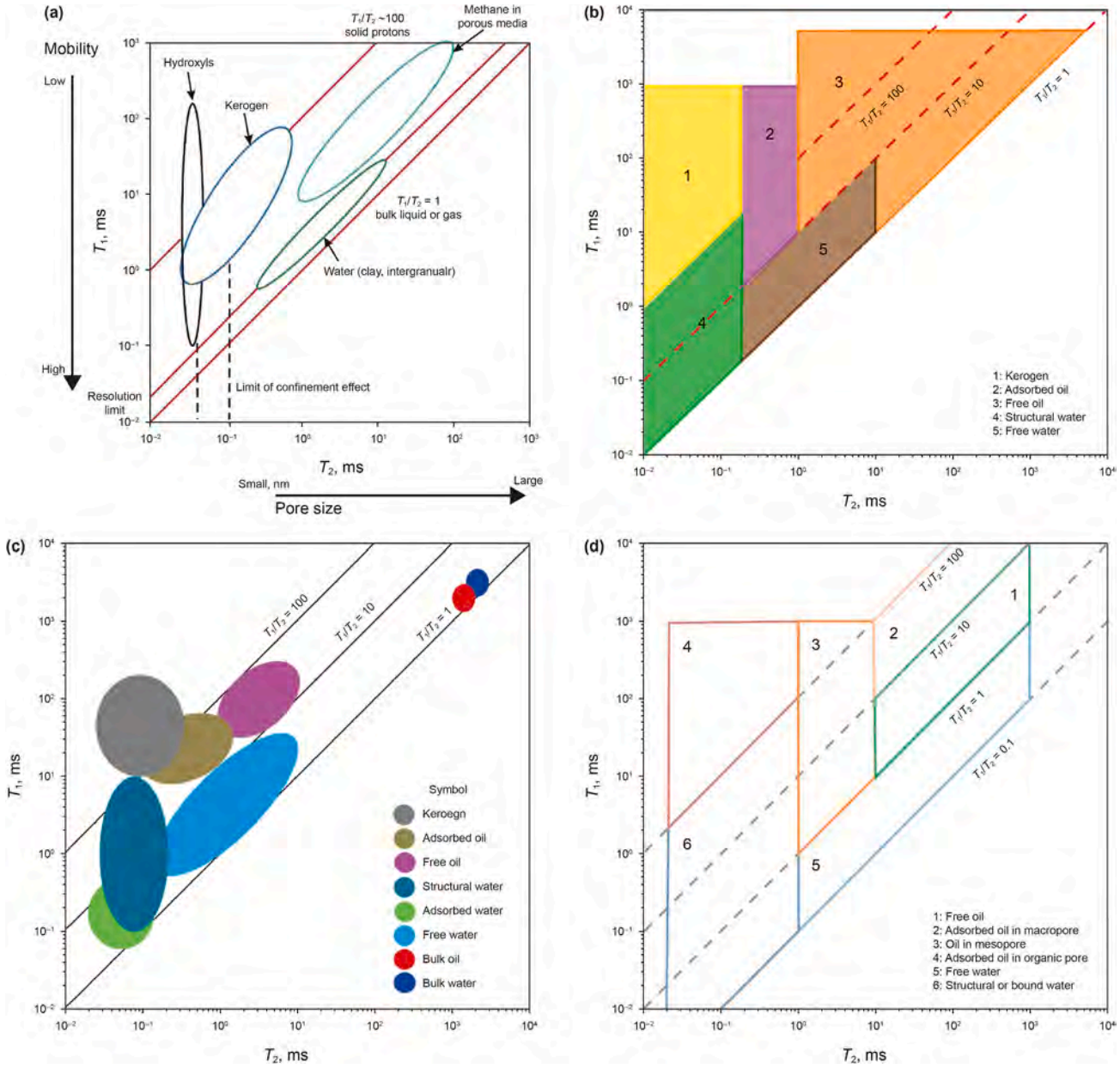

Fig. 7. Two-dimensional NMR T_1–T_2 spectrum (Li et al., 2018; Liu et al., 2020c; Nie et al., 2024; Zhang et al., 2023b).

3.7. Comparative analysis of various characterization methods

Table 4 comparatively analyzes the advantages and disadvantages, applicable conditions and characterization accuracy of various characterization methods. Among them, NMR is the most promising characterization technique. Each method has certain limitations. It should be characterized jointly by multiple methods.

3.8. In-situ characterization techniques of shale

In-situ characterization techniques are particularly useful for capturing the heterogeneity of shale (kerogen, mineral composition, porosity, etc.) at the microscopic scale (Chen et al., 2014a, 2014b). The most common in-situ techniques used for characterizing shale and mudstone include optical and electron microscopy, Raman, fluorescence and infrared spectroscopy (Chen et al., 2014a; Hackley et al., 2017; Henry et al., 2019; Klaver et al., 2015; Yasin et al., 2024). Among them, infrared spectroscopy has great potential for in-situ, rapid, and non-destructive identification and characterization of the heterogeneity of shale (Luo et al., 2021). This section mainly discusses infrared spectroscopy technology.

Fourier-transform infrared spectroscopy (FTIR) is based on the response of different materials to infrared light beams (Abarghani et al., 2020). Various functional groups, chemical bond isomers, and positional isomers all influence the position and intensity of the spectrum, exhibiting distinct characteristics on the spectrum (Chen et al., 2014a). Ganz and Kalkreuth (1987) introduced the 'A' and 'C' factors for the identification of kerogen types and thermal maturity. The 'A' factor is an indicator of the average petroleum generation potential of shale (Ganz and Kalkreuth, 1987). The 'C' factor is an indicator of the relative abundance of oxygen content (Craddock et al., 2015).

Traditional FTIR techniques include transmission FTIR (e.g., potassium bromide (KBr) pellet FTIR), attenuated total reflectance

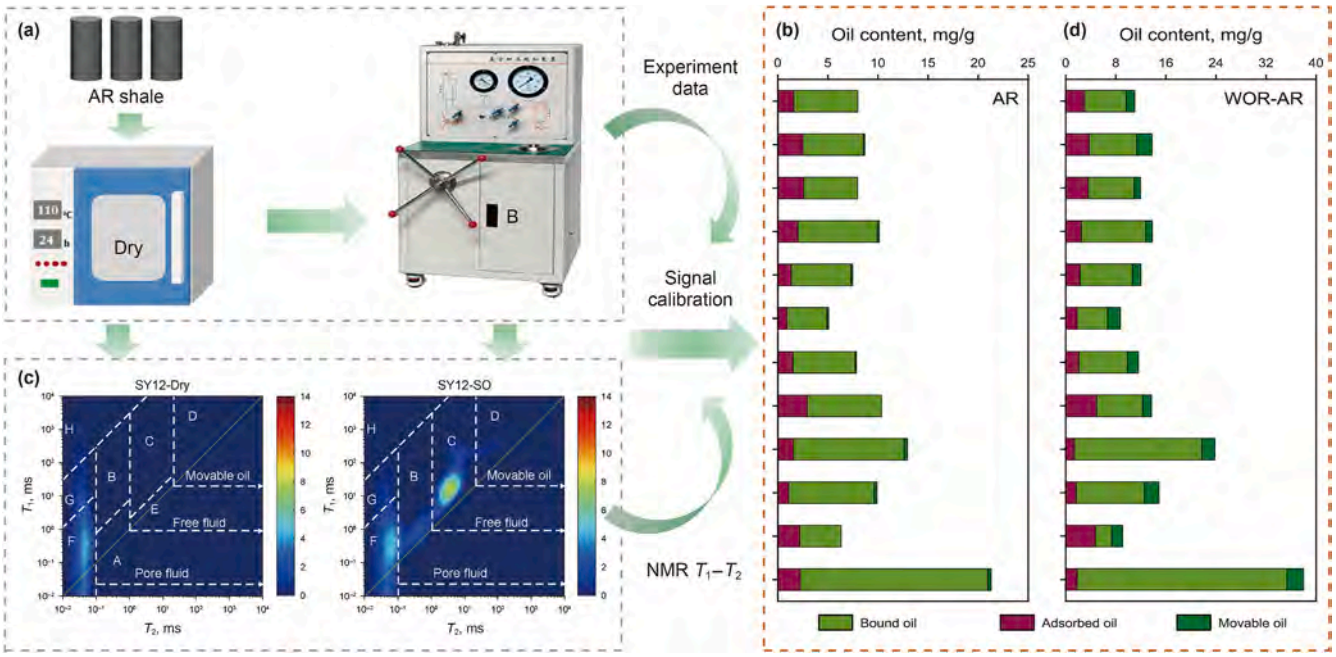

Fig. 8. Characterizing the content of oil in various states using NMR T_1–T_2 (Zhang et al., 2024).

Table 4
Comparison of various characterization methods.

Methods	Applicable conditions	Characterization accuracy	Advantages	Disadvantages
Solvent extraction	Analyze shale samples rich in free oil and partially adsorbed oil.	High quantitative accuracy for free oil.	Simple operation; the content of free oil is more accurate.	The extraction efficiency is affected by factors such as solvent polarity, type, and temperature.
Rock pyrolysis	Applicable to various types of shale, especially samples with high TOC content.	The evaluation of the total oil content potential is relatively accurate.	Evaluate the oil potential of OM, including free oil and solid OM; Suitable for batch analysis.	The S_1 peak (free hydrocarbons) is greatly affected by experimental conditions.
Vacuum imbibition	Suitable for irregular shale fragments.	Distinguish the content of ad-/absorbed oil and free oil.	Obtain organic/inorganic saturation and porosity.	Long experimental cycle.
Molecular simulation	Applicable to the study of the occurrence mechanism of microscopic shale oil.	The description of microscopic processes and molecular-level distributions is rather detailed.	Reveal the occurrence state and distribution mechanism of shale oil in pores at the molecular scale.	Depend on model parameters and assumptions; large amount of computation.
NMR	Applicable to various types of shale.	High quantitative accuracy for the state of fluid occurrence.	Non-destructive and fast; obtain information on pore structure and fluid distribution.	Its ability to distinguish between high-viscosity and low-fluidity oils is limited.

(ATR) FTIR, and diffuse reflectance infrared Fourier-transform (DRIFT) spectroscopy (Greene et al., 2004; Li et al., 2007; Lis et al., 2005). Traditional FTIR requires sample grinding and homogenization, which can be time-consuming and may lead to the loss of heterogeneity information and alterations in chemical properties. Micro-FTIR can avoid the destructive and potentially contaminating grinding of samples. Micro-FTIR is suitable for characterizing the heterogeneity of shale at higher resolutions (Chen et al., 2014a). It can perform in-situ measurements in areas larger than 20 μm × 20 μm (Mastalerz and Bustin, 1995). Its principle is based on the specific absorption characteristics of infrared light due to chemical bonds in the matrix and minerals. However, micro-FTIR also has a diffraction limit.

The latest research involves the combination of atomic force microscopy (AFM) with infrared spectroscopy (IR), known as AFM-IR (Dazzi and Prater, 2016). The AFM tip extracts spatially resolved vibrational resonance information by detecting the sample's response to thermal expansion from infrared light absorption, achieving chemical resolution at the nanoscale that far exceeds the Abbe diffraction limit (Dendisová et al., 2018; Jarzembski et al., 2018). AFM-IR can achieve a resolution of up to 10 nm (Dazzi et al., 2010). In addition, AFM-IR can provide information on the mechanical stiffness of the sample, morphological details, and the spatial distribution of specific functional groups (Dazzi and Prater, 2016).

3.9. Characterization of shale oil content and mobility

At present, the main methods for characterizing oil content include geochemical method, oil saturation method, material balance method, laser confocal technology, formation energy analysis, logging evaluation, and NMR (Guan et al., 2022; Li et al., 2020a; Wang et al., 2022a, 2025b). The geochemical method characterizes shale oil content by measuring the chloroform bitumen "A" content and the free hydrocarbon content (S_1) in rocks (Nikolaev and Kazak, 2019). However, during coring, transportation, storage, and processing, the loss of light hydrocarbons can lead to an underestimation of oil content. The loss of light

hydrocarbons from shale samples can occur up to C_{15} (Jiang et al., 2016a). Therefore, correction procedures should be implemented when using these parameters to evaluate oil content. Restoration of light hydrocarbons is commonly achieved through a range of techniques, including closed extraction (Wang, 2015), pressure-retained coring and liquid nitrogen freezing (Shao et al., 2024), gas chromatography (Song et al., 2013), pyrolysis (Zhu et al., 2015), hydrocarbon generation kinetic component simulation (Xue et al., 2016), formation energy analysis (Chen and Jiang, 2020), hydrocarbon generation and expulsion mass balance method (Chen et al., 2018b), and well-site mobile full-diameter core (MFDC) NMR (Shi et al., 2023).

At present, there are four methods to calculate the original oil saturation. (1) Direct method. Directly obtain the original fluid saturation from special core samples (pressure-retained coring or sealed coring). (2) Indirect method. First, the residual oil saturation of the core was measured using methods such as distillation, extraction, and NMR, and then the original oil saturation was obtained through loss correction (Fu et al., 2020; Handwerger et al., 2011; Spears et al., 2011; Tan et al., 2018). (3) Logging method. Using a fluid saturation interpretation model suitable for shale reservoirs, well log data (including resistivity logging, dielectric logging, and NMR logging) were inverted to obtain the original oil saturation (Tan et al., 2015; Wang et al., 2022b). (4) Laboratory simulation. By restoring cores saturated with different fluids to their in-situ state, the original fluid saturation can then be determined using instruments such as NMR or nano-CT (Ali et al., 2020). The laser confocal technique excites oil-bearing shale samples using a laser light source and measures the fluorescence intensity to extract fluorescence characteristics. By separating and recombining multiple fluorescence signals, three-dimensional digital imaging and quantitative analysis of crude oil in micron-to nanometer-scale pores was achieved (Shao et al., 2020). This method can rapidly and finely characterize the distribution of light and heavy oils within pores and identify micro-migration phenomena (Gentzis et al., 2021; Lu et al., 2023). However, the presence of fluorescent minerals may lead to an overestimation of oil content.

The logging method usually calculates oil content using the density logging curve (Liu et al., 2014a). Using logging methods can provide continuous oil content data, but it is necessary to consider the influence of data quality and prediction models on the accuracy of the results. In contrast, NMR logging provides information about pores and fluids, offering unique advantages for the evaluation of complex reservoirs (Liu et al., 2021c). NMR logging combined with pyrolysis has become a commonly used approach for determining oil saturation (Piedrahita and Aguilera, 2017). The material balance method is based on the principle that the mass of oil-generating OM in shale remains constant throughout the process of thermal evolution. Li et al. (2020a) used a hydrocarbon generation statistical model to simulate the variations of the hydrogen index and hydrocarbon generation potential index during shale evolution, and proposed a quantifiable oil and gas expulsion efficiency. The formation energy method evaluates crude oil content and mobility by measuring and inverting the energy state of oil and gas within the shale pore system in the subsurface. The NMR technique quantifies shale oil content by analyzing the spectral distribution and signal intensity of different components, or by applying a T_2 cutoff value to distinguish fluid types within the pore system. In the latest research, Wang et al. (2025b) utilized well-site MFDC NMR, laboratory oil–water restoration, and two-dimensional T_1–T_2 NMR techniques to quantify in-situ shale oil content.

The principal techniques for characterizing movable oil in shale comprise the oil saturation index (OSI) method (Jarvie, 2012), multistep pyrolysis (Jiang et al., 2016b), multi-solvent extraction (Zhang et al., 2020a), formation energy analysis (Chen et al., 2019b), swelling experiments (Li et al., 2016), MD simulations (Sui et al., 2020), and NMR (Li et al., 2020b). From a geochemical perspective, approaches such as the OSI method, the swelling method, multistep pyrolysis, and multi-solvent extraction are based on the concept that oil in shale initially saturates the adsorption sites of the OM, and only the surplus beyond this capacity is regarded as movable oil. The formation energy method evaluates shale oil primarily from a production perspective, defining movable oil as that recovered when the formation energy has decayed to a specific threshold.

However, these characterization methods have certain limitations in application. Jarvie (2012) argued that when the OSI exceeds 100 mg/g, the system enters the hydrocarbon expulsion stage and shale oil begins to exhibit mobility. This approach is currently widely employed for marine shale oil, whereas its applicability to continental shale oil is limited due to the pronounced heterogeneity in S_1 and TOC. The swelling method exhibits three primary limitations (Hu et al., 2021): (1) It may lead to an overestimation of shale porosity. (2) Substantial loss of light hydrocarbons often occurs during sample preservation and preparation. (3) The method requires numerous experimental parameters, rendering the analytical process relatively complex. Due to computational limitations, MD simulations can only study fluid flow in pores of tens of nanometers. Currently, NMR technology is the most popular method for studying shale oil mobility at the core scale from the perspective of pore structure. It is generally classified into three main approaches: (1) Integration with centrifugation techniques. (2) Integration with heating methods. (3) Use of two-dimensional NMR maps. Existing research methods can only investigate shale oil mobility from a single perspective. Considering the nano-scale pore development, complex fluid distribution, and the diverse composition of inorganic minerals and OM in shale reservoirs, a comprehensive investigation integrating multiple experimental methods has become imperative.

At present, many scholars have studied the conditions for the mobility of shale oil. For example, Liu et al. (2023d) suggested that in the Jiyang Sag of the Bohai Bay Basin, the lower limit of the OSI for movable oil is less than 50 mg/g, the lower limit of TOC is 1%, and the lower limit of porosity is 2.2%. Yu (2023), based on NMR and pore structure tests, found that the lower limit of oil-bearing porosity in the Songliao Basin is 4%, and the lower limit of oil-bearing permeability is 0.02 mD. Zhu et al. (2019b) investigated the changes in oil content and pore structure of shale before and after organic solvent extraction, and concluded that the mobility of retained oil requires an oil content greater than 0.7% and an average pore diameter exceeding 12.1 nm. Gong et al. (2020) employed NMR in combination with centrifugation to determine that the movable oil content in inorganic pores ranges from 20% to 80%, whereas that in OM pores is less than 10%. Using geochemical indicator methods, Wu (2023) determined that the mobility threshold of shale oil in the Fengcheng Formation of the Junggar Basin is defined by a minimum free oil content of 2.0 mg/g.

4. Occurrence space

4.1. Space types and genesis

Shale reservoirs primarily consist of three types of spaces: organic pores, inorganic pores, and fractures (Fig. 9) (Loucks et al., 2012; Wei et al., 2023a). Organic pores are the residual pores from hydrocarbon generation of OM, including residual pores from

kerogen hydrocarbon generation and the cracking of crude oil into gas (Curtis, 2002). Its pore diameter mainly ranges from 10 nm to 200 nm (Gao, 2019). The development degree and connectivity of organic pores are controlled by factors such as lithofacies, mineral composition, type of OM, thermal evolution degree, structural deformation, and stress intensity (Mastalerz et al., 2013; Wu et al., 2019). During the processes of OM accumulation and thermal evolution, numerous tiny pores and fractures continuously form within the OM. High maturity leads to a longer hydrocarbon expulsion time, which promotes the development of pores (Yang et al., 2013). Organic-rich shale has more microporous space compared to organic-poor shale, allowing it to retain more liquid hydrocarbons (Rexer et al., 2013).

Inorganic pores include InterP and IntraP (Loucks et al., 2012). InterP are formed by the gaps that remain after mineral particles or mineral aggregates undergo compaction during the diagenesis. These pores are primarily influenced by sedimentation and diagenesis (Dou et al., 2023). InterP are distributed within the accumulation of mineral particles, with pore sizes mostly at the micron level. These pores are relatively large and have good connectivity, providing ample space for the storage of oil. IntraP are the pores located within inorganic mineral particles, primarily distributed in minerals with unstable chemical properties (Zheng et al., 2019). There are two main types of IntraP. One type is the intercrystalline pores found in inorganic minerals, as well as the pyrite intercrystalline pores. The other type is the dissolution pores formed within minerals due to organic acids released during hydrocarbon generation (Kong, 2023).

Microfractures serve as the main microscopic pathways for oil migration and also provide the storage space. Microfractures are typically dominated by diagenetic shrinkage fractures, intergranular fractures in mineral particles, clay shrinkage fractures, hydrocarbon generation pressure fractures, inter-laminar fractures, and structural fractures (Dou et al., 2023; Kong, 2023; Niu et al., 2025). The factors controlling the formation of microfractures are very complex. External factors include tectonic stress, diagenesis, and hydrocarbon generation pressure, while internal factors include rock properties, lithofacies, and mineral composition.

It is widely accepted in the petroleum industry that bedding fractures occur within shale formations under high-pressure conditions. These fractures generally develop along lamination contacts, bedding planes, and lithologic boundaries (Lai et al., 2022; Li et al., 2024c; Zeng et al., 2016). In high-pressure subsurface formations, bedding fractures are generally closed or semi-closed (Pang et al., 2023b; Zhang et al., 2021). Nevertheless, they may become open under specific conditions, including hydrocarbon generation-induced overpressure, abnormally high pore pressures, tectonic activities (e.g., within fault and fold zones), magmatic activities, dissolution of fracture-filling materials, and hydraulic fracturing (Cobbold et al., 2013; Ismat, 2012; Liu et al., 2023a; Matthaei et al., 1995; Xin et al., 2022b).The opening width of bedding fractures is highly variable, with apertures commonly filled by bitumen, OM, and a variety of inorganic minerals (Lash and Engelder, 2005; Pang, 2023). As the degree of filling increases, the effectiveness of natural fractures gradually decreases, thus reducing their contribution to reservoir productivity (Laubach et al., 2004; Liu et al., 2021a). The development of matrix-type shale oil reservoirs is challenging, and their productivity is generally low without hydraulic fracturing. Fracture-type shale oil reservoirs are characterized by high hydrocarbon enrichment, high initial production rates, and a rapid decline in productivity (Zhang et al., 2021). Therefore, fractures are closely related to the development of shale oil.

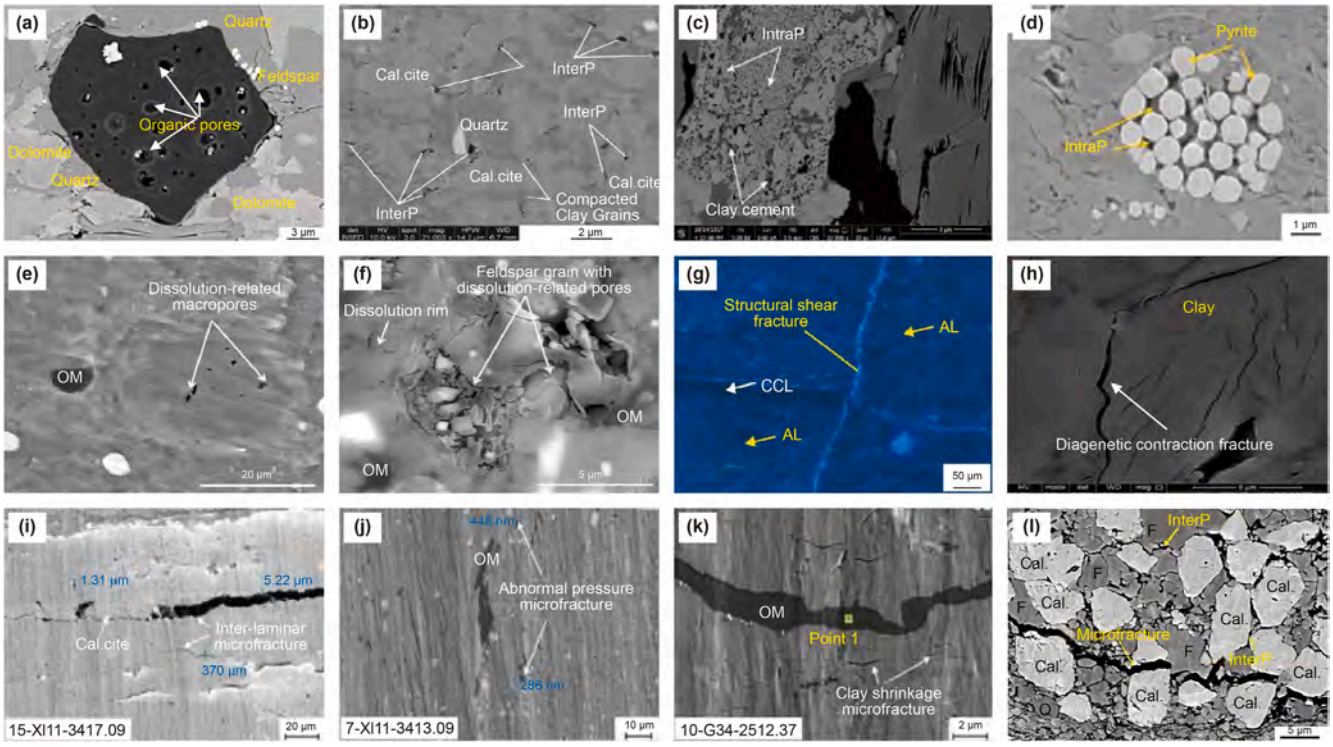

Fig. 9. Shale oil occurrence spaces: **(a)** organic pores; **(b)** InterP; **(c)** clay intercrystalline pores; **(d)** pyrite intercrystalline pores; **(e)** calcite dissolution pores; **(f)** feldspar dissolution pores; **(g)** structural fracture; **(h)** diagenetic shrinkage fracture; **(i)** interlayer fractures; **(j)** abnormal pressure fractures; **(k)** clay shrinkage fractures; **(l)** intergranular fracture in minerals. AL: argillaceous laminae; CCL: calcareous laminae; Cal.: calcite; F: feldspar; Q: quartz. (Chen et al., 2019a; Li et al., 2019d; Liu et al., 2020a; Loucks et al., 2012; Rao et al., 2024; Xiao et al., 2024; Xin et al., 2022b; Yang et al., 2016; Zhang et al., 2021).

Shi et al. (2022) found that different pore spaces have varying pore sizes. The pore diameter of calcite intercrystalline pores generally ranges from 10 μm to 30 μm, with a maximum pore diameter reaching several hundred micrometers. The intercrystalline pores of dolomite are well-developed due to the high resistance of dolomite crystals to compaction, with diameters ranging from 0.6 μm to 4 μm. The intercrystalline pores of clay minerals are plate-like and thin, with very small pore diameters (<1 μm); they develop in thin parallel laminae and weakly laminated layers (Shi et al., 2022). The diameter of pyrite intercrystalline pores typically ranges from 100 nm to 10 μm. Organic pores have irregular shapes, with pore diameters of less than 1 μm.

4.2. Discrepancies in the occurrence space

4.2.1. Discrepancies among laminated shale

There are certain discrepancies in the storage space types among different laminae (Dou et al., 2023; Hua et al., 2021, 2022a, 2022b). Clay-rich laminated shales develop InterP (Gao et al., 2017). Laminae developed with brittle minerals are prone to forming natural fractures (Bowker, 2007). Organic pores are primarily found in organic-rich laminae, while dissolution pores are more commonly observed within calcite-rich laminae (Shi et al., 2020; Xin et al., 2022b). Shi et al. (2022) compiled a statistical summary of six types of laminae in the Dongying Depression, along with their shale oil occurrence spaces (Fig. 10). The types of storage space are primarily composed of InterP of clay minerals and InterP of calcite, with the least amount of organic pores. Generally, in laminated shale reservoirs with good continuity, there are more InterP of calcite, InterP of dolomite, and interlaminar microfractures, while laminated shale reservoirs with poor continuity have relatively higher amounts of InterP of clay minerals and shrinkage fractures. Xin et al. (2022a) found that the siliceous laminae are primarily composed of InterP between rigid particles (quartz and feldspar), which exhibit triangular or elongated shapes (Fig. 11). Additionally, quartz and feldspar can reduce the compaction effect on pores, thereby enhancing connectivity (Schieber, 2010). The mixed laminae develop InterP between rigid particles and InterP between clay flakes. The main pores in the dolomite laminae are InterP between rigid particles (dolomite and feldspar), along with minor dissolution pores. The calcite laminae develop InterP and IntraP associated with dissolution.

4.2.2. Discrepancies between laminated shale and massive shale

Laminated shale reservoirs also exhibit certain differences compared to massive shale. Xin et al. (2022b) found that the laminated shale samples have higher porosity, larger macropore volume, better connectivity, and more developed microfractures compared to the massive samples. Based on Fig. 12(c) and (d), the incremental pore volume of laminated samples is higher than that of massive samples. The difference lies in the average pore throat diameter, with the mesoporous volume of laminated samples being greater than that of massive samples. The average porosity of laminated samples (4.2%) is greater than that of massive samples (2.4%). The mercury withdrawal efficiency is defined as the ratio of the mercury saturation at the lowest pressure at the end of the extraction phase to the mercury saturation at the highest pressure at the end of the injection phase. Samples with high withdrawal efficiency possess larger pore throat volumes, indicating good pore connectivity (Wardlaw and Taylor, 1976). The average withdrawal efficiency of massive samples is 13.5%, while the average withdrawal efficiency of laminated samples is 31.1%. The differences between massive shale and laminated shale are primarily attributed to three factors: the arrangement and combination of minerals, organic–inorganic interactions, and interlaminated fractures.

In addition, a high OM abundance, a high content of brittle minerals, and a specific thermal maturity are the fundamental conditions for the formation of dominant shale facies (Cao et al., 2019; Wu et al., 2016). Among these, the organic carbon content determines hydrocarbon generation potential, the pore structure determines storage performance and connectivity, and brittle minerals influence fracturing effectiveness. Therefore, the identification of favorable facies needs to comprehensively consider the matching relationships among these three factors (Zhang et al., 2017).

4.3. Controlling factors of occurrence space differentiation

The pore development mechanism in shale is highly complex, and the pore evolution is influenced by multiple factors. This

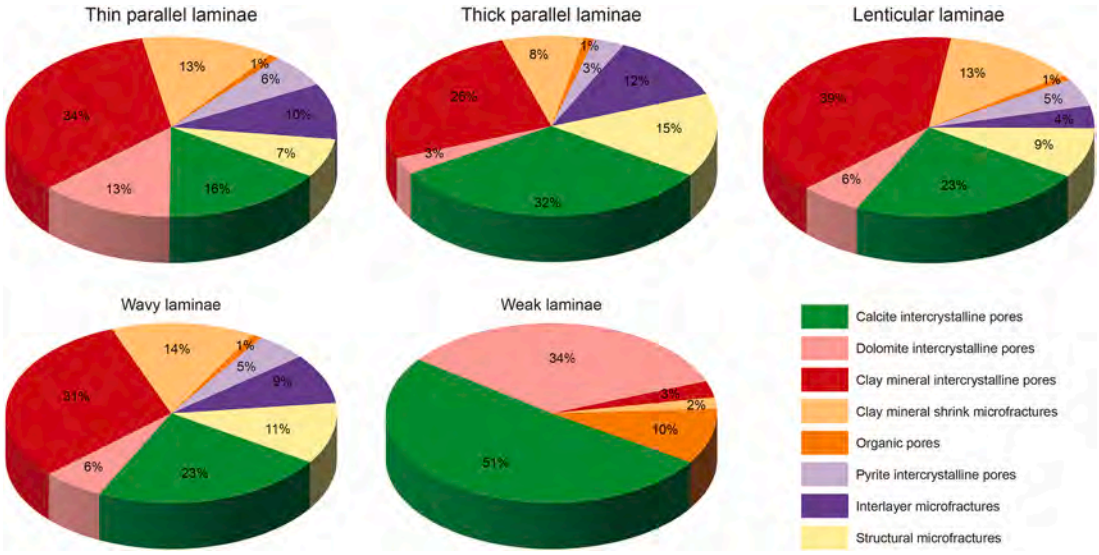

Fig. 10. Proportions of storage space in various laminae of the Dongying Sag (modified from Shi et al., 2022).

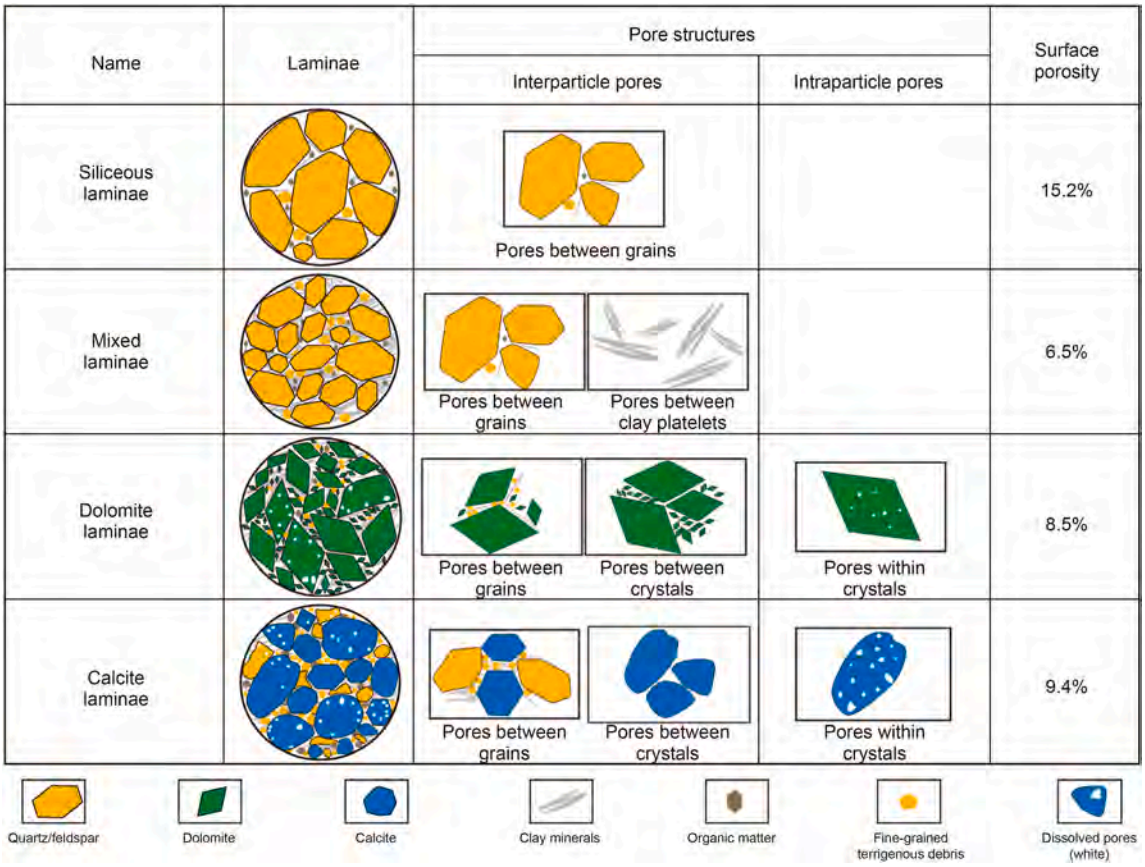

Fig. 11. Storage space in different laminae of Cangdong Sag (Xin et al., 2022a). The differences in storage space between Dongying Sag and Cangdong Sag are primarily controlled by mineral composition. Dongying Sag is mainly composed of clay minerals, while Cangdong Sag is dominated by rigid minerals such as quartz and feldspar.

section focuses on the impact of sedimentary tectonics and diagenesis on the occurrence space of shale oil.

4.3.1. Sedimentary tectonics

Sedimentary tectonics control the occurrence space through changes in the sedimentary environment (Qu et al., 2024). The interaction between OM and inorganic matter in shale controls the evolution of pores (Curtis, 1978). The thermal evolution of OM generates CO_2 and organic acids (Xin et al., 2022a). Organic acids can dissolve aluminosilicate minerals and carbonate minerals, forming secondary pores such as dissolution pores and microfractures (Zhang et al., 2009). Generally, there are more dissolution pores in laminated shale reservoirs compared to massive shale reservoirs. This may be due to the more limited fluid migration distance in the massive shale reservoirs. In contrast, fluids can migrate more easily laterally along the interfaces of the laminated shale reservoirs (Heydari and Wade, 2002; Liang et al., 2018; Zhang et al., 2016).

Xin et al. (2022b) discovered that laminated shale exhibits better continuity and a higher density of microfractures compared to massive shale in the Bohai Bay Basin (Fig. 13). Moreover, microfractures in the region are widely developed parallel to the laminae. The dehydration of clay minerals, differential compaction, pressure-solution, OM contraction, and overpressure resulting from hydrocarbon generation all contribute to the formation of microfractures (Davudov et al., 2020; He et al., 2022; Jiu et al., 2013; Zeng and Li, 2009; Meng et al., 2018; Pang et al., 2023b; Wang et al., 2020; Zhang et al., 2019a). The formation of parallel fractures can be attributed to two reasons: (1) Flat kerogen particles aligned parallel to the laminae may induce laminae-parallel fractures (Lash and Engelder, 2005; Vernik, 1994); (2) The tensile strength applied perpendicular to the laminae may be lower than that applied parallel to the laminae (Lash and Engelder, 2005; Meng et al., 2017). Additionally, in the fractures of rock samples from the Bohai Bay Basin (Fig. 14), dissolved remnants of feldspar were observed, along with some incompletely corroded silicate and carbonate mineral particles (Xin et al., 2022b). This phenomenon indicates that the microfractures (Fig. 13) were not artificially induced during the sample preparation process. These minerals bear part of the overburden load of the maximum principal stress.

4.3.2. Diagenesis

Diagenesis generally influences the evolution of pore space in shale through clay mineral transformation, mechanical compaction and the thermal evolution of OM (Wang et al., 2023b; Zhang et al., 2020b). Due to the high content of plastic components in shale, the mineral particles are relatively fine, resulting in relatively weak resistance to compaction. Under compaction, pore water is expelled, and intergranular pores gradually decrease (Liu et al., 2019). When montmorillonite transforms into illite, the lack of particle support leads to a reduction in the size of primary pores (Deng et al., 2020). In addition, the precipitation of silica generates authigenic minerals, which increases the brittleness of the rock. This process may also create interlayer fractures, enhancing the

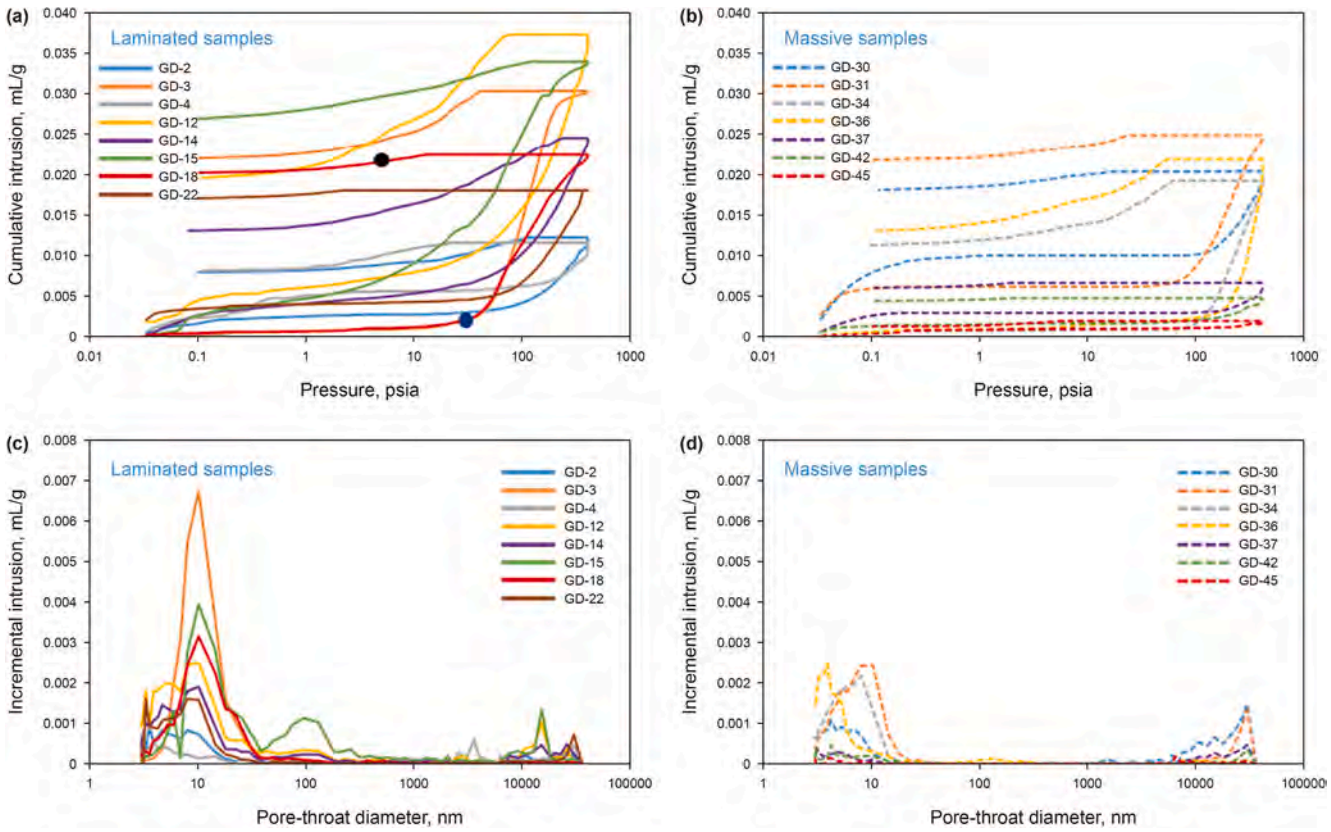

Fig. 12. Pore size distribution curves of laminated samples and massive samples from the Bohai Bay Basin: **(a)** mercury intrusion–extrusion curves of laminated samples; **(b)** mercury intrusion–extrusion curves of massive samples; **(c)** pore size distribution curves of laminated samples; **(d)** pore size distribution curves of massive samples (Xin et al., 2022b).

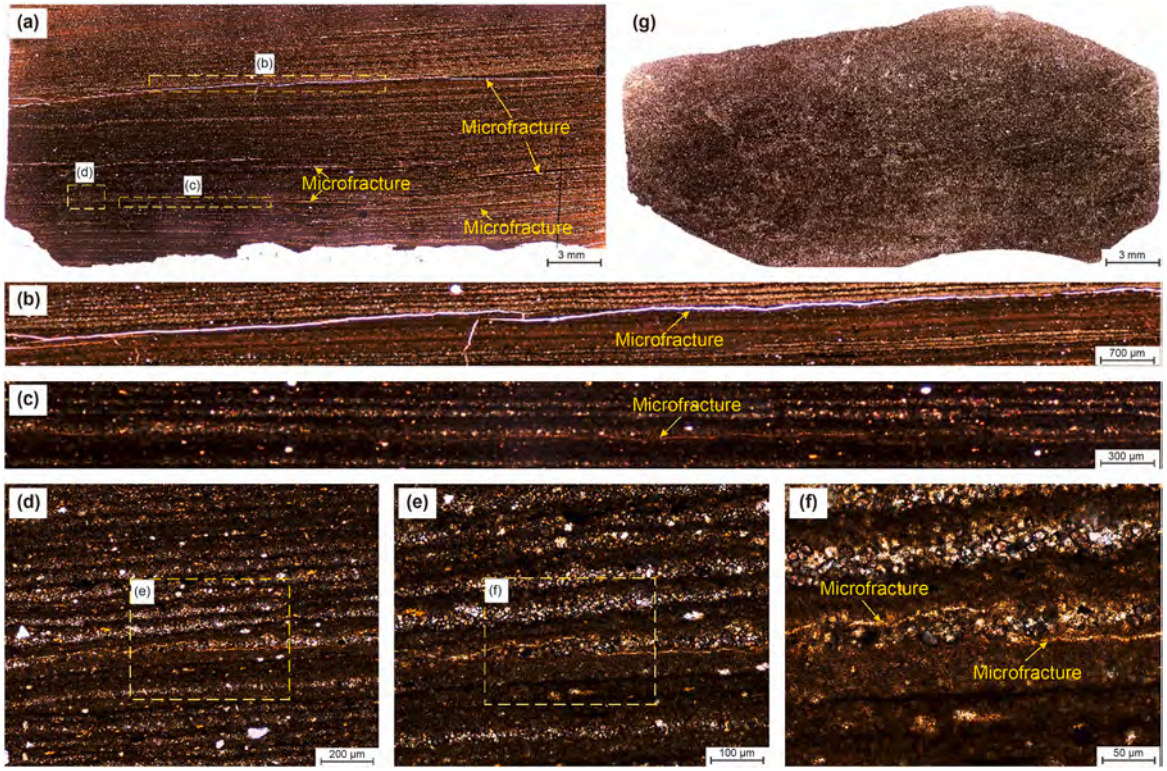

Fig. 13. Photomicrographs of the microfracture distribution in the shale samples from Bohai Bay Basin. **(a)–(f)** laminated samples; **(g)** massive sample (Xin et al., 2022b).

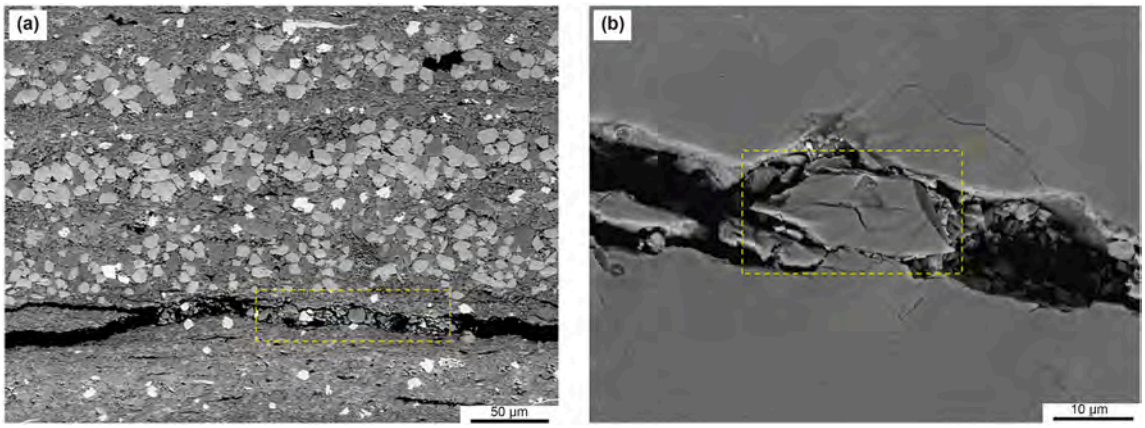

Fig. 14. Backscattered electron images of horizontal fractures in a shale sample from Bohai Bay Basin: **(a)** a horizontal fracture containing incompletely corroded silicate and carbonate mineral particles (yellow rectangle); **(b)** a horizontal fracture containing incompletely corroded feldspar (yellow rectangle) (Xin et al., 2022b).

storage capacity of the shale (Sun, 2017). During the thermal evolution of OM, oxygen-containing functional groups are removed, resulting in the production of organic acids and the release of carbon dioxide (Heydari and Wade, 2002; Zhang et al., 1994). The neutralization effect of organic acids causes the dissolution of aluminosilicate minerals and carbonate minerals, resulting in the generation of secondary pores (Heydari and Wade, 2002; Wan et al., 2025; Zhang et al., 2009).

4.4. Pore size of shale oil occurrence

4.4.1. Main pore size for shale oil occurrence

Clearly identifying the main pore sizes in which shale oil is stored is crucial for its production (Chen et al., 2018a). Typically, changes in shale pore size before and after organic solvent extraction are used to determine the main pore size range for shale oil (Chen et al., 2018a; Liu et al., 2020a; Wu et al., 2022b). Table 5 summarizes the main pore sizes for oil storage in different lithofacies of shale. There are certain discrepancies in the main pore size range of shale reservoirs, typically ranging from a few nanometers to several hundred nanometers. In addition, the main pore size range in laminated shale reservoirs is greater than that in massive shale reservoirs. The pore sizes in quartz-rich siltstone laminae and carbonate mineral laminae are larger than those in clay mineral laminae. Siltstone laminae have larger pore sizes compared to mudstone laminae, organic-rich laminae, and tuff laminae.

4.4.2. Lower limit of pore size

Various methods are typically employed, including solvent extraction, stepwise pyrolysis, NMR, centrifugation, N_2 adsorption, ESEM, and FE-SEM, to determine the pore size lower limits for movable oil and free oil (Bao, 2018; Guo et al., 2023, 2024; Sun et al., 2017; Wang et al., 2019c; Wu et al., 2022b). Table 6 summarizes the lower limit of pore size (LLPS). The LLPS of movable oil and free oil differs slightly, usually from a few nanometers to several hundred nanometers. The LLPS of movable oil in massive shale reservoirs is 3.5–40 nm, and the LLPS of free oil in pure shale reservoirs is 3–15 nm. The LLPS of movable oil in laminated shale is 88.4–217.22 nm. The LLPS of movable oil in lamellar shale is between 150 and 300 nm, while the LLPS of free oil in these reservoirs is 30–40 nm. The LLPS of movable oil is ranked as follows: lamellar shale > laminated shale > pure shale. The LLPS of free oil in lamellar shale reservoirs is significantly greater than that in pure shale.

5. Influencing factors of shale oil occurrence

5.1. Organic matter

5.1.1. Abundance of OM

The total organic carbon (TOC) content is used to represent the abundance of OM (Xu et al., 2022). The TOC content determines

Table 5
Summary of the main pore sizes for oil storage in shale. CI: confidence intervals.

References	Reservoirs	Lithofacies	Main pore size
Rylander et al. (2013)	Eagle Ford	Shale	≥250 nm (n = 10, 95% CI)
Saraji and Piri (2015)	Bakken	Shale	10–100 nm (n = 8, 95% CI)
Chen et al. (2018a)	Bohai Bay Basin	Shale	2–30 nm (n = 2, 95% CI)
Goral et al. (2019)	Vaca Muerta	Shale	5–75 nm (n = 2, 95% CI)
Dang et al. (2022)	Ordos Basin	Shale	2–25 nm (n = 16, 95% CI)
Wu (2023)	Junggar Basin	Felsic shale	5–40 nm (n = 18, 95% CI)
		Carbonate shale	6–50 nm (n = 18, 95% CI)
		Mixed shale	3–10 nm (n = 18, 95% CI)
Zhu et al. (2024)	Junggar Basin	Shale	>300 nm (n = 17, 95% CI)
Wang et al. (2019c)	Bohai Bay Basin	Organic-rich shale/laminae	<100 nm (n = 29, 95% CI)
An (2023)	Ordos Basin	Homogeneous shale	30–80 nm (n = 4, 95% CI)
		Felsic laminated shale	3–100 nm (n = 4, 95% CI)
		Tuffaceous laminated shale	7–30 nm (n = 4, 95% CI)
Wu et al. (2022a)	Junggar Basin	Quartz-rich siltstone laminae	<15–20 μm
		Carbonate mineral laminae	<15–20 μm
		Clay mineral laminae	50–200 nm
Wu et al. (2022a)	Ordos Basin	Felsic sandstone laminae	>500 nm
		Clay mineral laminae	30–300 nm
Xie et al. (2024)	Bohai Bay Basin	Laminated gray dolomitic shale	19.57–47.51 nm (n = 5, 95% CI)
		Laminated felsic shale	11.59–36.41 nm (n = 3, 95% CI)
		Massive shale	6.41–8.92 nm (n = 3, 95% CI)

Table 6
Summary of the LLPS for shale oil occurrence./: no data.

References	Basins	Lithofacies	LLPS of movable oil, nm	LLPS of free oil, nm
Sun et al. (2017)	Bohai Bay Basin	Shale	10–25	/
Bao (2018)	Bohai Bay Basin	Shale	/	10
Wang et al. (2019c)	Bohai Bay Basin	Shale	30	5
Wu et al. (2022b)	Junggar Basin	Shale	3.5–19	/
Wu (2023)	Junggar Basin	Felsic shale	8	5
		Carbonate shale	13	6
		Mixed shale	28	3
Guo et al. (2023)	Santanghu Basin	Massive shale	10	/
Guo et al. (2024)	Kailu Basin	Shale	40	15
Hua (2023)	Ordos Basin	Organic-rich laminae	194.30	/
		Felsic laminae	217.22	/
		Tuffaceous laminae	155.70	/
		Clay laminae	120.72	/
Hua (2023)	Songliao Basin	Clay laminae	88.40	/
		Calcareous laminae	163.15	/
		Felsic laminae	83.97	/
Yu (2023)	Songliao Basin	Lamellar shale	150–300	30–40

shale oil generation potential (Pang et al., 2023a). From Fig. 15, with the increase of TOC values, the contents of both free oil and adsorbed oil also increase. However, the correlation coefficient between adsorbed oil with TOC is greater than that of free oil. The adsorption capacity of OM is reflected in three aspects (Dang et al., 2022; Li et al., 2020d; Qu et al., 2024; Yang et al., 2024). (1) The residual hydrocarbon generation pores developed in OM can provide a certain storage space for adsorbed oil. (2) OM typically has a large specific surface area, which can provide numerous sites for the adsorption of shale oil. (3) The surface of OM is rich in oil-affinitive groups, which can produce high-energy adsorption sites.

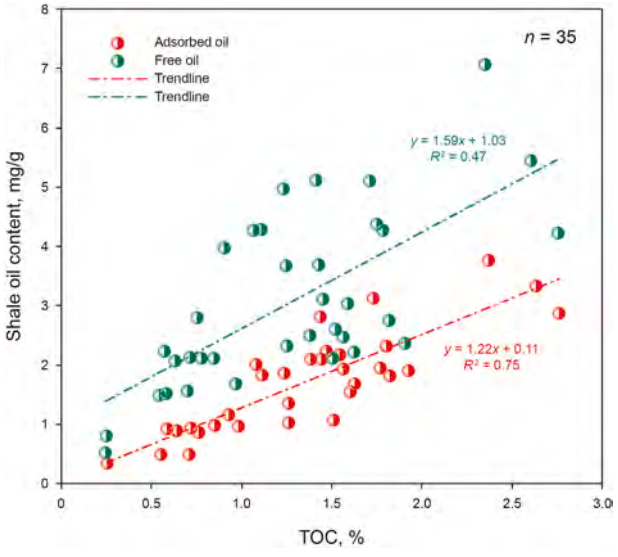

Fig. 15. Relationship between shale oil content and TOC in the Gaoyou Sag, Subei Basin (multi-temperature pyrolysis experiment results) (Gong et al., 2024).

5.1.2. Maturity of OM

Maturity controls the adsorption capacity of fluids (Xu et al., 2022). In the early stage of hydrocarbon generation, the degree of compaction is low, and the formation has relatively high porosity. At this time, the generated hydrocarbons are rich in heavy hydrocarbons, especially non-hydrocarbons and asphaltenes. Shale oil predominantly exists in an adsorbed state on the surfaces of kerogen and minerals (Bagri et al., 2010; Dang et al., 2022). As thermal maturity increases, kerogen undergoes cracking. Consequently, more light oil (saturated hydrocarbons and aromatic hydrocarbons) is generated, and the content of adsorbed oil discreases (Jiang et al., 2016b; Li et al., 2023a; Wang et al., 2019c).

Maturity controls the content of free oil by influencing the oil and gas content and pore structure (Xu et al., 2022). When R_o < 0.5%, bitumen and a small amount of poorly flowing free oil/gas are generated (Fig. 16) (Zhang et al., 2019f). When 0.5% < R_o < 0.7%, the thermal degradation capacity gradually increases, leading to a gradual increase in the amount of generated oil and gas. When 0.7% < R_o < 1.0%, it is the main phase for the significant generation of hydrocarbons from source rocks (Zhao et al., 2020). When 1.0% < R_o < 1.3%, macromolecular OM undergoes cracking to generate light hydrocarbons. When R_o > 1.3%, residual liquid hydrocarbons and heavy gaseous hydrocarbons are further cracked, ultimately producing stable methane gas, carbonaceous asphaltene, and graphite (Xu et al., 2016; Zhang et al., 2019f).

5.2. Inorganic mineral

The influence of mineral composition on the occurrence of shale oil mainly includes the adsorption capacity of the minerals (Loucks et al., 2012; Wang and Chang, 2024) and the developmental characteristics of the storage space (Gong et al., 2024). Generally, the adsorption capacity of OM and clay minerals for oil is stronger than that of inorganic minerals (such as feldspar, quartz, and calcite) (Chen et al., 2021; Liang et al., 2022b; Zhu et al., 2023). Li et al. (2016) found that the adsorption capacity follows the order: clay minerals > quartz > carbonate minerals, as clay minerals have a larger pore surface area compared to non-clay minerals, thus providing more adsorption sites (Xu et al., 2022). Additionally, illite has the strongest adsorption capacity for shale oil among clay minerals, followed by montmorillonite (Cooles et al., 1986; Zhang et al., 2015).

The differences in mineral composition of shale directly affect the development and preservation of shale pores (Loucks et al., 2012). Gou et al. (2023) proposed a model illustrating the occurrence space and mineral composition. Their research indicates that the mineral distribution in dolomitic and siliceous shales is

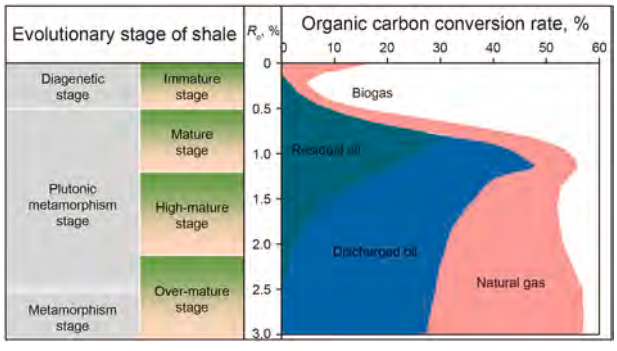

Fig. 16. Evolution model of hydrocarbon generation and expulsion in argillutite in China (modified from Zhang et al., 2019f).

uniform, retaining a significant amount of original InterP. Therefore, dolomitic and siliceous shales have a higher number of pores and larger pore diameters. Argillaceous shales have relatively weak resistance to compaction, but during their evolution, mineral transformations and dehydration shrinkage occur, generating numerous pores and microfractures within the clay minerals (Sun et al., 2021; Wan et al., 2025; Zhao et al., 2022). For mixed shales, fine-grained clay particles fill the spaces between quartz and carbonates. As a result, most of the InterP get blocked, leading to smaller pore diameters.

5.3. Burial history and depth

The increase in burial depth leads to higher formation temperatures and pressures, which affect hydrocarbon generation and storage capacity, further influencing the occurrence states and space. Increased pressure reduces porosity in shale (Rimstidt et al., 2017). In addition, rising temperatures promote the pyrolysis of OM and increase the amount of hydrocarbons (Yang et al., 2020). Porosity typically undergoes three evolutionary stages with increasing burial depth (Li et al., 2016; Pang et al., 2023a). From Fig. 17(a), the porosity gradually decreases at burial depths of less than 2.5 km, increases between 2.5 km and 3 km, and then decreases again at depths greater than 3 km (Li et al., 2016). The reasons for this can be analyzed in three stages. In the early stage, the decrease in shale porosity is primarily due to the compaction and cementation processes, which cause larger pores to transform into smaller pores (Zhang et al., 2019c). In the next stage, the shale reservoir enters the 'oil window' phase, where OM pores begin to develop. Hydrocarbon generation causes a sharp increase in fluid pressure, which counteracts the effective stress of the overlying rock, thereby enhancing the porosity of the shale (Zhang et al., 2014). In addition, during the pyrolysis of kerogen, acidic fluids dissolve unstable minerals, promoting the formation of pores (Deng et al., 2020). Therefore, the porosity increases with increasing burial depth. In the final stage, the pyrolysis of shale oil leads to a reduction in molecular weight, facilitating flow and decreasing reservoir pressure. At the same time, the intensified compaction and pressure release together result in a decrease in reservoir porosity. Fig. 17 (b) presents the variation of adsorbed oil ratio with depth. It can be observed that with increasing burial depth, adsorbed oil ratio in both lamellar and laminae shale gradually decreases. Wang et al. (2019c) suggested that with increasing depth, the viscosity/density of oil decreases, the saturated hydrocarbon content increases (resulting in lighter oil). This weakens the capacity of oil to adhere to the pore wall surfaces.

The tectonic activity can also have a certain impact on the occurrence of shale oil. Fault activity generates a large number of fractures, allowing shale gas to escape along these fractures, which reduces formation pressure and causes organic pores to close under compaction (Xiang et al., 2024). Fu et al. (2023) found that the shale oil productivity is higher inside fault systems than outside them. The reason is that many fractures develop within fault systems, improving the connectivity of the shale reservoir and facilitating the occurrence of shale oil. The inversion structure formed by tectonic uplift can break shale along mechanically weak positions, generating bedding fractures that facilitate the migration of shale oil (Fu et al., 2023). Additionally, the later the tectonic uplift occurs, the longer the burial history of the source rocks, leading to higher maturity and a greater accumulation of free oil.

The rigid basement of the Huangling uplift (granite) has an impact on the thermal evolution of OM (Ge et al., 2013). The insulating effect of the rigid basement results in a lower thermal maturity of the source rocks surrounding the Huangling uplift, with an average maturity of about 2% (Xiang et al., 2024). When the thermal maturity exceeds 3.5%, the carbonization of OM leads to a reduction in organic pores (Xiang et al., 2024). Therefore, the insulating effect of the rigid basement allows the thermal evolution of OM to remain in a favorable stage. At the same time, the rigid basement protects the shale pores from damage during tectonic movements (Bao et al., 2018; Zhang et al., 2019b). Tectonic activity also affects the TOC content and the type of OM. When tectonic activity is active, the TOC content increases, and the OM is predominantly Type I. As tectonic activity weakens, the TOC content decreases, and the OM is Type II_1-II_2 (Huang et al., 2015).

5.4. Pore size

Pore size controls the occurrence state and flow of shale oil (Jin et al., 2021; Wang et al., 2019c). Small pores have a larger specific

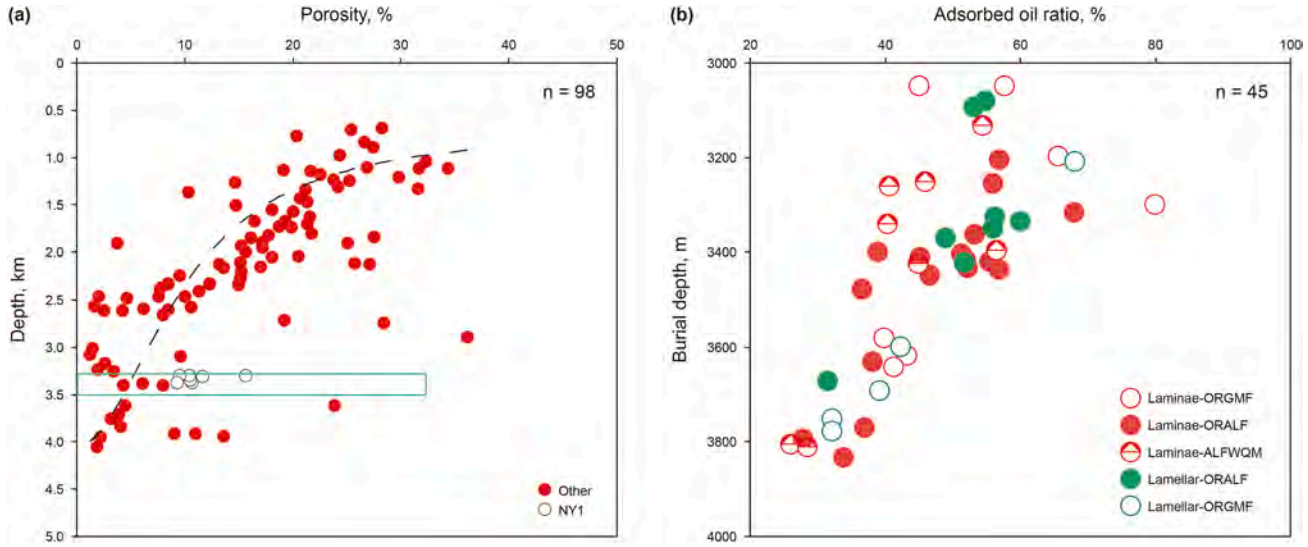

Fig. 17. Variation in porosity and adsorbed oil ratio with depth in the Bohai Bay Basin: **(a)** porosity (Li et al., 2016); **(b)** adsorbed oil ratio (stepwise pyrolysis experiment results modified from Wang et al., 2019c).

surface area and a higher proportion of adsorbed oil, while large pores have a higher content of free oil (Jiang et al., 2020; Wang et al., 2019c). Sun et al. (2024) found that only adsorbed fluids exist in pores of 3 nm. However, in pores of 5 nm and 8 nm, both adsorbed fluid and bulk phase fluid coexist. This can be analyzed from the perspective of fluid forces. As shown in Fig. 18, in smaller pores, fluid molecules experience opposing forces from interactions between fluid near-wall (INW) and fluid far-wall force, which partially cancels out the INW force. Fluid molecules are all adsorbed onto the pore surface, with no bulk phase fluid present. As the pore increases, the alkane molecules move further away from the surface, and the forces exerted by the surface on the fluid weaken. Free oil appears at the center of the pore.

5.5. Reservoir temperature and pressure

Fei et al. (2023) found that an increase in temperature leads to a decrease in the density of n-octane (Fig. 19(a)–(e)). High temperatures intensify the thermodynamic motion of hydrocarbon molecules and enhance their diffusion capacity. This indicates that hydrocarbon molecules are more easily desorbed from kerogen, and the adsorbed layer gradually disappears (Guo et al., 2020; Wang et al., 2023a). In addition, the increase in temperature promotes the absorption of hydrocarbons by kerogen while reducing the number of adsorbed hydrocarbons (Fig. 19(f) and (g)). From molecular simulations, pressure has almost no effect on the adsorption of oil (Pernyeszi et al., 1998; Wu, 2018). However, under high-pressure conditions in the formation, some gas may dissolve in oil, which enhances its mobility but decreases its adsorption capacity (Wang et al., 2019c; Zhang et al., 2019e).

5.6. Shale oil components

Alkanes, aromatics, resins, and asphaltenes are the main components of shale oil (Cao et al., 2021). These components interact and affect the states of each other (Jin et al., 2021; Wang et al., 2019c, 2025c). Typically, light components exist in a free state in the pores, while heavier components are more easily adsorbed onto the walls (Wang et al., 2022c). The adsorption mechanisms of each component differ. Non-polar components and oil molecules with polar functional groups are adsorbed on kerogen through van der Waals forces and Coulombic forces, respectively (Fei et al., 2023). Previous studies have found that kerogen preferentially adsorbs indole, nonanone, methyl octyl sulfide, and molecules containing benzene rings (Sun et al., 2023; Zhang et al., 2023f). Asphaltenes have a stronger affinity for kerogen compared to methane (a light component) (Yang et al., 2020).

5.7. Formation water

Formation water also affects the states of oil in nanopores (Li et al., 2020c). High concentrations of formation water cause water molecules to aggregate in clusters, forming water bridges (Fig. 20(a)) (Xiong et al., 2020; Zhang et al., 2019e). Water bridges can inhibit the adsorption and diffusion of oil (Li et al., 2023c). Water film weakens the interactions between oil and the pore surfaces, facilitating the flow of oil (Zhang et al., 2019d). Kim and Devegowda (2022) found that hydrogen bonds formed between polar components and water cause asphaltenes/resins to exhibit affinity for water. (Fig. 20(b)). In addition, high salinity leads to a reduction in the thickness of the water bridge while causing ion aggregation, which hinders the flow of oil (Xiong and Devegowda, 2022). Saltwater can coat the surface of montmorillonite, leading to the distribution of non-polar components in the nanopores (Zhang et al., 2019d). Na^+ and Cl^- adsorb on the surface of calcite, enhancing the hydrophilicity of calcite and weakening its adsorption of oil molecules (Zhao et al., 2019). Fei et al. (2023) found that under aqueous conditions, water clusters form and adsorb near the N, S, and O-containing groups on the surface of kerogen, which blocks the matrix pores and reduces the content of absorbed oil.

5.8. Shale wettability

The distribution of fluids in oil-bearing shales is strongly influenced by wettability. Variability in wettability due to heterogeneous compositions and pore systems significantly affects the occurrence state of shale oil (e.g., pore-size distribution, storage sites, and free-to-adsorbed ratio) (Li et al., 2023b; Siddiqui et al., 2019; Suekuni et al., 2024; Zhang et al., 2023e). Typically, in water-wet shale formations, water occupies the small pores as a continuous phase, whereas hydrocarbons tend to accumulate in the larger pores (Pan et al., 2020). In contrast, in oil-wet shale formations, oil is often adsorbed onto the pore walls. Due to the complex mineral composition and abundant OM in shale, its wettability exhibits strong heterogeneity. Therefore, the mechanisms of oil-water coexistence within shale pores remain challenging to elucidate.

Gao et al. (2023) used laser scanning confocal microscopy (LSCM) combined with saturated oil experiment to measure the oil content of shale samples with different wettability from the Mahu Sag, Junggar Basin. As shown in Fig. 21, samples 2 and 4 (oil-wet) have the highest oil content, at 37%. In contrast, sample 1 (water-wet) has the lowest oil content, at 26.3%. It can be seen that shale oil has a greater enrichment capacity in oil-wet pore systems. In addition, the heavy oil content in samples 2 and 4 is higher than that of light oil, whereas the water-wet sample 1 shows the

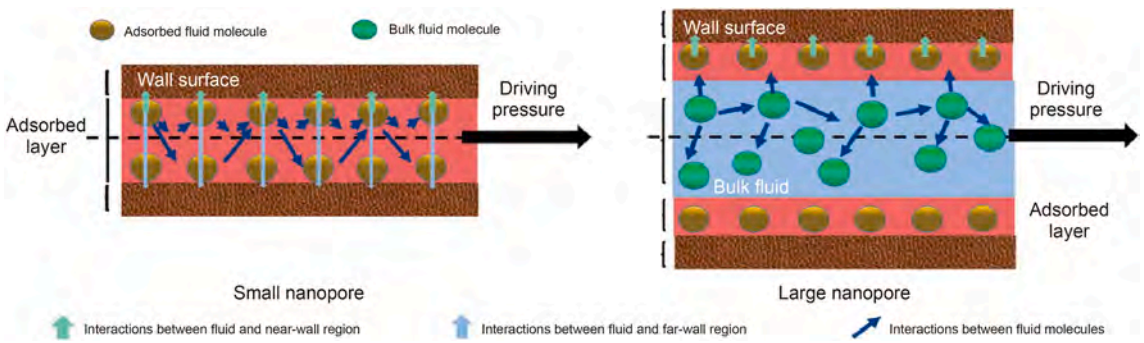

Fig. 18. Fluid distribution and force analysis (Sun et al., 2024).

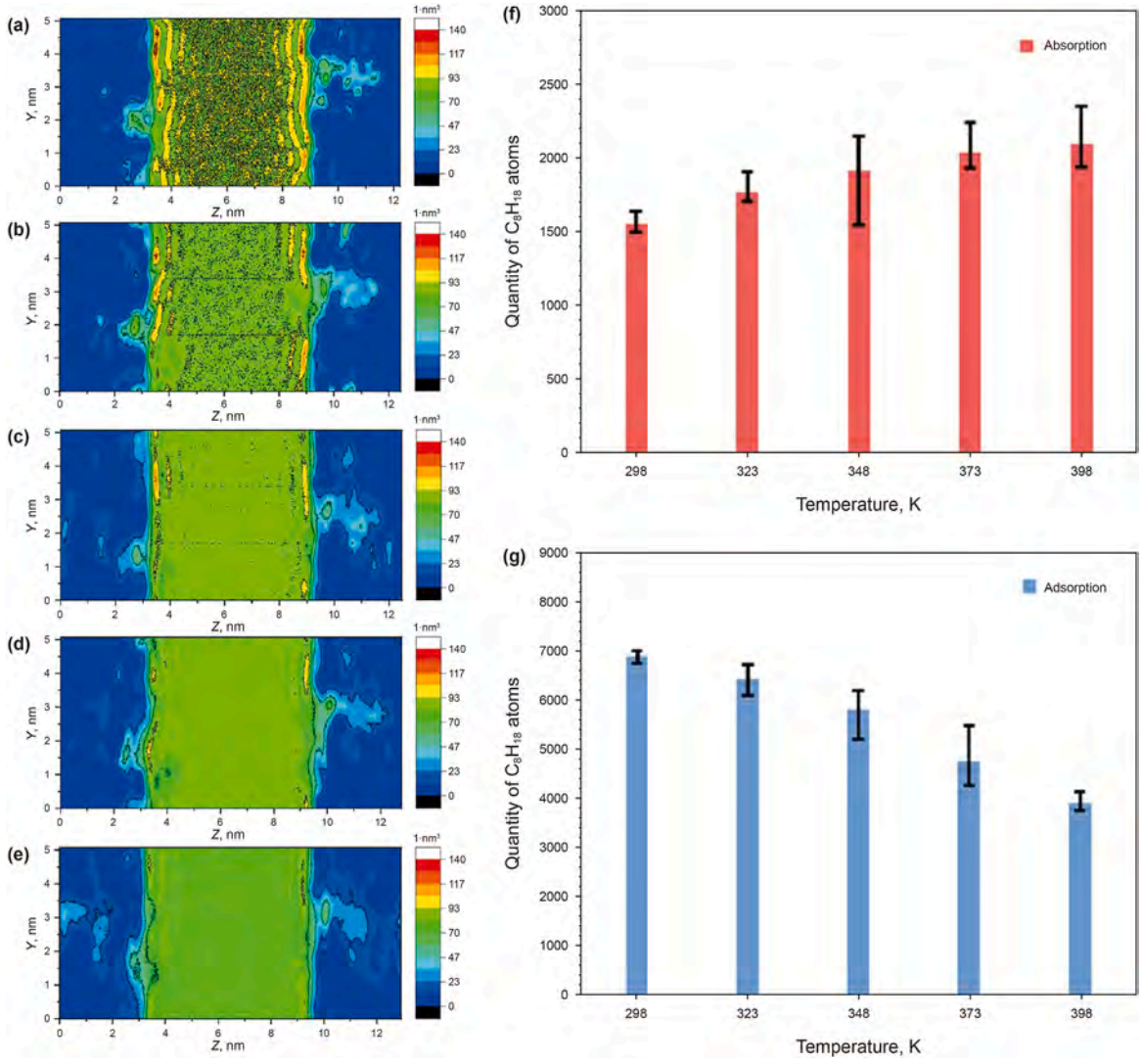

Fig. 19. Number density contour maps and the number of octane atoms adsorbed and absorbed by kerogen: **(a)** 298 K; **(b)** 323 K; **(c)** 348 K; **(d)** 373 K; **(e)** 398 K; **(f)** absorption; **(g)** adsorption (Fei et al., 2023).

opposite trend. This indicates that heavy components interact more strongly with oil-wet inorganic minerals and OM, and are therefore more significantly affected by wettability.

6. The enrichment patterns of shale oil

Due to differences in thermal maturity, burial depth, lithology, OM content, mineral composition, pore structure, diagenesis, formation water content, and laminae types, the occurrence mechanism of shale oil is complex. Currently, the research on the occurrence mechanism of shale oil is conducted by establishing occurrence models (Fan et al., 2023; Gong et al., 2023; He et al., 2025c; Li et al., 2022, 2024a; Liang et al., 2022a; Ma et al., 2024a; Niu et al., 2025; Wang et al., 2019c; Zhang et al., 2023a). This section summarizes the enrichment patterns of shale oil in both pure shale and laminated shale reservoirs. The main storage space of the Permian Lucaogou Formation in eastern Junggar Basin is a heterogeneous pore-throat system composed of InterP and solution pores (Fig. 22(a)–I, II) (He et al., 2025c). Micropores mainly contain adsorbed and irreducible oil. Mesopores contain significant amounts of irreducible oil, moderate amounts of movable oil, and small quantities of adsorbed oil. Macropores primarily accommodate movable oil (Fig. 22(a)–IV). In addition, the presence of abundant OM and carbonate minerals increases the content of free oil and adsorbed oil.

The pore water and retained oil in the marine-continental transitional shale reservoir are stored competitively in non-micropores, significantly affecting the enrichment of retained oil (Fig. 22(b)) (Fan et al., 2023). Pore water is mainly present in the pores <2 nm, 2–10 nm, and >10 nm of inorganic substances in the forms of filling, adsorption and water-clusters, respectively. Retained oil primarily exists in a filling or dissolved state in the micropores and small non-micropores of OM, while in the large non-micropores, it mainly exists in the form of oil-clusters. Li et al. (2022) found that the oil occurrence state in the Bohai Bay Basin varies significantly with depth. The Es^3 member contains a significant amount of kerogen-absorbed oil and a small portion of clay-adsorbed oil, which decreases with increasing depth (Fig. 22(c)). In contrast, the Es^4 member is enriched with a large amount of kerogen-adsorbed oil and free oil. This is attributed to the reduced swelling ability of kerogen and the increased development of organic pores in relatively mature shale.

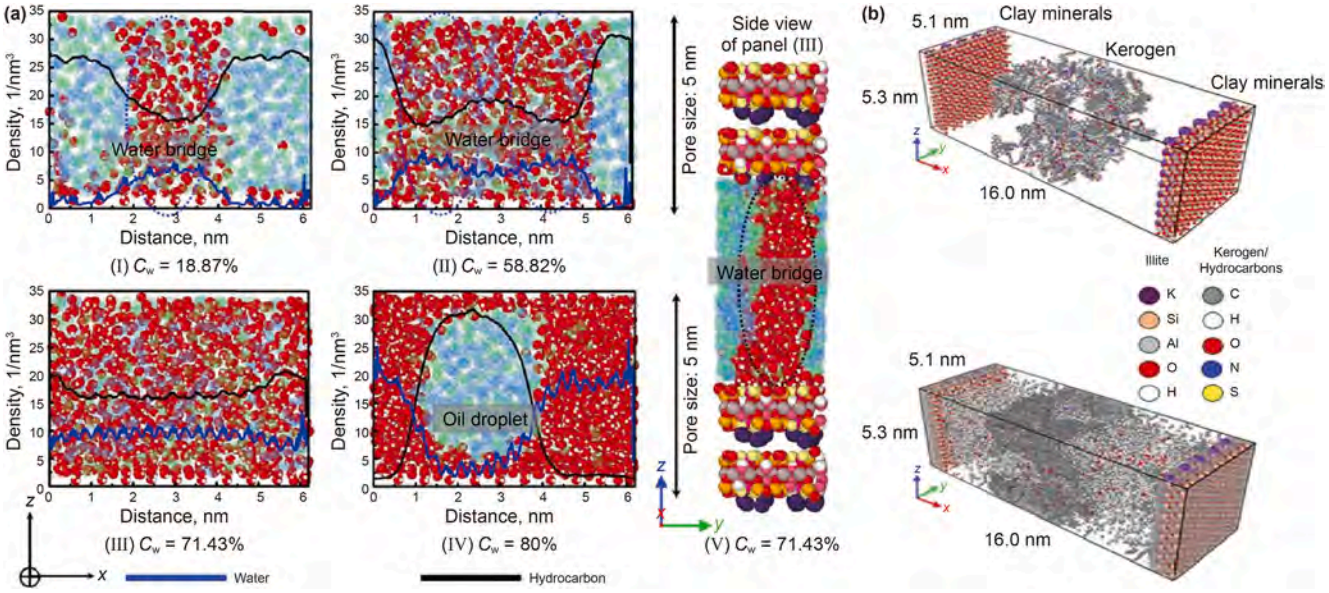

Fig. 20. **(a)** Equilibrium configurations and number density profiles in the 5 nm pore; **(b)** the mixed-wet system and the fluid-saturated mixed-wet system after equilibration. C_w: concentration of water (Kim and Devegowda, 2022; Xiong et al., 2020).

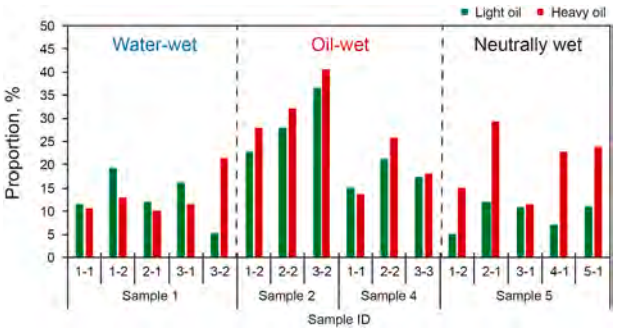

Fig. 21. Shale oil content and wettability in Mahu Sag, Junggar Basin (LSCM combined with saturated oil experiment) (Gao et al., 2023).

Zhang et al. (2023a) established four shale oil occurrence models for different lithologies (Fig. 22(d)). Mudstone has a high OM content, primarily storing adsorbed oil in kerogen and mineral surfaces. The highest amount of adsorbed oil is found in the tuffaceous/silty mudstone. Mudstone exhibits limited development of dissolution pores; therefore, free oil is primarily hosted in the bedding fractures. In contrast, siltstone and carbonate rocks have a higher oil content than mudstone, with free oil hosted in fractures and dissolution pores. In summary, the Lucaogou Formation mudstone has considerable hydrocarbon generation potential and contains abundant adsorbed oil. Siltstone and carbonate rocks, contain significant amounts of free oil and have considerable development potential.

The reservoir types of the Fengcheng Formation in Junggar Basin include sandwich-type shale oil reservoirs (STSOR) and laminated-type shale oil reservoirs (LTSOR) (Fig. 23(a)) (Gong et al., 2023). They are primarily characterized by inorganic intercrystalline pores and dissolved pores, with STSOR also developing microfractures. The free oil content in STSOR is higher than the adsorbed oil content, while in LTSOR, the free oil content is similar to the adsorbed oil content. STSOR contains more free oil, and its storage capacity is significantly better than that of LTSOR. Liang et al. (2022a) found that hydrocarbons in lacustrine shale reservoirs exist in a free state within dissolved pores, recrystallized intercrystalline pores, and various fractures, while they are present in an adsorbed state within organic pores, pyrite intercrystalline pores, and flocculation pores (Fig. 23(b)). When R_o > 0.5%, hydrocarbons are in an adsorbed state within OM. As R_o continues to increase, more hydrocarbons are expelled into adjacent recrystallized intercrystalline pores and structural fractures in a free state. The remaining hydrocarbons are adsorbed onto the surfaces of organic pores and mineral particles (R_o > 1.3%), while also existing in a free state within fractures (Fig. 23(b)).

The differential occurrence of crude oil in the Chang 7_3 submember of laminated shale is characterized by the following features (Fig. 23(c)) (Niu et al., 2025): (1) In the organic-rich laminated shale, hydrocarbon generation-induced fractures and bedding fractures are the main occurrence space for lighter components. (2) In the rigid laminae (sandy laminae, tuffaceous laminae, and mixed laminae), abundant interparticle pores, dissolution pores, bedding fractures, hydrocarbon generation-induced fractures, and microfractures serve as the primary spaces for the migration and accumulation of shale oil. (3) Heavy oil in various types of laminated formations is primarily adsorbed onto OM or the surfaces of dissolution pores. (4) The spatial superposition of different laminae and the combination patterns of multi-scale pores and fractures jointly determine the degree of oil enrichment between laminae. When the maturity of the Kongdian Formation shale reservoir in Bohai Bay Basin is low (Fig. 23(d)–I), the content of adsorbed oil is higher than that of free oil (Ma et al., 2024a). As thermal maturity increases, the amount of light oil increases, while the amount of heavy hydrocarbons decreases. This promotes the migration of oil into the larger pores of the mineral matrix (Fig. 23(d)–II).

7. Occurrence mechanisms guide development practices

A deeper understanding of the occurrence mechanisms of shale oil can guide field development and improve resource utilization efficiency. The guidance provided by the shale oil occurrence mechanisms primarily manifests in resource assessment, drilling site selection, completion design, and development strategies. The

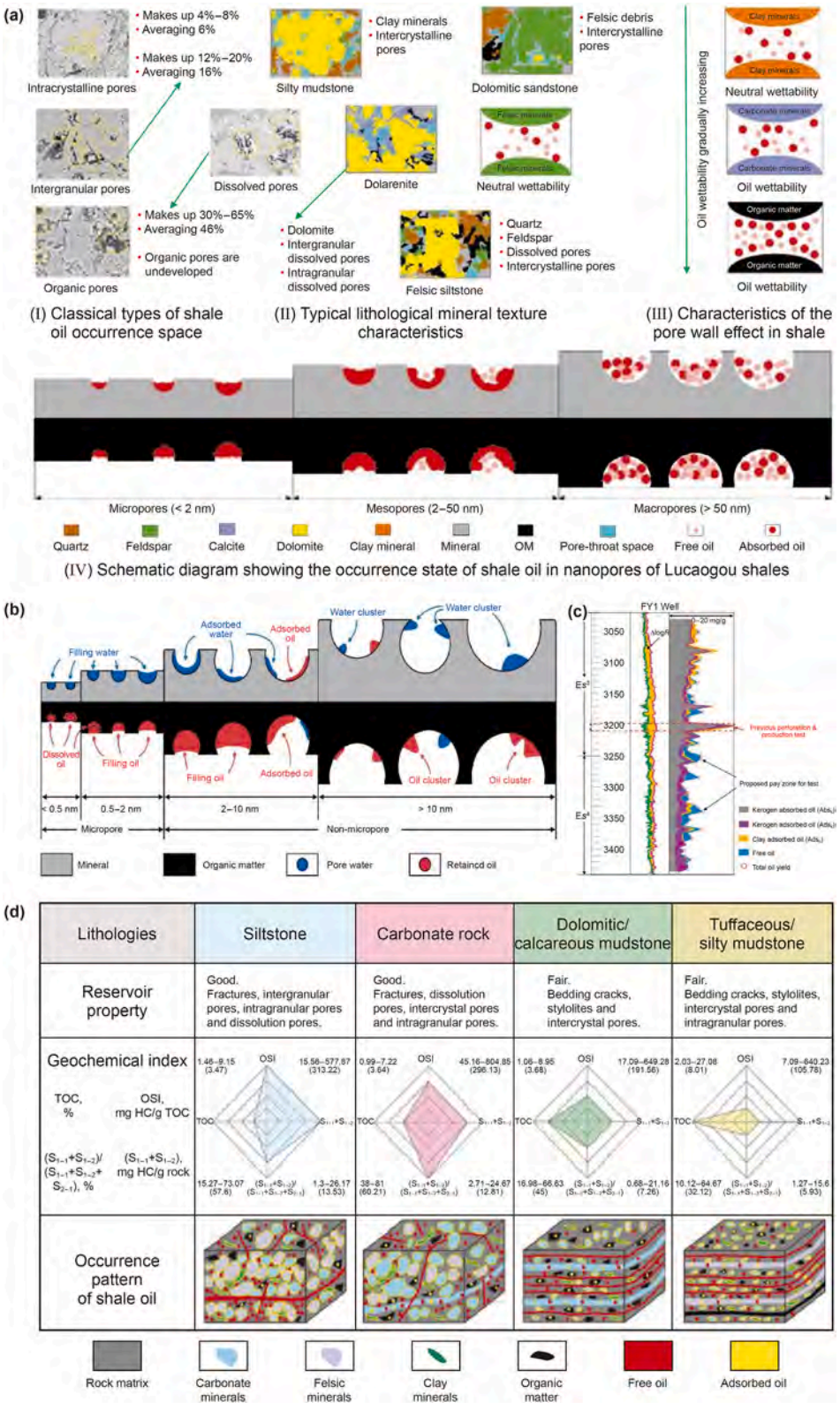

Fig. 22. Shale oil occurrence model in pure shale reservoirs (modified from Fan et al., 2023; He et al., 2025c; Li et al., 2022; Zhang et al., 2023a).

occurrence state of shale oil directly affects its recoverability and resource potential. Niu et al. (2025) used a multi-solvent stepwise continuous extraction method combined with weighing to calculate the free, transitional, and adsorbed shale oil content from over 80 shale cores taken from more than 20 wells in the Chang 7_3 sub-member of the Ordos Basin. In non-laminated shale, shale oil is primarily distributed in microfractures, with a content ranging from 1.084 mg/g to 8.759 mg/g, and the free state accounts

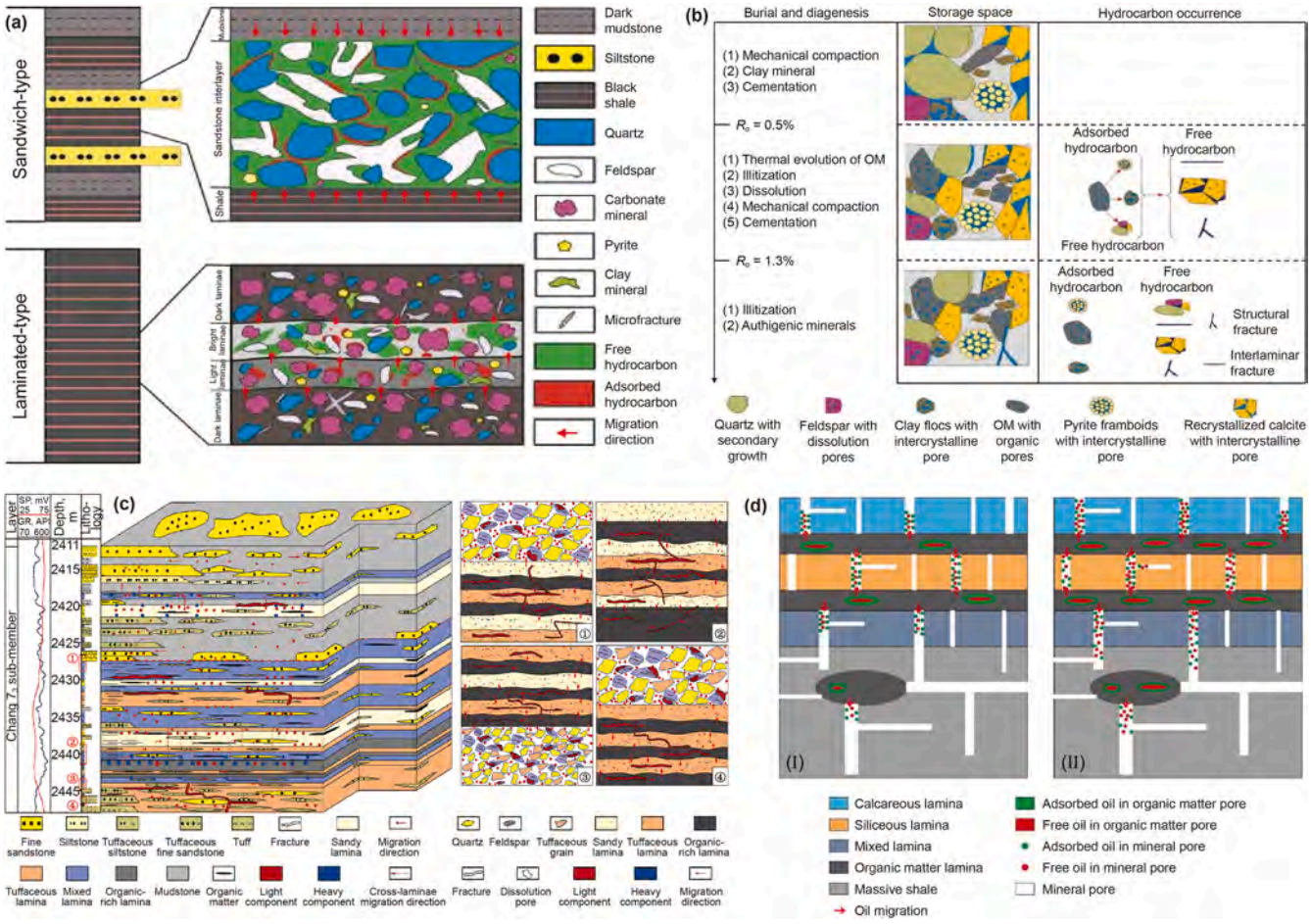

Fig. 23. Shale oil occurrence model in laminated shale reservoirs (modified from (Gong et al., 2023; Liang et al., 2022a; Ma et al., 2024a; Niu et al., 2025)).

for 29%. In sandy laminated shale, shale oil (which is relatively lighter) is predominantly found in dissolution pores, with a content ranging from 2.958 mg/g to 17.654 mg/g, and the free state accounts for 42%. In tuffaceous laminated shale, shale oil is primarily distributed in hydrocarbon generation-induced fractures and bedding fractures, with a content ranging from 5.008 mg/g to 16.211 mg/g, and the free state accounts for 35%. In organic-rich laminated shale, shale oil mainly occurs in the interlayer fractures of clay minerals and a small number of dissolution pores. The shale oil content ranges from 3.527 mg/g to 12.536 mg/g, with the free state accounting for 17%. The micro-nano pore fractures in rigid laminated shales, such as sandy and tuffaceous laminae, provide advantageous storage space for light oil. In contrast, the oil quality in organic-rich laminated shales is relatively heavier.

It is evident that sandy and tuffaceous laminated shales have significant development potential and should be prioritized for development. For the non-laminated shales and tuffaceous laminated shales, where the storage space is primarily fractures, development strategies should focus on enhancing the conductivity of these fractures. Additionally, hydraulic fracturing is also necessary to connect natural fractures and create a complex fracture network. Fu et al. (2023) found that the Qingshankou Formation in the Songliao Basin is characterized by the development of high-density faults. The presence of numerous fractures near faults promotes the accumulation and mobility of shale oil. Therefore, drilling within the fault system should be prioritized, as it can increase shale oil recovery and reduce development costs.

8. Challenges and recommendations

According to our review, existing studies seem to have addressed all issues related to the occurrence mechanisms of shale oil in laminated shale reservoirs. However, there are still some challenges in reality. There are multiple schemes for the classification of shale laminae, and there is no consensus on classification standards and focal points. Currently, there are various methods for studying the states of oil in shale pores, but each individual method has inherent limitations, making precise characterization difficult. The oil content in different types of laminae, especially the content, location, and LLPS in various states within the laminae, remains to be explored. The micro-scale migration of oil between laminae through the kerogen, inorganic pore, and microfractures should not be overlooked. It remains to be investigated whether there exists a micro-migration and enrichment pattern between adjacent shale laminae.

In response to the challenges mentioned above, it is recommended to strengthen theoretical research in the following areas: (1) Establish classification standards for millimeter-scale laminae. The scheme proposed by Hua (2023), which classifies millimeter-scale laminae based on X-ray diffraction fluorescence spectroscopy and key elements, can be referenced. (2) In the quantitative characterization of the states of shale oil, it is important to combine multiple methods, particularly utilizing 2D NMR technology. (3) The distribution and migration of shale oil between different laminae can be studied from both experimental and simulation perspectives. High-resolution techniques such as SEM,

CT, and NMR can be used to accurately characterize the pore structure, connectivity, and oil distribution characteristics of laminae. On the basis of understanding the occurrence of shale oil, further studies on the migration of shale oil between different laminae can be conducted using online NMR core flooding experiments and microfluidic chip experiments. In particular, the combination of two-dimensional NMR T_1–T_2, NMR interface scanning, and NMR imaging techniques represents the most promising approach for studying fluid crossflow between laminae. Finally, based on experimental parameters and findings, a multi-scale, multi-physics numerical simulation model can be established to simulate the mechanisms of fluid migration between laminae.

9. Conclusions

1) The main deposition mechanisms of laminae include biological processes, chemical processes, biogeochemical processes, and mechanical processes. The formation of laminae are influenced by paleoclimate and paleogeography. The classification schemes for shale laminae have not been standardized. In major shale oil-bearing basins in China, such as the Bohai Bay, Songliao, Ordos, and Junggar basins, the classification methods primarily focus on lamina composition.
2) There are many quantitative evaluation methods for the oil content and mobility of shale. At present, two-dimensional NMR combined with other methods has become the main characterization approach. The main pore size range for shale oil occurrence varies, generally from a few nanometers to several hundred nanometers. The lower limit of pore size for free oil and movable oil in laminated shale reservoirs is significantly greater than that in pure shale.
3) The discrepancies in the occurrence space of different laminated shale reservoirs are primarily controlled by mineral composition, sedimentary structure, and diagenesis. In high-pressure subsurface formations, bedding fractures are generally closed or semi-closed. They may become open under specific conditions, including hydrocarbon generation-induced overpressure, abnormally high pore pressure, tectonic activities, magmatic activities, dissolution of fracture-filling materials, and hydraulic fracturing.
4) The main factors influencing shale oil occurrence include organic matter, inorganic minerals, burial depth, pore size, temperature, fluid components, shale wettability and formation water. Pure shales and organic-rich laminated shales mainly accumulate adsorbed oil within organic matter nanopores, exhibiting high hydrocarbon generation potential. In contrast, rigid laminated shales tend to accumulate free oil in intergranular mineral pores and fractures, demonstrating greater development potential.

CRediT authorship contribution statement

Qian Sang: Writing – review & editing, Supervision, Project administration. **Xue-Qiang Guo:** Writing – original draft, Methodology, Investigation, Formal analysis, Conceptualization. **Ming-Zhe Dong:** Writing – review & editing, Funding acquisition.

Conflict of interest

The authors declare that they have no conflict of interest.

Acknowledgements

This work was financially supported by the National Natural Science Foundation of China (Project No. 42090024).

References

Abarghani, A., Gentzis, T., Shokouhimehr, M., et al., 2020. Chemical heterogeneity of organic matter at nanoscale by AFM-Based IR spectroscopy. Fuel 261, 116454. https://doi.org/10.1016/j.fuel.2019.116454.
Abourriche, A., Oumam, M., Mouhssim, A., et al., 2004. New pitches with enhanced graphitization ability obtained from Moroccan oil shales. J. Anal. Appl. Pyrolysis 71 (2), 935–944. https://doi.org/10.1016/j.jaap.2003.12.004.
Alharthy, N., Teklu, T., Kazemi, H., et al., 2018. Enhanced oil recovery in liquid-rich shale reservoirs: Laboratory to field. SPE Reservoir Eval. Eng. 21 (1), 137–159. https://doi.org/10.2118/175034-PA.
Ali, M., Ali, S., Mathur, A., et al., 2020. Organic shale spontaneous imbibition and monitoring with NMR to evaluate in-situ saturations, wettability and molecular sieving. In: Unconventional Resources Technology Conference. https://doi.org/10.15530/urtec-2020-3096.
Amer, M.W., Alhesan, J.S.A., Marshall, M., et al., 2022. Energy efficient method of supercritical extraction of oil from oil shale. Energy Convers. Manag. 252, 115108. https://doi.org/10.1016/j.enconman.2021.115108.
An, C., 2023. Reservoir Characteristics and Oil-bearing Evaluation of Laminated Shale in Chang 7 Member of Ordos Basin. Master Thesis. China University of Petroleum, Beijing (in Chinese).
Anderson, R.Y., Dean, W.E., 1988. Lacustrine varve formation through time. Palaeogeogr. Palaeoclimatol. Palaeoecol. 62 (1–4), 215–235. https://doi.org/10.1016/0031-0182(88)90055-7.
Awramik, S.M., Buchheim, H.P., 2015. Giant stromatolites of the Eocene green river formation (Colorado, USA). Geology 43 (8), 691–694. https://doi.org/10.1130/G36793.1.
Baas, J.H., Best, J.L., Peakall, J., et al., 2009. A phase diagram for turbulent, transitional, and laminar clay suspension flows. J. Sediment. Res. 79 (4), 162–183. https://doi.org/10.2110/jsr.2009.025.
Bagri, A., Grantab, R., Medhekar, N.V., et al., 2010. Stability and formation mechanisms of carbonyl- and hydroxyl-decorated holes in graphene oxide. J. Phys. Chem. C 114, 12053–12061. https://doi.org/10.1021/jp908801c.
Bao, S.J., Zhai, G.Y., Zhou, Z., et al., 2018. The evolution of the Huangling uplift and its control on the accumulation and preservation of shale gas. China Geol. 1 (3), 346–353. https://doi.org/10.31035/cg2018052.
Bao, S.Y., 2018. Effective reservoir spaces of Paleogene shale oil in the Dongying Depression, Bohai Bay Basin. Petroleum Geology & Experiment 40 (4), 479–484 (in Chinese).
Ben Dor, Y., Neugebauer, I., Enzel, Y., et al., 2019. Varves of the Dead Sea sedimentary record. Quat. Sci. Rev. 215, 173–184. https://doi.org/10.1016/j.quascirev.2019.04.011.
Birdwell, J.E., Washburn, K.E., 2015. Multivariate analysis relating oil shale geochemical properties to NMR relaxometry. Energy Fuels 29 (4), 2234–2243. https://doi.org/10.1021/ef502828k.
Bloembergen, N., Purcell, E.M., Pound, R.V., 1948. Relaxation effects in nuclear magnetic resonance absorption. Phys. Rev. 73 (7), 679–712. https://doi.org/10.1103/PhysRev.73.679.
Boehrer, B., Schultze, M., 2008. Stratification of lakes. Rev. Geophys. 46 (2). https://doi.org/10.1029/2006RG000210.
Bowker, K.A., 2007. Shale gas production, Fort Worth Basin: Issues and discussion. AAPG (Am. Assoc. Pet. Geol.) Bull. 91 (4), 523–533. https://doi.org/10.1306/06190606018.
Cao, X.N., Jiang, Z.X., Zhu, D.Y., et al., 2019. Lithofacies types and reservoir characteristics of continental shales of Ziliujing Formation in northeastern Sichuan Basin. Nat. Gas Geosci. 30 (12), 1782–1793 (in Chinese).
Cao, Z., Jiang, H., Zeng, J.H., et al., 2021. Nanoscale liquid hydrocarbon adsorption on clay minerals: A molecular dynamics simulation of shale oils. Chem. Eng. J. 420, 127578. https://doi.org/10.1016/j.cej.2020.127578.
Chen, F.W., Zhao, H.Q., Lu, S.F., et al., 2019a. The effects of composition, laminar structure and burial depth on connected pore characteristics in a shale oil reservoir, the Raoyang Sag of the Bohai Bay Basin, China. Mar. Petrol. Geol. 101, 290–302. https://doi.org/10.1016/j.marpetgeo.2018.12.012.
Chen, F.W., Zhao, H.Q., Wang, S.P., et al., 2019b. Evaluation of movable shale oil reserves in the Es^{1L} of the Raoyang sag, Jizhong Depression. Oil Gas Geol. 40 (3), 593–601 (in Chinese).
Chen, G.H., Lu, S.F., Zhang, J.F., et al., 2018a. A method for determining oil-bearing pore size distribution in shales: a case study from the Damintun Sag, China. J. Petrol. Sci. Eng. 166, 673–678. https://doi.org/10.1016/j.petrol.2018.03.082.
Chen, H.A., Fu, L.Q., 2025. Impact of pore structure on imbibition characteristics in Qingshankou Formation shale oil reservoirs, Songliao Basin. Special Oil Gas Reservoirs 32 (3), 94–103 (in Chinese).
Chen, J.J., 2024. Study on the Characteristics of Shale Oil Reservoirs in the Second Member of Kongdian Formation in Cangdong Sag. Master thesis. China University of Petroleum (Beijing). Beijing (in Chinese).
Chen, J.Q., Pang, X.Q., Pang, H., et al., 2018b. Hydrocarbon evaporative loss evaluation of lacustrine shale oil based on mass balance method: Permian Lucaogou

Formation in Jimusaer Depression, Junggar Basin. Mar. Petrol. Geol. 91, 422–431. https://doi.org/10.1016/j.marpetgeo.2018.01.021.
Chen, S.J., Li, P., Zhang, J.C., et al., 2021. Measurement of shale wettability using calorimetry: Experimental results and model. Energy Fuels 35 (21), 17446–17462. https://doi.org/10.1021/acs.energyfuels.1c02289.
Chen, X.H., Zhang, M., 2017. Composition characteristics of the saturated hydrocarbon of the sequential extracts from the oil-bearing shales with different polarity reagents. Pet. Geol. Oilfield Dev. Daqing 36 (3), 168–174 (in Chinese).
Chen, Y.H., Liu, D.D., Fan, Q.Q., et al., 2023. Oil mobility evaluation of fine-grained sedimentary rocks with high heterogeneity: A case study of the Lucaogou Formation in the Jimusar Sag, Junggar Basin, NW China. Energy Fuels 37 (11), 7679–7695. https://doi.org/10.1021/acs.energyfuels.3c00438.
Chen, Y.Y., Furmann, A., Mastalerz, M., et al., 2014a. Quantitative analysis of shales by KBr-FTIR and micro-FTIR. Fuel 116, 538–549. https://doi.org/10.1016/j.fuel.2013.08.052.
Chen, Y.Y., Mastalerz, M., Schimmelmann, A., 2014b. Heterogeneity of shale documented by micro-FTIR and image analysis. J. Microsc. 256 (3), 177–189. https://doi.org/10.1111/jmi.12169.
Chen, Z.H., Jiang, C.Q., 2020. An integrated mass balance approach for assessing hydrocarbon resources in a liquid-rich shale resource play: An example from Upper Devonian Duvernay Formation, western Canada sedimentary basin. J. Earth Sci. 31 (6), 1259–1272. https://doi.org/10.1007/s12583-020-1088-1.
Cobbold, P.R., Zanella, A., Rodrigues, N., et al., 2013. Bedding-parallel fibrous veins (beef and cone-in-cone): Worldwide occurrence and possible significance in terms of fluid overpressure, hydrocarbon generation and mineralization. Mar. Petrol. Geol. 43, 1–20. https://doi.org/10.1016/j.marpetgeo.2013.01.010.
Cooles, G.P., Mackenzie, A.S., Quigley, T.M., 1986. Calculation of petroleum masses generated and expelled from source rocks. Org. Geochem. 10 (1–3), 235–245. https://doi.org/10.1016/0146-6380(86)90026-4.
Craddock, P.R., Le Doan, T.V., Bake, K., et al., 2015. Evolution of kerogen and bitumen during thermal maturation via semi-open pyrolysis investigated by infrared spectroscopy. Energy Fuels 29 (4), 2197–2210. https://doi.org/10.1021/ef5027532.
Curtis, C.D., 1978. Possible links between sandstone diagenesis and depth-related geochemical reactions occurring in enclosing mudstones. J. Geol. Soc. 135 (1), 107–117. https://doi.org/10.1144/gsjgs.135.1.0107.
Curtis, J.B., 2002. Fractured shale-gas systems. AAPG (Am. Assoc. Pet. Geol.) Bull. 86 (11), 1921–1938. https://doi.org/10.1306/61EEDDBE-173E-11D7-8645000102C1865D.
Dang, W., Zhang, J.C., Nie, H.K., et al., 2022. Microscopic occurrence characteristics of shale oil and their main controlling factors: A case study of the 3rd submember continentalshale of Member 7 of Yanchang Formation in Yan'an area, Ordos Basin. Acta Pet. Sin. 43 (4), 507–523 (in Chinese).
Davudov, D., Moghanloo, R.G., Zhang, Y.X., 2020. Interplay between pore connectivity and permeability in shale sample. Int. J. Coal Geol. 220, 103427. https://doi.org/10.1016/j.coal.2020.103427.
Dazzi, A., Glotin, F., Carminati, R., 2010. Theory of infrared nanospectroscopy by photothermal induced resonance. Journal of Applied Physics 107 (12), 124519. https://doi.org/10.1063/1.3429214.
Dazzi, A., Prater, C.B., 2016. AFM-IR: Technology and applications in nanoscale infrared spectroscopy and chemical imaging. Chem. Rev. 117 (7), 5146–5173. https://doi.org/10.1021/acs.chemrev.6b00448.
Dendisová, M., Jeništová, A., Parchaňská-Kokaislová, A., et al., 2018. The use of infrared spectroscopic techniques to characterize nanomaterials and nanostructures: A review. Anal. Chim. Acta 1031, 1–14. https://doi.org/10.1016/j.aca.2018.05.046.
Deng, Y., Chen, S.Y., Pu, X.G., et al., 2020. Characteristics and controlling factors of shale oil reservoir spaces in the Bohai Bay Basin. Acta Geol. Sin. Engl. Ed. 94 (2), 253–268. https://doi.org/10.1111/1755-6724.14286.
Dong, M.Z., Li, Y.J., Sang, Q., et al., 2019. Reservoir conditions and mechanism of shale oil flow. Oil Gas Geol. 40 (3), 636–644 (in Chinese).
Dou, W., Sun, P.C., Ouyang, Z.Y., et al., 2023. Influence of lamination development on shale reservoirs: A case study of shales from the upper Es4 and lower Es3 sub-member in the Dongying Sag of the Bohai Bay Basin. Journal of Northeast Petroleum University 47 (4), 14–28 (in Chinese).
Falk, K., Pellenq, R., Ulm, F.J., et al., 2015. Effect of chain length and pore accessibility on alkane adsorption in kerogen. Energy Fuels 29 (12), 7889–7896. https://doi.org/10.1021/acs.energyfuels.5b02015.
Fan, Q.Z., Cheng, P., Tian, H., et al., 2023. Distribution and occurrence of pore water and retained oil in nanopores of marine–terrestrial transitional shales during oil generation and expulsion: Implications from a thermal simulation experiment on shale plug samples. Mar. Petrol. Geol. 150, 106125. https://doi.org/10.1016/j.marpetgeo.2023.106125.
Fan, Z.Q., Song, X., Wang, D.Y., et al., 2025. Poroelastic solutions of a semipermeable borehole under nonhydrostatic in situ stresses within transversely isotropic media. Int. J. GeoMech. 25 (2), 04024342. https://doi.org/10.1061/IJGNAI.GMENG-10261.
Fang, L.Y., Hua, Y., Meng, Z.Z., et al., 2019. Molecular dynamics simulations on the orientation of n-alkanes with different lengths on graphene. Surf. Sci. 690, 121468. https://doi.org/10.1016/j.susc.2019.121468.
Fang, Y.J., Li, Z.X., Yang, E., et al., 2024. Molecular dynamics simulation study on the occurrence of shale oil in hybrid nanopores. Molecules 29 (2), 312. https://doi.org/10.3390/molecules29020312.
Fei, J.S., Wang, M., Li, J.B., et al., 2023. Molecular dynamics simulation of adsorption and absorption behavior of shale oil in realistic kerogen slits. Energy Fuels 37 (5), 3654–3671. https://doi.org/10.1021/acs.energyfuels.2c03842.
Fleury, M., Romero-Sarmiento, M., 2016. Characterization of shales using T_1–T_2 NMR maps. J. Petrol. Sci. Eng. 137, 55–62. https://doi.org/10.1016/j.petrol.2015.11.006.
Frogner, P., Gíslason, S.R., Óskarsson, N., 2001. Fertilizing potential of volcanic ash in ocean surface water. Geology 29 (6), 487–490. https://doi.org/10.1130/0091-7613(2001)029<0487:FPOVAI>2.0.CO;2.
Fu, E., He, W.D., 2024. The development and utilization of shale oil and gas resources in China and economic analysis of energy security under the background of global energy crisis. J. Pet. Explor. Prod. Technol. 14 (8–9), 2315–2341. https://doi.org/10.1007/s13202-024-01818-3.
Fu, J.H., Li, S.X., Hou, Y.T., et al., 2020. Breakthrough of risk exploration of Class II shale oil in Chang 7 member of Yanchang Formation in the Ordos Basin and its significance. China Petroleum Exploration 25 (1), 78–92 (in Chinese).
Fu, X.F., Su, X.C., Gong, L., et al., 2023. Control of faults and fractures on shale oil enrichment. Geoenergy Sci. Eng. 228, 212080. https://doi.org/10.1016/j.geoen.2023.212080.
Fu, X.L., Meng, Q.A., Zheng, Q., et al., 2022. Cyclicity of organic matter abundance and lithofacies paleogeography of Gulong shale in songliao Basin. Pet. Geol. Oilfield Dev. Daqing 41 (3), 38–52 (in Chinese).
Ganz, H., Kalkreuth, W., 1987. Application of infrared spectroscopy to the classification of kerogent ypes and the evaluation of source rock and oil shale potentials. Fuel 66 (5), 708–711.
Gao, F.L., 2019. Reservoir Characteristics of Continental Shale and its Influences on Gas-bearing Properties. Ph.D. Thesis. China University of Petroleum (Beijing), Beijing (in Chinese).
Gao, F.L., Song, Y., Jiang, Z.X., et al., 2017. Influence of clay minerals on shale storage space and adsorptive capacity. Special Oil Gas Reservoirs 24 (3), 1–8 (in Chinese).
Gao, H.C., Zheng, R.C., Xiao, Y.K., et al., 2015. Origin of the salt rock of Paleogene Shahejie Formation in Dongpu Sag, Bohai Bay Basin: Evidences from sedimentology and geochemistry. Acta Pet. Sin. 36 (1), 19–32 (in Chinese).
Gao, R., Bai, D., Yu, B., et al., 2024. Ground fracturing of multi-strata for strong ground pressure control in extra-thick coal seams with hard roofs: Numerical simulation and case study. Eng. Fract. Mech. 303, 110129. https://doi.org/10.1016/j.engfracmech.2024.110129.
Gao, R., Kuang, T.J., Meng, X.B., et al., 2020. Effects of ground fracturing with horizontal fracture plane on rock breakage characteristics and mine pressure control. Rock Mech. Rock Eng. 54 (6), 3229–3243. https://doi.org/10.1007/s00603-020-02294-x.
Gao, Z.Y., Duan, L.F., Jiang, Z.X., et al., 2023. Using laser scanning confocal microscopy combined with saturated oil experiment to investigate the pseudo in-situ occurrence mechanism of light and heavy components of shale oil in sub-micron scale. J. Petrol. Sci. Eng. 220, 111234. https://doi.org/10.1016/j.petrol.2022.111234.
Ge, X., Shen, C.B., Yang, Z., et al., 2013. Low-temperature thermochronology constraints on the Mesozoic–Cenozoic exhumation of the Huangling massif in the Middle Yangtze Block, central China. J. Earth Sci. 24 (4), 541–552. https://doi.org/10.1007/s12583-013-0348-8.
Gentzis, T., Carvajal-Ortiz, H., Harry Xie, Z., et al., 2021. An integrated geochemical, spectroscopic, and petrographic approach to examining the producibility of hydrocarbons from liquids-rich unconventional formations. Fuel 298, 120357. https://doi.org/10.1016/j.fuel.2021.120357.
Gong, D.Y., Bai, L.X., Gao, Z.Y., et al., 2023. Occurrence mechanisms of laminated-type and sandwich-type shale oil in the Fengcheng Formation of Mahu Sag, Junggar Basin. Energy Fuels 37 (18), 13960–13975. https://doi.org/10.1021/acs.energyfuels.3c02625.
Gong, H.J., Jiang, Z.X., Zhu, F., et al., 2024. Quantitative characterization and control factors of shale oil occurrencestate in the shale of member 2 of funing Formation in the Gaoyou Sag, Subei Basin. Journal of Northeast Petroleum University 48 (2), 59–71 (in Chinese).
Gong, H.J., Zhu, C.F., Zhang, Y.L., et al., 2020. Experimental evaluation on the oil saturation and movability in the organic and inorganic matter of shale. Energy Fuels 34 (7), 8063–8073. https://doi.org/10.1021/acs.energyfuels.0c00831.
Goral, J., Walton, I., Andrew, M., et al., 2019. Pore system characterization of organic-rich shales using nanoscale-resolution 3D imaging. Fuel 258, 116049. https://doi.org/10.1016/j.fuel.2019.116049.
Gou, Q.Y., Xu, S., Hao, F., et al., 2019. Full-scale pores and micro-fractures characterization using FE-SEM, gas adsorption, nano-CT and micro-CT: A case study of the Silurian Longmaxi Formation shale in the Fuling area, Sichuan Basin, China. Fuel 253, 167–179. https://doi.org/10.1016/j.fuel.2019.04.116.
Gou, Q.Y., Xu, S., Hao, F., et al., 2023. Petrography and mineralogy control the nm–μm-scale pore structure of saline lacustrine carbonate-rich shales from the Jianghan Basin, China. Mar. Petrol. Geol. 155, 106399. https://doi.org/10.1016/j.marpetgeo.2023.106399.
Greene, E.F., Tauch, S., Webb, E., et al., 2004. Application of diffuse reflectance infrared Fourier transform spectroscopy (DRIFTS) for the identification of potential diagenesis and crystallinity changes in teeth. Microchem. J. 76 (1–2), 141–149. https://doi.org/10.1016/j.microc.2003.11.006.
Guan, M., Liu, X.P., Jin, Z.J., et al., 2022. Quantitative characterization of various oil contents and spatial distribution in lacustrine shales: Insight from petroleum

compositional characteristics derived from programed pyrolysis. Mar. Petrol. Geol. 138, 105522. https://doi.org/10.1016/j.marpetgeo.2021.105522.
Guo, F.G., Wang, S., Feng, Q.H., et al., 2020. Adsorption and absorption of supercritical methane within shale kerogen slit. J. Mol. Liq. 320, 114364. https://doi.org/10.1016/j.molliq.2020.114364.
Guo, P.C., Cui, X.D., Dong, X.D., et al., 2024. The characterization of occurrence state and pore size lower limit of shale oil in Jiufotang Formation of Jiaolige Subsag, Ludong Sag. Journal of Northeast Petroleum University 48 (3), 14–22 (in Chinese).
Guo, R.L., Liang, X.W., Zhou, X.P., et al., 2025. Effect of extractable organic matter on nanopore structure and heterogeneity in Triassic Yanchang lacustrine shale of the Ordos basin, China. J. Asian Earth Sci. 287, 106577. https://doi.org/10.1016/j.jseaes.2025.106577.
Guo, X.B., Zhou, L.F., Pan, Y.S., et al., 2023. Pore structure and oil-bearing property of laminated and massive shale of Lucaogou Formation in Malang Sag, Santanghu Basin. Geol. J. 59 (3), 980–999. https://doi.org/10.1002/gj.4904.
Hackley, P.C., Walters, C.C., Kelemen, S.R., et al., 2017. Organic petrology and microspectroscopy of Tasmanites microfossils: Applications to kerogen transformations in the early oil window. Org. Geochem. 114, 23–44. https://doi.org/10.1016/j.orggeochem.2017.09.002.
Hage, S., Cartigny, M.J.B., Sumner, E.J., et al., 2019. Direct monitoring reveals initiation of turbidity currents from extremely dilute river plumes. Geophys. Res. Lett. 46 (20), 11310–11320. https://doi.org/10.1029/2019GL084526.
Hampton, M., 1975. Competence of fine-grained debris flows. J. Sediment. Res. 45 (4), 834–844. https://doi.org/10.1306/212F6E5B-2B24-11D7-8648000102C1865D.
Handwerger, D.A., Suarez-Rivera, R., Vaughn, K.I., et al., 2011. Improved petrophysical core measurements on tight shale reservoirs using retort and crushed samples. In: SPE Annual Technical Conference and Exhibition. https://doi.org/10.2118/147456-MS.
Hay, B.J., Honjo, S., Kempe, S., et al., 1990. Interannual variability in particle flux in the southwestern Black sea. Deep-Sea Res. 37 (6), 911–928. https://doi.org/10.1016/0198-0149(90)90103-3.
He, J.Y., Leng, J.Y., He, W.J., et al., 2025a. Quality and oil-bearing properties of argillaceous hydrocarbon source rocks across different lithofacies of Permian Lucaogou Formation in Jimsar Sag, Junggar Basin: a case study of well J10025. Petroleum Geology & Experiment 47 (3), 606–620 (in Chinese).
He, S., Qin, Q.R., Qin, Z.J., et al., 2022. Natural fracture development characteristics and their relationship with gas contents — a case study of Wufeng–Longmaxi Formation in Luzhou area, southern Sichuan Basin, China. ACS Omega 7 (38), 34066–34079. https://doi.org/10.1021/acsomega.2c03318.
He, W.J., Li, Z.M., Li, C.R., et al., 2025b. Hydrocarbon generation, expulsion, and retention characteristics of the Permian Fengcheng shale and Lucaogou shale in the Junggar Basin: implications for the exploration of lacustrine shale oil. Front. Earth Sci. 12. https://doi.org/10.3389/feart.2024.1525983.
He, X.B., Luo, Q., Li, X., et al., 2025c. Microscopic occurrence mechanism of shale oil in saline lacustrine shale: insights from NMR and Micro-CT combined with saturated oil, centrifuged and solvent extraction experiments. Nat. Resour. Res. 34, 2089–2116. https://doi.org/10.1007/s11053-025-10486-x.
Heard, T.G., 2008. Ichnology and Sedimentology of Deep-marine Clastic Systems, Middle Eocene, Ainsa-Jaca Basin, Spanish Pyrenees. Ph.D. thesis. University of London, University College, London (United Kingdom).
Henry, D.G., Jarvis, I., Gillmore, G., et al., 2019. Raman spectroscopy as a tool to determine the thermal maturity of organic matter: Application to sedimentary, metamorphic and structural geology. Earth Sci. Rev. 198, 102936. https://doi.org/10.1016/j.earscirev.2019.102936.
Heydari, E., Wade, W.J., 2002. Massive recrystallization of low-Mg calcite at high temperatures in hydrocarbon source rocks: Implications for organic acids as factors in diagenesis. AAPG (Am. Assoc. Pet. Geol.) Bull. 86, 1285–1303. https://doi.org/10.1306/61EEDC7E-173E-11D7-8645000102C1865D.
Hou, L.H., Luo, X., Lin, S.H., et al., 2021. Quantitative measurement of retained oil in organic-rich shale — a case study on the Chang 7 Member in the Ordos Basin, China. Front. Earth Sci. 9, 662586. https://doi.org/10.3389/feart.2021.662586.
Hu, T., Liu, Y., Jiang, F.J., et al., 2024. A novel method for quantifying hydrocarbon micromigration in heterogeneous shale and the controlling mechanism. Energy 288, 129712. https://doi.org/10.1016/j.energy.2023.129712.
Hu, T., Pang, X.Q., Jiang, F.J., et al., 2021. Movable oil content evaluation of lacustrine organic-rich shales: Methods and a novel quantitative evaluation model. Earth Sci. Rev. 214, 103545. https://doi.org/10.1016/j.earscirev.2021.103545.
Hua, G.L., 2023. Laminate Structure Development and Continental Shale Oil Intrasource Accumulation Process: Case Studies of Member 1 of the Qingshankou Formation in the Songliao Basin and Member 7 of the Yanchang Formation in the Ordos Basin. Ph.D. thesis. China University of Geosciences (Beijing), Beijing. https://doi.org/10.27493/d.cnki.gzdzy.2023.000193 (in Chinese).
Hua, G.L., Wu, S.T., Qiu, Z., et al., 2021. Lamination texture and its effect on reservoir properties: A case study of Longmaxi Shale, Sichuan Basin. Acta Sedimentol. Sin. 39 (2), 281–296. https://doi.org/10.14027/j.issn.1000-0550.2020.110 (in Chinese).
Hua, G.L., Wu, S.T., Zhang, J.Y., et al., 2022a. Laminar structure and reservoir quality of shales with high clay mineral content in the Qingshankou Formation, Songliao Basin. Energies 15 (17), 6132. https://doi.org/10.3390/en15176132.
Hua, G.L., Wu, S.T., Zhang, J.Y., et al., 2022b. Laminar structure differences and heterogeneities in reservoirs in continental organic-rich shales: the Cretaceous Nenjiang Formation in the Songliao Basin. Interpretation 10 (3), SD89–SD106. https://doi.org/10.1190/int-2021-0156.1.
Huang, C.Y., Zhang, J.C., Wang, H., et al., 2015. Lacustrine shale deposition and variable tectonic accommodation in the rift basins of the Bohai Bay Basin in eastern China. J. Earth Sci. 26 (5), 700–711. https://doi.org/10.1007/s12583-015-0602-3.
Irwin, M.L., 1965. General theory of epeiric clear water sedimentation. AAPG (Am. Assoc. Pet. Geol.) Bull. 49 (4), 445–459. https://doi.org/10.1306/A6633632-16C0-11D7-8645000102C1865D.
Ismat, Z., 2012. Evolution of fracture porosity and permeability during folding by cataclastic flow: Implications for syntectonic fluid flow. Rocky Mt. Geol. 47 (2), 133–155. https://doi.org/10.2113/gsrocky.47.2.133.
Jarvie, D.M., 2012. Shale resource systems for oil and gas: Part 2 — Shale-oil resource systems. In: Breyer, J.A. (Ed.), Shale Reservoirs — Giant Resources for the 21st Century, vol. 97. AAPG Memoir. https://doi.org/10.1306/13321447M973489.
Jarzembski, A., Shaskey, C., Park, K., 2018. Review: Tip-based vibrational spectroscopy for nanoscale analysis of emerging energy materials. Front. Energy 12 (1), 43–71. https://doi.org/10.1007/s11708-018-0524-8.
Jia, C.Z., Zheng, M., Zhang, Y.F., 2016. Some key issues on the unconventional petroleum systems. Petroleum Research 1 (2), 113–122. https://doi.org/10.1016/S2096-2495(17)30036-4.
Jiang, C.F., Wang, X.Z., Zhang, L.X., et al., 2013. Geological characteristics of shale and exploration potential of continental shale gas in 7th member of Yanchang Formation, southeast Ordos Basin. Geology in China 40 (6), 1880–1888 (in Chinese).
Jiang, C.Q., Chen, Z.H., Mort, A., et al., 2016a. Hydrocarbon evaporative loss from shale core samples as revealed by Rock-Eval and thermal desorption-gas chromatography analysis: its geochemical and geological implications. Mar. Petrol. Geol. 70, 294–303. https://doi.org/10.1016/j.marpetgeo.2015.11.021.
Jiang, H., 2010. Dynamical mechanism and depositional responses of turbidity current sedimentation. Oil Gas Geol. 31 (4), 428–435 (in Chinese).
Jiang, Q.G., Li, M.W., Qian, M.H., et al., 2016b. Quantitative characterization of shale oil in different occurrence states and its application. Petroleum Geology & Experiment 38 (6), 842–849 (in Chinese).
Jiang, Z.X., Li, T.W., Gong, H.J., et al., 2020. Characteristics of low-mature shale reservoirs in Zhanhua sag and their influence on the mobility of shale oil. Acta Pet. Sin. 41 (12), 1587–1600 (in Chinese).
Jiang, Z.X., Wang, Y.Z., Wang, L., et al., 2022. Review on provenance, transport-sedimentation dynamics and multi-source hydrocarbon sweet spots of continental fine-grained sedimentary rocks. Oil Gas Geol. 43 (5), 1039–1048 (in Chinese).
Jiang, Z.X., Zhang, J.G., Kong, X.X., et al., 2023. Research progress and development direction of continental shale oil and gas deposition and reservoirs in China. Acta Pet. Sin. 44 (1), 45–71 (in Chinese).
Jin, Z.J., Wang, G.P., Liu, G.X., et al., 2021. Research progress and key scientific issues of continental shale oil in China. Acta Pet. Sin. 42 (7), 821–835 (in Chinese).
Jiu, K., Ding, W.L., Huang, W.H., et al., 2013. Fractures of lacustrine shale reservoirs, the Zhanhua Depression in the Bohai Bay Basin, eastern China. Mar. Petrol. Geol. 48, 113–123. https://doi.org/10.1016/j.marpetgeo.2013.08.009.
Khatibi, S., Ostadhassan, M., Xie, Z.H., et al., 2019. NMR relaxometry a new approach to detect geochemical properties of organic matter in tight shales. Fuel 235, 167–177. https://doi.org/10.1016/j.fuel.2018.07.100.
Kim, C., Devegowda, D., 2022. Molecular dynamics study of fluid-fluid and solid-fluid interactions in mixed-wet shale pores. Fuel 319, 123587. https://doi.org/10.1016/j.fuel.2022.123587.
Klaver, J., Desbois, G., Littke, R., et al., 2015. BIB-SEM characterization of pore space morphology and distribution in postmature to overmature samples from the Haynesville and Bossier Shales. Mar. Petrol. Geol. 59, 451–466. https://doi.org/10.1016/j.marpetgeo.2014.09.020.
Kong, X.X., Jiang, Z.X., Han, C., et al., 2016. Laminations characteristics and reservoir significance of fine-grained carbonate in the lower 3rd member of Shahejie Formation of Shulu sag. Petroleum Geology and Recovery Efficiency 23 (4), 19–26. https://doi.org/10.13673/j.cnki.cn37-1359/te.2016.04.003.
Kong, X.X., Jiang, Z.X., Han, C., et al., 2017. Genesis and implications of the composition and sedimentary structure of fine-grained carbonate rocks in the Shulu sag. J. Earth Sci. 28 (6), 1047–1063. https://doi.org/10.1007/s12583-016-0927-x.
Kong, X.Y., 2023. Shale Pore Structure and its Control on Shale Oil Occurrence in Jurassic Da'Anzhai Member, Central Sichuan Basin. Ph.D. thesis. China University of Petroleum (Beijing), Beijing. https://doi.org/10.27643/d.cnki.gsybu.2023.000128 (in Chinese).
Korb, J.P., Nicot, B., Louis-Joseph, A., et al., 2014. Dynamics and wettability of oil and water in oil shales. J. Phys. Chem. C 118 (40), 23212–23218. https://doi.org/10.1021/jp508659e.
Lai, J., Liu, B.C., Li, H.B., et al., 2022. Bedding parallel fractures in fine-grained sedimentary rocks: Recognition, formation mechanisms, and prediction using well log. Pet. Sci. 19 (2), 554–569. https://doi.org/10.1016/j.petsci.2021.10.017.
Larsen, C.P.S., MacDonald, G.M., 1993. Lake morphometry, sediment mixing and the selection of sites for time resolution paleoecological studies. Quat. Sci. Rev. 12, 781–791. https://doi.org/10.1016/0277-3791(93)90017-G.
Lash, G.G., Engelder, T., 2005. An analysis of horizontal microcracking during catagenesis: Example from the Catskill delta complex. AAPG (Am. Assoc. Pet. Geol.) Bull. 89 (11), 1433–1449. https://doi.org/10.1306/05250504141.

Laubach, S.E., Reed, R.M., Olson, J.E., et al., 2004. Coevolution of crack-seal texture and fracture porosity in sedimentary rocks: Cathodoluminescence observations of regional fractures. J. Struct. Geol. 26 (5), 967–982. https://doi.org/10.1016/j.jsg.2003.08.019.

Lazar, O.R., Bohacs, K.M., Macquaker, J.H.S., et al., 2015a. Capturing key attributes of fine-grained sedimentary rocks in outcrops, cores, and thin sections: nomenclature and description guidelines. J. Sediment. Res. 85 (3), 230–246. https://doi.org/10.2110/jsr.2015.11.

Lazar, O.R., Bohacs, K.M., Schieber, J., et al., 2015b. Mudstone Primer: Lithofacies Variations, Diagnostic Criteria, and sedimentologic–stratigraphic Implications at Lamina to Bedset Scale. SEPM Society for Sedimentary Geology. https://doi.org/10.2110/sepmcsp.12.

Li, C.R., Pang, X.Q., Huo, Z.P., et al., 2020a. A revised method for reconstructing the hydrocarbon generation and expulsion history and evaluating the hydrocarbon resource potential: example from the first member of the Qingshankou Formation in the Northern Songliao Basin, Northeast China. Mar. Petrol. Geol. 121, 104577. https://doi.org/10.1016/j.marpetgeo.2020.104577.

Li, J.B., Huang, W.B., Lu, S.F., et al., 2018. Nuclear magnetic resonance T_1–T_2 map division method for hydrogen-bearing components in continental shale. Energy Fuels 32 (9), 9043–9054. https://doi.org/10.1021/acs.energyfuels.8b01541.

Li, J.B., Jiang, C.Q., Wang, M., et al., 2020b. Adsorbed and free hydrocarbons in unconventional shale reservoir: a new insight from NMR T_1–T_2 maps. Mar. Petrol. Geol. 116, 104311. https://doi.org/10.1016/j.marpetgeo.2020.104311.

Li, J.B., Lu, S.F., Chen, G.H., et al., 2019a. A new method for measuring shale porosity with low-field nuclear magnetic resonance considering non-fluid signals. Mar. Petrol. Geol. 102, 535–543. https://doi.org/10.1016/j.marpetgeo.2019.01.013.

Li, J.B., Wang, M., Jiang, C.Q., et al., 2022. Sorption model of lacustrine shale oil: Insights from the contribution of organic matter and clay minerals. Energy 260, 125011. https://doi.org/10.1016/j.energy.2022.125011.

Li, J.Q., Lu, S.F., Xie, L.J., et al., 2017. Modeling of hydrocarbon adsorption on continental oil shale: A case study on *n*-alkane. Fuel 206, 603–613. https://doi.org/10.1016/j.fuel.2017.06.017.

Li, J.Q., Lu, S.F., zhang, J., et al., 2019b. Quantitative evaluation models of adsorbed and free shale oil and its microscopic occurrence mechanism. Oil Gas Geol. 40 (3), 583–592 (in Chinese).

Li, J.R., Yang, Z., Wang, Z.Y., et al., 2023a. Quantitative characterization and main controlling factors of shale oil occurrence in Permian Fengcheng Formation, Mahu Sag, Junggar Basin. Petroleum Geology & Experiment 45 (4), 681–692 (in Chinese).

Li, J.S., Jin, A.M., Zhu, R., et al., 2024a. Micro-occurrence characteristics and charging mechanism in continental shale oil from Lucaogou Formation in the Jimsar Sag, Junggar Basin, NW China. PLoS One 19 (2), e0297104. https://doi.org/10.1371/journal.pone.0297104.

Li, M.W., Chen, Z.H., Ma, X.X., et al., 2019c. Shale oil resource potential and oil mobility characteristics of the Eocene–Oligocene Shahejie Formation, Jiyang Super-Depression, Bohai Bay Basin of China. Int. J. Coal Geol. 204, 130–143. https://doi.org/10.1016/j.coal.2019.01.013.

Li, M.W., Chen, Z.H., Qian, M.H., et al., 2020c. What are in pyrolysis S_1 peak and what are missed? Petroleum compositional characteristics revealed from programed pyrolysis and implications for shale oil mobility and resource potential. Int. J. Coal Geol. 217, 103321. https://doi.org/10.1016/j.coal.2019.103321.

Li, M.W., Jin, Z.J., Dong, M.Z., et al., 2020d. Advances in the basic study of lacustrine shale evolution and shale oil accumulation. Petroleum Geology & Experiment 42 (4), 489–505 (in Chinese).

Li, P., Nie, H.K., Zhang, J.C., et al., 2023b. Characteristics and model of heterogeneous wettability in a marine–continental transitional shale reservoir: insights from organic matter, minerals, and microstructure. Energy Fuels 37 (9), 6450–6464. https://doi.org/10.1021/acs.energyfuels.2c04256.

Li, Q.Q., Bao, Z.D., Xiao, Y.X., et al., 2021. Research advances and prospect of mixed deposition. Acta Sedimentol. Sin. 39 (1), 153–167. https://doi.org/10.14027/j.issn.1000-0550.2020.140 (in Chinese).

Li, R., Chen, Z.X., Wu, K.L., et al., 2023c. Shale gas transport in nanopores with mobile water films and water bridge. Pet. Sci. 20 (2), 1068–1076. https://doi.org/10.1016/j.petsci.2022.08.015.

Li, W., Zhu, X.M., Duan, H.L., et al., 2020f. Characteristics and forming mechanism of laminae fine-grained sedimentary rock of the Paleogene Funing Formation in Gaoyou and Jinhu sags, Subei Basin. J. Palaeogeogr. 22 (3), 469–482 (in Chinese).

Li, W.H., Zhang, M.S., Nan, Y.L., et al., 2020e. Molecular dynamics study on CO_2 storage in water-filled kerogen nanopores in shale reservoirs: effects of kerogen maturity and pore size. Langmuir 37 (1), 542–552. https://doi.org/10.1021/acs.langmuir.0c03232.

Li, Y., Wang, Z.S., Pan, Z.J., et al., 2019d. Pore structure and its fractal dimensions of transitional shale: a cross-section from east margin of the Ordos Basin, China. Fuel 241, 417–431. https://doi.org/10.1016/j.fuel.2018.12.066.

Li, Z., Bao, S.Y., Zhu, R.F., et al., 2024b. Progress in experimental techniques and research methods for shale oil occurrence characteristics and mobility. Petroleum Geology and Recovery Efficiency 31 (4), 84–95. https://doi.org/10.13673/j.pgre.202405070.

Li, Z., Zou, Y.R., Xu, X.Y., et al., 2016. Adsorption of mudstone source rock for shale oil — experiments, model and a case study. Org. Geochem. 92, 55–62. https://doi.org/10.1016/j.orggeochem.2015.12.009.

Li, Z.L., Fan, C.Y., Hui, X., et al., 2024c. Research progress and trend of bedding-parallel fractures in unconventional sedimentary reservoirs. Acta Sedimentol. Sin. 42 (4), 1150–1163. https://doi.org/10.14027/j.issn.1000-0550.2022.124 (in Chinese).

Li, Z.S., Fredericks, P.M., Rintoul, L., et al., 2007. Application of attenuated total reflectance micro-fourier transform infrared (ATR-FTIR) spectroscopy to the study of coal macerals: Examples from the Bowen Basin, Australia. Int. J. Coal Geol. 70 (1–3), 87–94. https://doi.org/10.1016/j.coal.2006.01.006.

Liang, C., Cao, Y.C., Liu, K.Y., et al., 2018. Diagenetic variation at the lamina scale in lacustrine organic-rich shales: Implications for hydrocarbon migration and accumulation. Geochem. Cosmochim. Acta 229, 112–128. https://doi.org/10.1016/j.gca.2018.03.017.

Liang, C., Wu, J., Cao, Y.C., et al., 2022a. Storage space development and hydrocarbon occurrence model controlled by lithofacies in the Eocene Jiyang Subbasin, East China: significance for shale oil reservoir formation. J. Petrol. Sci. Eng. 215, 110631. https://doi.org/10.1016/j.petrol.2022.110631.

Liang, S., Wang, J.M., Liu, Y.K., et al., 2022b. Oil occurrence states in shale mixed inorganic matter nanopores. Front. Earth Sci. 9. https://doi.org/10.3389/feart.2021.833302.

Lin, P.X., Lin, C.M., Yao, Y., et al., 2017. Characteristics and causes of analcime distributed in dolostone of the member 3 of Paleogene Shahejie Formation in Beitang Sag, Bohai Bay Basin. J. Palaeogeogr. 19 (2), 241–256 (in Chinese).

Liu, B., Wang, Y., Tian, S.S., et al., 2022. Impact of thermal maturity on the diagenesis and porosity of lacustrine oil-prone shales: Insights from natural shale samples with thermal maturation in the oil generation window. Int. J. Coal Geol. 261, 104079. https://doi.org/10.1016/j.coal.2022.104079.

Liu, C., Lu, S.F., Xue, H.T., 2014a. Variable-coefficient $\Delta\log R$ model and its application in shale organic evaluation. Prog. Geophys. 29 (1), 312–317 (in Chinese).

Liu, C., Xu, X.Y., Liu, K.Y., et al., 2020a. Pore-scale oil distribution in shales of the Qingshankou formation in the Changling Sag, Songliao Basin, NE China. Mar. Petrol. Geol. 120, 104553. https://doi.org/10.1016/j.marpetgeo.2020.104553.

Liu, C.L., Wang, P.X., 2013. The role of algal blooms in the formation of lacustrine petroleum source rocks — evidence from Jiyang depression, Bohai Gulf Rift Basin, eastern China. Palaeogeogr. Palaeoclimatol. Palaeoecol. 388, 15–22. https://doi.org/10.1016/j.palaeo.2013.07.024.

Liu, D.S., Liu, J.Q., Lv, H.Y., 1998. Progress in high-resolution paleoenvironment research from Maar Lake. Quat. Sci. 4, 289–296 (in Chinese).

Liu, G.H., Huang, Z.L., Jiang, Z.X., et al., 2015. The characteristic and reservoir significance of lamina in shale from Yanchang Formation of Ordos Basin. Nat. Gas Geosci. 26 (3), 408–417 (in Chinese).

Liu, G.P., Jin, Z.J., Zeng, L.B., et al., 2023a. Natural fractures in deep continental shale oil reservoirs: a case study from the Permian Lucaogou Formation in the Eastern Junggar Basin, Northwest China. J. Struct. Geol. 174, 104913. https://doi.org/10.1016/j.jsg.2023.104913.

Liu, G.P., Zeng, L.B., Zhu, R.K., et al., 2021a. Effective fractures and their contribution to the reservoirs in deep tight sandstones in the Kuqa Depression, Tarim Basin, China. Mar. Petrol. Geol. 124, 104824. https://doi.org/10.1016/j.marpetgeo.2020.104824.

Liu, H., Huang, Y.Q., Cai, M., et al., 2023c. Practice and development suggestions of hydraulic fracturing technology in the Gulong shale oil reservoirs of Songliao Basin, NE China. Petrol. Explor. Dev. 50 (3), 688–698. https://doi.org/10.1016/S1876-3804(23)60420-3.

Lis, G.P., Mastalerz, M., Schimmelmann, A., et al., 2005. FTIR absorption indices for thermal maturity in comparison with vitrinite reflectance R_o in type-II kerogens from Devonian black shales. Org. Geochem. 36 (11), 1533–1552. https://doi.org/10.1016/j.orggeochem.2005.07.001.

Liu, H.M., Bao, Y.S., Zhang, S.C., et al., 2023b. Structural characteristics of continental carbonate-rich shale and shale oil movability: a case study of the Paleogene Shahejie Formation shale in Jiyang Depression, Bohai Bay Basin, China. Petrol. Explor. Dev. 50 (6), 1320–1332. https://doi.org/10.1016/S1876-3804(24)60469-6.

Liu, H.M., Li, Z., Bao, S.Y., et al., 2023d. Geology of shales in prolific shale-oil well BYP5 in the Jiyang Depression, Bohai Bay Basin. Oil Gas Geol. 44 (6), 1405–1417 (in Chinese).

Liu, J.P., Xian, B.Z., Ji, Y.L., et al., 2020b. Alternating of aggradation and progradation dominated clinothems and its implications for sediment delivery to deep lake: the Eocene Dongying Depression, Bohai Bay Basin, East China. Mar. Petrol. Geol. 114, 104197. https://doi.org/10.1016/j.marpetgeo.2019.104197.

Liu, Q., Yuan, X.J., Lin, S.H., et al., 2014b. The classification of lacustrine mudrock and research on its' depositional environment. Acta Sedimentol. Sin. 32 (6), 1016–1025. https://doi.org/10.14027/j.cnki.cjxb.2014.06.003 (in Chinese).

Liu, W.Q., Qiao, Y., Bo, J.F., et al., 2019. Geochemistry of mudstones from the Upper Permian Dalong Formation in the Enshi area, western Hubei, and its implications for weathering, provenance and tectonic setting. J. Lanzhou Univ. 55 (2), 158–167. https://doi.org/10.13885/j.issn.0455-2059.2019.02.003 (in Chinese).

Liu, X.Y., Yang, W.W., Li, S.X., et al., 2021b. Occurrence states and quantitative characterization of lacustrine shale oil from Yanchang Formation in Ordos Basin. Nat. Gas Geosci. 32 (12), 1762–1770 (in Chinese).

Liu, Y.H., Wang, C.Z., Liu, Z.H., et al., 2021c. A logging method for evaluating oil-bearing property of shale oil: case study of Jimusar Sag in Junggar Basin. Nat. Gas Geosci. 32 (7), 1084–1091 (in Chinese).

Liu, Y.Q., Zhou, D.W., Nan, Y., et al., 2018. Permian mantle-derived carbonatite originated exhalative sedimentary rocks in North Xinjiang. J. Palaeogeogr. 20 (1), 49–63 (in Chinese).

Liu, Z.S., Liu, D.M., Cai, Y.D., et al., 2020c. Application of nuclear magnetic resonance (NMR) in coalbed methane and shale reservoirs: a review. Int. J. Coal Geol. 218, 103261. https://doi.org/10.1016/j.coal.2019.103261.
Loucks, R.G., Reed, R.M., Ruppel, S.C., et al., 2012. Spectrum of pore types and networks in mudrocks and a descriptive classification for matrix-related mudrock pores. AAPG (Am. Assoc. Pet. Geol.) Bull. 96 (6), 1071–1098. https://doi.org/10.1306/08171111061.
Loucks, R.G., Ruppel, S.C., 2007. Mississippian Barnett Shale: Lithofacies and depositional setting of a deep-water shale-gas succession in the Fort Worth Basin, Texas. AAPG (Am. Assoc. Pet. Geol.) Bull. 91 (4), 579–601. https://doi.org/10.1306/11020606059, 2007.
Lu, F., Li, Z.Y., Yang, Z., et al., 2023. Characterization of oil-bearing properties in submicron shale pores by laser scanning confocal microscopy technology: A case study of shale in Lucaogou Formation, Junggar Basin. Petroleum Geology & Experiment 45 (1), 193–202 (in Chinese).
Luo, B., Shu, Z.G., Chen, Y.L., et al., 2021. Mineral heterogeneity characterization of the lacustrine Yanchang Shales, Ordos Basin using micro-Fourier transform infrared spectroscopy (micro-FTIR) technique. Geofluids 2021, 1–10. https://doi.org/10.1155/2021/5585701.
Lv, J.H., Hu, T., Zhang, W., et al., 2025. Microscopic oil occurrence in the Permian alkaline lacustrine shales: Fengcheng Formation, Mahu Sag, Junggar basin. Pet. Sci. 22 (4), 1407–1427. https://doi.org/10.1016/j.petsci.2025.01.005.
Ma, B.Y., Hu, Q.H., Pu, X.G., et al., 2024a. Occurrence mechanism and controlling factors of shale oil from the Paleogene Kongdian Formation in Cangdong Sag, Bohai Bay Basin, East China. J. Mar. Sci. Eng. 12 (9), 1557. https://doi.org/10.3390/jmse12091557.
Ma, J., Wu, C.D., Wang, Y.Z., et al., 2017. Paleoenvironmental reconstruction of a saline lake in the Tertiary: Evidence from aragonite laminae in the northern Tibet Plateau. Sediment. Geol. 353, 1–12. https://doi.org/10.1016/j.sedgeo.2017.03.002.
Ma, W.J., Luo, X., Tao, S.Z., et al., 2020. Modified pyrolysis experiments and indexes to re-evaluate petroleum expulsion efficiency and productive potential of the Chang 7 shale, Ordos Basin, China. J. Petrol. Sci. Eng. 186, 106710. https://doi.org/10.1016/j.petrol.2019.106710.
Ma, X., Xu, J.Q., Liu, W.H., et al., 2024b. Developing characteristics of shale lamination and their impact on reservoir properties in the deep Wufeng–Longmaxi Formation shale of the southern Sichuan Basin. Minerals 14 (2), 171. https://doi.org/10.3390/min14020171.
Ma, Y.Q., Fan, M.J., Lu, Y.C., et al., 2016. Climate-driven paleolimnological change controls lacustrine mudstone depositional process and organic matter accumulation: Constraints from lithofacies and geochemical studies in the Zhanhua Depression, eastern China. Int. J. Coal Geol. 167, 103–118. https://doi.org/10.1016/j.coal.2016.09.014.
Macquaker, J.H.S., Bentley, S.J., Bohacs, K.M., 2010a. Wave-enhanced sediment-gravity flows and mud dispersal across continental shelves: reappraising sediment transport processes operating in ancient mudstone successions. Geology 38 (10), 947–950. https://doi.org/10.1130/G31093.1.
Macquaker, J.H.S., Keller, M.A., Davies, S.J., 2010b. Algal blooms and "marine snow": mechanisms that enhance preservation of organic carbon in ancient fine-grained sediments. J. Sediment. Res. 80 (11), 934–942. https://doi.org/10.2110/jsr.2010.085.
Mastalerz, M., Bustin, R.M., 1995. Application of reflectance micro-Fourier transform-infrared spectrometry in studying coal macerals-comparison with other fourier-transform infrared techniques. Fuel 74 (4), 536–542. https://doi.org/10.1016/0016-2361(95)98356-J.
Mastalerz, M., Schimmelmann, A., Drobniak, A., et al., 2013. Porosity of Devonian and Mississippian New Albany Shale across a maturation gradient: Insights from organic petrology, gas adsorption, and mercury intrusion. AAPG (Am. Assoc. Pet. Geol.) Bull. 97 (10), 1621–1643. https://doi.org/10.1306/04011312194.
Matthaei, S.K., Henley, R.W., Heinrich, C.A., 1995. Gold precipitation by fluid mixing in bedding-parallel fractures near carbonaceous slates at the Cosmopolitan Howley gold Deposit, northern Australia. Econ. Geol. 90 (8), 2123–2142. https://doi.org/10.2113/gsecongeo.90.8.2123.
Meng, Q.F., Hooker, J., Cartwright, J., 2017. Genesis of natural hydraulic fractures as an indicator of basin inversion. J. Struct. Geol. 102, 1–20. https://doi.org/10.1016/j.jsg.2017.07.001.
Meng, Q.F., Hooker, J., Cartwright, J., 2018. Displacive widening of calcite veins in shale: Insights into the force of crystallization. J. Sediment. Res. 88 (3), 327–343. https://doi.org/10.2110/jsr.2018.18.
Mukhametdinova, A., Habina-Skrzyniarz, I., Kazak, A., et al., 2021. NMR relaxometry interpretation of source rock liquid saturation — A holistic approach. Mar. Petrol. Geol. 132, 105165. https://doi.org/10.1016/j.marpetgeo.2021.105165.
Neil, C.W., Hjelm, R.P., Hawley, M.E., et al., 2023. Small-angle neutron scattering investigation of oil recovery in mineralogically distinct Wolfcamp Shale strata. Energy Fuels 37 (7), 4937–4947. https://doi.org/10.1021/acs.energyfuels.2c03964.
Nie, S.J., Yang, F., Luo, L., et al., 2024. Experimental investigation on the oil occurrence and mobility of lacustrine shales in offshore area of China using 1D/2D nuclear magnetic resonance and centrifugal techniques. Int. J. Coal Geol. 294, 104618. https://doi.org/10.1016/j.coal.2024.104618.
Nikolaev, M.Y., Kazak, A.V., 2019. Liquid saturation evaluation in organic-rich unconventional reservoirs: A comprehensive review. Earth Sci. Rev. 194, 327–349. https://doi.org/10.1016/j.earscirev.2019.05.012.
Ning, F.X., Wang, X.J., Hao, X.F., et al., 2017. Occurrence mechanism of shale oil with different lithofacies in Jiyang depression. Acta Pet. Sin. 38 (2), 185–195 (in Chinese).
Niu, X.B., Lyu, C.F., Feng, S.B., et al., 2025. Lamina combination characteristics and differential shale oil enrichment mechanisms of continental organic-rich shale: A case study of Triassic Yanchang Formation Chang 7_3 sub-member, Ordos Basin, NW China. Petrol. Explor. Dev. 52 (2), 316–329. https://doi.org/10.1016/S1876-3804(25)60569-6.
Ojala, A.E.K., Francus, P., Zolitschka, B., et al., 2012. Characteristics of sedimentary varve chronologies – a review. Quat. Sci. Rev. 43, 45–60. https://doi.org/10.1016/j.quascirev.2012.04.006.
Pan, B., Yin, X., Iglauer, S., 2020. A review on clay wettability: From experimental investigations to molecular dynamics simulations. Adv. Colloid Interface Sci. 285, 102266. https://doi.org/10.1016/j.cis.2020.102266.
Pang, X.J., 2023. Petrophysical Response Mechanism and Logging Evaluation of Shale Oil Reservoirs in the Gulong Sag, Songliao Basin, China. Ph.D. thesis. China University of Petroleum (Beijing), Beijing. https://doi.org/10.27643/d.cnki.gsybu.2023.000820 (in Chinese).
Pang, X.J., Wang, G.W., Kuang, L.C., et al., 2023b. Lamellation fractures in shale oil reservoirs: recognition, prediction and their influence on oil enrichment. Mar. Petrol. Geol. 148, 106032. https://doi.org/10.1016/j.marpetgeo.2022.106032.
Pang, X.Q., Li, M., Li, B.Y., et al., 2023a. Main controlling factors and movability evaluation of continental shale oil. Earth Sci. Rev. 243, 104472. https://doi.org/10.1016/j.earscirev.2023.104472.
Perez, F., Devegowda, D., 2019. Spatial distribution of reservoir fluids in mature kerogen using molecular simulations. Fuel 235, 448–459. https://doi.org/10.1016/j.fuel.2018.08.024.
Pernyeszi, T., Patzkó, Á., Berkesi, O., et al., 1998. Asphaltene adsorption on clays and crude oil reservoir rocks. Colloids Surf. A Physicochem. Eng. Asp. 137, 373–384. https://doi.org/10.1016/S0927-7757(98)00214-3.
Piedrahita, J., Aguilera, R., 2017. Estimating oil saturation index OSI from NMR logging and comparison with Rock-Eval pyrolysis measurements in a shale oil reservoir. In: SPE Canada Unconventional Resources Conference. https://doi.org/10.2118/185073-MS.
Praet, N., Van Daele, M., Collart, T., et al., 2020. Turbidite stratigraphy in proglacial lakes: Deciphering trigger mechanisms using a statistical approach. Sedimentology 67 (5), 2332–2359. https://doi.org/10.1111/sed.12703.
Qiu, H.Y., 2023. Characteristics of Continental Shale Laminae Pore Structure and Its Controlling Mechanism on Shale Oil and Gas Enrichment: A Case Study of Jurassic System in Northeast Sichuan. Ph.D. thesis. China University of Petroleum (Beijing), Beijing. https://doi.org/10.27643/d.cnki.gsybu.2023.000274 (in Chinese).
Qu, Y.Q., Ouyang, S.Q., Gao, J.W., et al., 2024. Pore space characteristics and migration changes in hydrocarbons in shale reservoir. Fractal and Fractional 8 (10), 588. https://doi.org/10.3390/fractalfract8100588.
Rao, Q., He, Z.L., Dong, T., et al., 2024. Pore and fracture characteristics and diagenetic evolution mechanisms of low-maturity lacustrine shales from the Paleogene Shahejie Formation in the Jiyang Depression, Bohai Bay Basin, Eastern China. Mar. Petrol. Geol. 170, 107154. https://doi.org/10.1016/j.marpetgeo.2024.107154.
Rexer, T.F.T., Benham, M.J., Aplin, A.C., et al., 2013. Methane adsorption on shale under simulated geological temperature and pressure conditions. Energy Fuels 27 (6), 3099–3109. https://doi.org/10.1021/ef400381v.
Rezaeyan, A., Kampman, N., Pipich, V., et al., 2023. Evolution of pore structure in organic-lean and organic-rich mudrocks. Energy Fuels 37 (21), 16446–16460. https://doi.org/10.1021/acs.energyfuels.3c02180.
Rimstidt, J.D., Chermak, J.A., Schreiber, M.E., 2017. Processes that control mineral and element abundances in shales. Earth Sci. Rev. 171, 383–399. https://doi.org/10.1016/j.earscirev.2017.06.010.
Rylander, E., Philip, M.S., Tianmin, J., et al., 2013. NMR T_2 distributions in the Eagle Ford shale: Reflections on pore size. In: SPE Unconventional Resources Conference/Gas Technology Symposium. https://doi.org/10.2118/164554-MS.
Sang, Q., Zhang, S.J., Li, Y.J., et al., 2018. Determination of organic and inorganic hydrocarbon saturations and effective porosities in shale using vacuum-imbibition method. Int. J. Coal Geol. 200, 123–134. https://doi.org/10.1016/j.coal.2018.10.010.
Saraji, S., Piri, M., 2015. The representative sample size in shale oil rocks and nano-scale characterization of transport properties. Int. J. Coal Geol. 146, 42–54. https://doi.org/10.1016/j.coal.2015.04.005.
Schieber, J., 2010. Common themes in the formation and preservation of intrinsic porosity in shales and mudstones — illustrated with examples across the Phanerozoic. In: SPE Unconventional Resources Conference/Gas Technology Symposium. https://doi.org/10.2118/132370-MS.
Schieber, J., 2016. Mud re-distribution in epicontinental basins — exploring likely processes. Mar. Petrol. Geol. 71, 119–133. https://doi.org/10.1016/j.marpetgeo.2015.12.014.
Schieber, J., Southard, J., Thaisen, K., 2007. Accretion of mudstone beds from migrating floccule ripples. Science 318 (5857), 1760–1763. https://doi.org/10.1126/science.1147001.
Schieber, J., Southard, J.B., Kissling, P., et al., 2013. Experimental deposition of carbonate mud from moving suspensions: Importance of flocculation and implications for modern and ancient carbonate mud deposition. J. Sediment. Res. 83 (11), 1025–1031. https://doi.org/10.2110/jsr.2013.77.

Schimmelmann, A., Lange, C.B., Schieber, J., et al., 2016. Varves in marine sediments: a review. Earth Sci. Rev. 159, 215–246. https://doi.org/10.1016/j.earscirev.2016.04.009.
Severson, B.L., Snurr, R.Q., 2007. Monte carlo simulation of n-alkane adsorption isotherms in carbon slit pores. J. Chem. Phys. 126, 134708. https://doi.org/10.1063/1.2713097.
Shanmugam, G., 2008. Chapter 5 Deep-water bottom currents and their deposits. In: Rebesco, M., Camerlenghi, A. (Eds.), Contourites. Developments in Sedimentology 60, 59–81. https://doi.org/10.1016/S0070-4571(08)10005-X.
Shao, H.M., Gao, B., Hong, S.X., et al., 2020. Progress and application of the experimental technologies for the shale oil reservoirs: A case study on Gulong area in Songliao Basin. Pet. Geol. Oilfield Dev. Daqing 39 (3), 97–106. https://doi.org/10.19597/J.ISSN.1000-3754.202004058 (in Chinese).
Shao, X.D., Song, Y., Jiang, L., et al., 2024. Graded evaluation and controls on in situ oil content within lacustrine shale of the Upper Cretaceous Qingshankou Formation, Songliao Basin, China. Energy Fuels 38 (14), 12925–12937. https://doi.org/10.1021/acs.energyfuels.4c02003.
Shi, J.H., Gong, L., Sun, S.Y., et al., 2019. Competitive adsorption phenomenon in shale gas displacement processes. RSC Adv. 9 (44), 25326–25335. https://doi.org/10.1039/C9RA04963K.
Shi, J.Y., Jin, Z.J., Liu, Q.Y., et al., 2022. Laminar characteristics of lacustrine organic-rich shales and their significance for shale reservoir formation: A case study of the Paleogene shales in the Dongying Sag, Bohai Bay Basin, China. J. Asian Earth Sci. 223, 104976. https://doi.org/10.1016/j.jseaes.2021.104976.
Shi, K.Y., Chen, J.Q., Pang, X.Q., et al., 2024. Average molecular structure model of shale kerogen: Experimental characterization, structural reconstruction, and pyrolysis analysis. Fuel 355, 129474. https://doi.org/10.1016/j.fuel.2023.129474.
Shi, Y.J., Cai, W.Y., Liu, G.Q., et al., 2023. Full diameter core 2D NMR spectrum characteristics of pore fluid in shale oil reservoir and evaluation method. China Petroleum Exploration 28 (3), 132–144 (in Chinese).
Shi, Z.S., Dong, D.Z., Wang, H.Y., et al., 2020. Reservoir characteristics and genetic mechanisms of gas-bearing shales with different laminae and laminae combinations: A case study of Member 1 of the Lower Silurian Longmaxi shale in Sichuan Basin, SW China. Petrol. Explor. Dev. 47 (4), 888–900. https://doi.org/10.1016/S1876-3804(20)60104-5.
Shi, Z.S., Qiu, Z., Dong, D.Z., et al., 2018. Laminae characteristics of gas-bearing shale fine-grained sediment of the Silurian Longmaxi Formation of Well Wuxi 2 in Sichuan Basin, SW China. Petrol. Explor. Dev. 45 (2), 358–368. https://doi.org/10.1016/S1876-3804(18)30040-5.
Siddiqui, M.A.Q., Chen, X., Iglauer, S., et al., 2019. A multiscale study on shale wettability: Spontaneous imbibition versus contact angle. Water Resour. Res. 55 (6), 5012–5032. https://doi.org/10.1029/2019WR024893.
Song, G.Q., Zhang, L.Y., Lu, S.F., et al., 2013. Resource evaluation method for shale oil and its application. Earth Sci. Front. 20 (4), 221–228 (in Chinese).
Song, M.S., Liu, H.M., Wang, Y., et al., 2020. Enrichment rules and exploration practices of Paleogene shale oil in Jiyang Depression, Bohai Bay Basin, China. Petrol. Explor. Dev. 47 (2), 242–253. https://doi.org/10.1016/S1876-3804(20)60043-X.
Song, Z.Z., Zhang, J., Jin, S.G., et al., 2024. The occurrences and mobility of shale oil in the pore space of terrestrial shale. Fuel 374, 132377. https://doi.org/10.1016/j.fuel.2024.132377.
Spears, R.W., Dudus, D., Foulds, A., et al., 2011. Shale gas core analysis: Strategies for normalizing between laboratories and a clear need for standard materials. SPWLA Annual Logging Symposium.
Suekuni, M.T., Ezazi, M., Kwon, G., et al., 2024. Assessment of kerogen wettability from contact angle goniometry. Energy Fuels 38 (3), 1864–1872. https://doi.org/10.1021/acs.energyfuels.3c03175.
Sui, H.G., Yao, J., 2016. Effect of surface chemistry for CH_4/CO_2 adsorption in kerogen: A molecular simulation study. J. Nat. Gas Sci. Eng. 31, 738–746. https://doi.org/10.1016/j.jngse.2016.03.097.
Sui, H.G., Zhang, F.Y., Wang, Z.Q., et al., 2020. Molecular simulations of oil adsorption and transport behavior in inorganic shale. J. Mol. Liq. 305, 112745. https://doi.org/10.1016/j.molliq.2020.112745.
Sun, B., Liu, X.P., Zhao, X.Z., et al., 2025a. Laminated shale oil system mobility and controlling factors of the Paleogene Shahejie Formation: Evidences from T_1–T_2 NMR experiments, multi-temperature pyrolysis and confocal laser scanning microscopy. Fuel 379, 133015. https://doi.org/10.1016/j.fuel.2024.133015.
Sun, C., 2017. The Characteristics, Formation and Evolution of Shale Oil Reservoir Space in Dongying Sag. Ph.D. thesis. Nanjing University, Nanjing (in Chinese).
Sun, C., Yao, S.P., Li, J.N., et al., 2017. Characteristics of pore structure and effectiveness of shale oil reservoir space in Dongying Sag, Jiyang Depression, Bohai Bay Basin. J. Nanosci. Nanotechnol. 17 (9), 6781–6790. https://doi.org/10.1166/jnn.2017.14478.
Sun, H., Li, T.H., Li, Z., et al., 2023. Shale oil redistribution-induced flow regime transition in nanopores. Energy 282, 128553. https://doi.org/10.1016/j.energy.2023.128553.
Sun, H.Q., Lv, Q., Fang, J.C., et al., 2025b. Development technology and direction of shale oil in continental rift basins. Acta Pet. Sin. 46 (8), 1589–1601 (in Chinese).
Sun, L.D., Liu, H., He, W.Y., et al., 2021. An analysis of major scientific problems and research paths of Gulong shale oil in Daqing Oilfield, NE China. Petrol. Explor. Dev. 48 (3), 527–540. https://doi.org/10.1016/S1876-3804(21)60043-5.
Sun, S., Gao, M.Y., Liang, S., et al., 2024. Hydrocarbon transportation in heterogeneous shale pores by molecular dynamic simulation. Molecules 29 (8), 1763. https://doi.org/10.3390/molecules29081763.
Sun, Z.T., Xin, H.G., Lv, C.F., et al., 2022. Occurrence states and organic geochemical characteristics of shale-type shale oil from Chang 7**3** sub-member in the Ordos Basin. Nat. Gas Geosci. 33 (8), 1304–1318 (in Chinese).
Tan, M.J., Mao, K.Y., Song, X.D., et al., 2015. NMR petrophysical interpretation method of gas shale based on core NMR experiment. J. Petrol. Sci. Eng. 136, 100–111. https://doi.org/10.1016/j.petrol.2015.11.007.
Tan, Z.W., Chen, Y., Liu, Y., et al., 2018. Research and application of core fluid saturation analysistechnique in low permeability reservoirs. 2018 International Field Exploration and Development Conference. Xi'An, China.
Tang, X.L., Jiang, S., Jiang, Z.X., et al., 2019. Heterogeneity of Paleozoic Wufeng–Longmaxi Formation shale and its effects on the shale gas accumulation in the Upper Yangtze Region, China. Fuel 239, 387–402. https://doi.org/10.1016/j.fuel.2018.11.022.
Thompson, J.B., Schultze-Lam, S., Beveridge, T.J., et al., 2003. Whiting events: Biogenic origin due to the photosynthetic activity of cyanobacterial picoplankton. Limnol. Oceanogr. 42 (1), 133–141. https://doi.org/10.4319/lo.1997.42.1.0133.
Tian, H., He, K., Huangfu, Y.H., et al., 2024a. Oil content and mobility in a shale reservoir in Songliao Basin, Northeast China: insights from combined solvent extraction and NMR methods. Fuel 357, 129678. https://doi.org/10.1016/j.fuel.2023.129678.
Tian, S.S., Dong, Z.T., Liu, B., et al., 2022. Characteristics of gaseous/liquid hydrocarbon adsorption based on numerical simulation and experimental testing. Molecules 27 (14), 4590. https://doi.org/10.3390/molecules27144590.
Tian, X., Duan, X.G., Sun, M.D., et al., 2024b. Evolution of fractal characteristics in shales with increasing thermal maturity: Evidence from neutron scattering, N_2 physisorption, and FE-SEM imaging. Energy 298, 131342. https://doi.org/10.1016/j.energy.2024.131342.
Tylmann, W., Zolitschka, B., 2020. Annually laminated lake sediments — recent progress. Quaternary 3 (1), 5. https://doi.org/10.3390/quat3010005.
Vernik, L., 1994. Hydrocarbon-generation-induced microcracking of source rocks. Geophysics 59 (4), 555–563. https://doi.org/10.1190/1.1443616.
Wan, J.L., Yu, Z.C., Yuan, Y.J., et al., 2025. Lithofacies classification and reservoir property of lacustrine shale, the Cretaceous Qingshankou Formation, Songliao Basin, Northeast China. Mar. Petrol. Geol. 173, 107262. https://doi.org/10.1016/j.marpetgeo.2024.107262.
Wan, T., Zhang, J., Wu, B.C., 2024. NMR and CT characterizing the influence of O**2** in air injection performance in shale oil cores. Fuel 356, 129639. https://doi.org/10.1016/j.fuel.2023.129639.
Wang, C., Zhang, B.Q., Hu, Q.H., et al., 2019a. Laminae characteristics and influence on shale gas reservoir quality of lower Silurian Longmaxi Formation in the Jiaoshiba area of the Sichuan Basin, China. Mar. Petrol. Geol. 109, 839–851. https://doi.org/10.1016/j.marpetgeo.2019.06.022.
Wang, C., Zhang, B.Q., Shu, Z.G., et al., 2019b. Shale lamination and its influence on shale reservoir quality of Wufeng Formation–Longmaxi Formation in Jiaoshiba area. Earth Sci. 44 (3), 972–982 (in Chinese).
Wang, E.Z., Feng, Y., Guo, T.L., et al., 2022a. Oil content and resource quality evaluation methods for lacustrine shale: a review and a novel three-dimensional quality evaluation model. Earth Sci. Rev. 232, 104134. https://doi.org/10.1016/j.earscirev.2022.104134.
Wang, F.Y., Chang, S.L., 2024. Molecular dynamics investigation of shale oil occurrence and adsorption in nanopores: Unveiling wettability and influencing factors. Chem. Eng. J. 481, 148380. https://doi.org/10.1016/j.cej.2023.148380.
Wang, G.M., Zhong, J.H., 2004. A review and the prospects of the researches on sedimentary mechanism of lacustrine laminae. Acta Petrol. Mineral. 23 (1), 43–48 (in Chinese).
Wang, H.Z., Mei, H.M., 1998. Paleolimnological information from the oil shale in the lower part of Sha 3 Formation, in Dongying Depression. J. Tongji Univ. Nat. Sci. 26 (3), 315–319 (in Chinese).
Wang, J., 2015. Low-temperature closed extraction technology of light hydrocarbons and itsapplication in evaluation of shale oil resource. China Petroleum Exploration 20 (3), 58–63 (in Chinese).
Wang, J.J., Zhang, P.F., Lu, S.F., et al., 2025a. Insights into microscopic oil occurrence characteristics in shales from the Paleogene Funing Formation in Subei Basin, China. Pet. Sci. 22 (1), 55–75. https://doi.org/10.1016/j.petsci.2024.07.025.
Wang, J.J., Zhang, P.F., Lu, S.F., et al., 2025b. In situ fluid content evaluation of shale oil reservoirs: insights from laboratory and wellsite mobile full-diameter core NMR. Nat. Resour. Res. 34 (3), 1725–1742. https://doi.org/10.1007/s11053-025-10465-2.
Wang, J.L., Zhu, Y.M., Gong, Y.P., et al., 2015a. Influential factors and forecast of microcrack development degree of Longmaxi Formation shales in Nanchuan region, Chongqing. Nat. Gas Geosci. 26 (8), 1579–1586 (in Chinese).
Wang, L., Zhang, Y.F., Zou, R., et al., 2025c. Applications of molecular dynamics simulation in studying shale oil reservoirs at the nanoscale: advances, challenges and perspectives. Pet. Sci. 22 (1), 234–254. https://doi.org/10.1016/j.petsci.2024.09.023.
Wang, M., Chen, Y., Bain, W.M., et al., 2020. Direct evidence for fluid overpressure during hydrocarbon generation and expulsion from organic-rich shales. Geology 48 (4), 374–378. https://doi.org/10.1130/G46650.1.
Wang, M., Li, M., Li, J.B., et al., 2022b. The key parameter of shale oil resource evaluation: oil content. Pet. Sci. 19 (4), 1443–1459. https://doi.org/10.1016/j.petsci.2022.03.006.

Wang, M., Ma, R., Li, J.B., et al., 2019c. Occurrence mechanism of lacustrine shale oil in the Paleogene Shahejie Formation of Jiyang Depression, Bohai Bay Basin, China. Petrol. Explor. Dev. 46 (4), 833–846. https://doi.org/10.1016/S1876-3804(19)60242-9.
Wang, M., Yu, C.Q., Fei, J.S., et al., 2023a. Molecular dynamics simulation of shale oil adsorption in kerogen and its implications. Oil Gas Geol. 44 (6), 1442–1452 (in Chinese).
Wang, S., 2022. Logging Characterization Method of Continental Shale Oil Reservoir Quality Variation in Junggar Basin — A Case Study of the Fengcheng Formation in Mahu Sag. Ph.D. thesis. China University of Petroleum (Beijing), Beijing (in Chinese).
Wang, S., Feng, Q.H., Javadpour, F., et al., 2015b. Oil adsorption in shale nanopores and its effect on recoverable oil-in-place. Int. J. Coal Geol. 147–148, 9–24. https://doi.org/10.1016/j.coal.2015.06.002.
Wang, S., Javadpour, F., Feng, Q.H., 2016. Molecular dynamics simulations of oil transport through inorganic nanopores in shale. Fuel 171, 74–86. https://doi.org/10.1016/j.fuel.2015.12.071.
Wang, S., Liang, Y.P., Feng, Q.H., et al., 2022c. Sticky layers affect oil transport through the nanopores of realistic shale kerogen. Fuel 310, 122480. https://doi.org/10.1016/j.fuel.2021.122480.
Wang, S.P., Ma, C.F., Sun, X., et al., 2023b. Lacustrine shale diagenesis — a case study of the second member of the Funing Formation in the Subei Basin. Processes 11 (7), 2009. https://doi.org/10.3390/pr11072009.
Wang, W.Q., Liu, H.M., Liu, Y.L., et al., 2022d. Texture and genesis of Paleogene lacustrine shale carbonate laminae in Dongying Sag, Jiyang Depresion, Bohai Bay Basin. Petroleum Geology and Recovery Efficiency 29 (3), 11–19. https://doi.org/10.13673/j.cnki.cn37-1359/te.202103027.
Wang, X.R., Sun, Y., Liu, R.H., et al., 2023c. Research progress into fine-grained sedimentary rock characteristics and formation in a continental lake basin. Acta Sedimentol. Sin. 41 (2), 349–377. https://doi.org/10.14027/j.issn.1000-0550.2021.117 (in Chinese).
Wang, Y., Liu, H.M., Song, G.Q., et al., 2019d. Lacustrine shale fine-grained sedimentary system in Jiyang Depression. Acta Pet. Sin. 40 (4), 395–410 (in Chinese).
Wardlaw, N.C., Taylor, R.P., 1976. Mercury capillary pressure curves and the interpretation of pore structure and capillary behavior in reservoir rocks. Bull. Can. Petrol. Geol. 24 (2), 225–262. https://doi.org/10.35767/gscpgbull.24.2.225.
Wei, J.G., Yang, E.L., Li, J.T., et al., 2023a. Nuclear magnetic resonance study on the evolution of oil water distribution in multistage pore networks of shale oil reservoirs. Energy 282, 128714. https://doi.org/10.1016/j.energy.2023.128714.
Wei, J.G., Zhang, A., Li, J.T., et al., 2023b. Study on microscale pore structure and bedding fracture characteristics of shale oil reservoir. Energy 278, 127829. https://doi.org/10.1016/j.energy.2023.127829.
Wilson, R.D., Schieber, J., 2014. Muddy prodeltaic hyperpycnites in the Lower Genesee Group of central New York, USA: Implications for mud transport in epicontinental seas. J. Sediment. Res. 84 (10), 866–874. https://doi.org/10.2110/jsr.2014.70.
Wu, C.Z., 2018. Molecular Dynamics Simulation of Shale Oil Occurrence Characteristics. Master thesis. China University of Petroleum (East China), Qingdao. https://doi.org/10.27644/d.cnki.gsydu.2018.001747 (in Chinese).
Wu, L.Y., Hu, D.F., Lu, Y.C., et al., 2016. Advantageous shale lithofacies of Wufeng Formation–Longmaxi Formation in Fuling gas field of Sichuan Basin, SW China. Petrol. Explor. Dev. 43 (2), 208–217. https://doi.org/10.1016/S1876-3804(16)30024-6.
Wu, S.T., Yang, Z., Zhai, X.F., et al., 2019. An experimental study of organic matter, minerals and porosity evolution in shales within high-temperature and high-pressure constraints. Mar. Petrol. Geol. 102, 377–390. https://doi.org/10.1016/j.marpetgeo.2018.12.014.
Wu, S.T., Zhu, R.K., Luo, Z., et al., 2022a. Laminar structure of typical continental shales and reservoir quality evaluation in central–western basins in China. China Petroleum Exploration 27 (5), 62–72 (in Chinese).
Wu, Y.P., 2023. Occurrence Mechanism and Movable Resource Potential of Alkaline Lacustrine Shale Oil in the Fengcheng Formation, Mahu Sag. Ph.D. thesis. China University of Petroleum (Beijing), Beijing. https://doi.org/10.27643/d.cnki.gsybu.2023.000356 (in Chinese).
Wu, Y.P., Liu, C.L., Jiang, F.J., et al., 2022b. Occurrence space and state of petroleum in lacustrine shale: Insights from two-step pyrolysis and the N_2 adsorption experiment. Energy Fuels 36 (18), 10920–10933. https://doi.org/10.1021/acs.energyfuels.2c02222.
Xi, K.L., Li, K., Cao, Y.C., et al., 2020. Laminae combination and shale oil enrichment patterns of Chang 7_3 sub-member organic-rich shales in the Triassic Yanchang Formation, Ordos Basin, NW China. Petrol. Explor. Dev. 47 (6), 1342–1353. https://doi.org/10.1016/S1876-3804(20)60142-8.
Xi, K.L., Zhang, Y.Y., Cao, Y.C., et al., 2023. Control of micro-wettability of pore-throat on shale oil occurrence: A case study of laminated shale of Permian Lucaogou Formation in Jimusar Sag, Junggar Basin, NW China. Petrol. Explor. Dev. 50 (2), 334–345. https://doi.org/10.1016/S1876-3804(23)60391-X.
Xiang, M., Xu, S., Wen, Y.R., et al., 2024. Influence of tectonic preservation conditions on the nanopore structure of shale reservoir: A case study of Wufeng–Longmaxi Formation shale in western Hubei area, south China. Pet. Sci. 21 (4), 2203–2217. https://doi.org/10.1016/j.petsci.2024.02.008.
Xiao, D.S., Zheng, L.H., Xing, J.L., et al., 2024. Coupling control of organic and inorganic rock components on porosity and pore structure of lacustrine shale with medium maturity: A case study of the Qingshankou Formation in the southern Songliao Basin. Mar. Petrol. Geol. 164, 106844. https://doi.org/10.1016/j.marpetgeo.2024.106844.
Xie, D.L., Zhao, X.Z., Jin, F.M., et al., 2024. Genesis of deep lacustrine subfacies laminated shale and influence factors on shale oil mobility in Cangdong sag, Bohai Bay Basin. Acta Pet. Sin. 45 (5), 804–816 (in Chinese).
Xin, B.X., Hao, F., Liu, X.F., et al., 2022a. Quantitative evaluation of pore structures within micron-scale laminae of lacustrine shales from the second member of the Kongdian Formation in Cangdong Sag, Bohai Bay Basin, China. Mar. Petrol. Geol. 144, 105827. https://doi.org/10.1016/j.marpetgeo.2022.105827.
Xin, B.X., Zhao, X.Z., Hao, F., et al., 2022b. Laminae characteristics of lacustrine shales from the Paleogene Kongdian Formation in the Cangdong Sag, Bohai Bay Basin, China: why do laminated shales have better reservoir physical properties? Int. J. Coal Geol. 260, 104056. https://doi.org/10.1016/j.coal.2022.104056.
Xiong, H., Devegowda, D., 2022. Fluid behavior in clay-hosted nanopores with varying salinity: Insights into molecular dynamics. SPE J. 27 (3), 1396–1410. https://doi.org/10.2118/209212-PA.
Xiong, H., Devegowda, D., Huang, L.L., 2020. Water bridges in clay nanopores: Mechanisms of formation and impact on hydrocarbon transport. Langmuir 36 (3), 723–733. https://doi.org/10.1021/acs.langmuir.9b03244.
Xu, J.L., Wang, R.T., Zan, L., 2023. Shale oil occurrence and slit medium coupling based on a molecular dynamics simulation. J. Petrol. Sci. Eng. 220, 111151. https://doi.org/10.1016/j.petrol.2022.111151.
Xu, L., Shen, R., Yang, H., et al., 2024. Utilizing atomic force microscopy for microstructural surface analysis and reservoir evaluation of shale. Arabian J. Sci. Eng. 50 (7), 5253–5263. https://doi.org/10.1007/s13369-024-09401-y.
Xu, X.H., Zheng, L.J., Ma, Z.L., 2016. Organic matter occurrence and hydrocarbon generation in shale. Petroleum Geology & Experiment 38 (4), 423–428 (in Chinese).
Xu, Y., Lun, Z.M., Pan, Z.J., et al., 2022. Occurrence space and state of shale oil: A review. J. Petrol. Sci. Eng. 211. https://doi.org/10.1016/j.petrol.2022.110183.
Xue, H.T., Tian, S.S., Wang, W.M., et al., 2016. Correction of oil content — one key parameter in shale oil resource assessment. Oil Gas Geol. 37 (1), 15–22 (in Chinese).
Yan, K.L., Jie, X.Y., Li, X.Q., et al., 2023. Microwave-enhanced methane cracking for clean hydrogen production in shale rocks. Int. J. Hydrogen Energy 48 (41), 15421–15432. https://doi.org/10.1016/j.ijhydene.2023.01.052.
Yan, Q., 2023. The Enrichment Mechanism of Inter-saltshale Oil — A Case Study of Upper Es^3 Sub-member in Liutunsag, Dongpu Depression. Ph.D. Thesis. China University of Geosciences, Beijing), Beijing. https://doi.org/10.27492/d.cnki.gzdzu.2023.000090 (in Chinese).
Yang, F., Ning, Z.F., Wang, Q., et al., 2016. Pore structure characteristics of lower Silurian shales in the southern Sichuan Basin, China: Insights to pore development and gas storage mechanism. Int. J. Coal Geol. 156, 12–24. https://doi.org/10.1016/j.coal.2015.12.015.
Yang, F., Liu, Y.S., Nie, S.J., et al., 2025. Molecular insights into the control mechanism of the solid–liquid interface interaction on shale oil occurrence: Grand canonical Monte Carlo and molecular dynamics simulations investigation. Langmuir 41 (4), 2191–2204. https://doi.org/10.1021/acs.langmuir.4c03561.
Yang, F., Nie, S.J., Jiang, S., et al., 2023. Occurrence characteristics of mobile hydrocarbons in lacustrine shales: Insights from solvent extraction and petrophysical characterization. Energy Fuels 38 (1), 374–386. https://doi.org/10.1021/acs.energyfuels.3c04047.
Yang, F., Ning, Z.F., Hu, C.P., et al., 2013. Characterization of microscopic pore structures in shale reservoirs. Acta Pet. Sin. 34 (2), 301–311 (in Chinese).
Yang, Y., 2024. Shale oil development techniques and application based on ternary-element storage and flow concept in Jiyang Depression, Bohai Bay Basin, East China. Petrol. Explor. Dev. 51 (2), 380–393. https://doi.org/10.1016/S1876-3804(24)60030-3.
Yang, Y.F., Liu, J., Yao, J., et al., 2020. Adsorption behaviors of shale oil in kerogen slit by molecular simulation. Chem. Eng. J. 387, 124054. https://doi.org/10.1016/j.cej.2020.124054.
Yang, Y.F., Song, H.S., Imani, G., et al., 2024. Adsorption behavior of shale oil and water in the kerogen-kaolinite pore by molecular simulations. J. Mol. Liq. 393, 123549. https://doi.org/10.1016/j.molliq.2023.123549.
Yasin, Q., Liu, B., Sun, M.D., et al., 2024. Automatic pore structure analysis in organic-rich shale using FIB-SEM and attention U-Net. Fuel 358, 130161. https://doi.org/10.1016/j.fuel.2023.130161.
Yawar, Z., Schieber, J., 2017. On the origin of silt laminae in laminated shales. Sediment. Geol. 360, 22–34. https://doi.org/10.1016/j.sedgeo.2017.09.001.
Yu, E.X., 2019. Depositional Environments and Inter-annual Paleoclimatic Characteristics of the Fine-grained Sedimentary Rocks of the First Member of the Nenjiang Formation in the Late Cretaceous Songliao Basin. Ph.D. thesis. China University of Geosciences (Beijing), Beijing. https://doi.org/10.27493/d.cnki.gzdzy.2019.000062 (in Chinese).
Yu, L.M., 2023. Comprehensive Evaluation of Sweet Spots Ininterlayer Shale Oil of the First Member of Qingshankou Formation in Daqingzijing Area of the Songliao Basin. Ph.D. thesis. Northeast Petroleum University, Daqing. https://doi.org/10.26995/d.cnki.gdqsc.2023.001253 (in Chinese).
Yu, Y.J., Wang, Y.H., Wang, H.Y., et al., 2022. Examining and applying the theory of "exploring petroleum inside source kitchens" for continental shale oil: A case study from the Kong 2 member of the Cangdong sag in the Bohai Bay Basin, China. Energy Rep. 8, 1174–1190. https://doi.org/10.1016/j.egyr.2021.11.254.

Zavala, C., Arcuri, M., Di Meglio, M., et al., 2021. Deltas: A new classification expanding Bates's concepts. J. Palaeogeogr. 10 (1), 1–15. https://doi.org/10.1186/s42501-021-00098-w.
Zeng, L.B., Li, X.Y., 2009. Fractures in sandstone reservoirs with ultra-low permeability: A case study of the Upper Triassic Yanchang Formation in the Ordos Basin, China. AAPG (Am. Assoc. Pet. Geol.) Bull. 93 (4), 461–477. https://doi.org/10.1306/09240808047.
Zeng, L.B., Lyu, W.Y., Li, J., et al., 2016. Natural fractures and their influence on shale gas enrichment in Sichuan Basin, China. J. Nat. Gas Sci. Eng. 30, 1–9. https://doi.org/10.1016/j.jngse.2015.11.048.
Zeng, X., Cai, J.G., Dong, Z., et al., 2018. Relationship between mineral and organic matter in shales: The case of Shahejie Formation, Dongying Sag, China. Minerals 8 (6), 222. https://doi.org/10.3390/min8060222.
Zhan, S.Y., Su, Y.L., Jin, Z.H., et al., 2020. Molecular insight into the boundary conditions of water flow in clay nanopores. J. Mol. Liq. 311, 113292. https://doi.org/10.1016/j.molliq.2020.113292.
Zhang, C.J., Cao, J., Xiang, B.L., et al., 2023a. Occurrence state of shale oil in saline lacustrine basins: a lithofacies perspective. J. Asian Earth Sci. 255, 105799. https://doi.org/10.1016/j.jseaes.2023.105799.
Zhang, C.J., Hu, Q.H., Wang, Q.M., et al., 2025. Effects of solvent extraction on pore structure properties and oil distribution in shales of alkaline lacustrine basins. Mar. Petrol. Geol. 171, 107207. https://doi.org/10.1016/j.marpetgeo.2024.107207.
Zhang, C.X., Jiang, F.J., Hu, T., et al., 2023b. Oil occurrence state and quantity in alkaline lacustrine shale using a high-frequency NMR technique. Mar. Petrol. Geol. 154, 106302. https://doi.org/10.1016/j.marpetgeo.2023.106302.
Zhang, H., Huang, H.P., Li, Z., et al., 2020a. Comparative study between sequential solvent-extraction and multiple isothermal stages pyrolysis: a case study on Eocene Shahejie Formation shales, Dongying Depression, East China. Fuel 263, 116591. https://doi.org/10.1016/j.fuel.2019.116591.
Zhang, H., Wang, Z.Z., Yang, L., et al., 2022. Quantitative evaluation of shale oil in different occurrence states in first member of Qingshankou Formation of Upper Cretaceous in south of Songliao Basin. J. Jilin Univ. (Earth Sci. Ed.) 52 (2), 315–327. https://doi.org/10.13278/j.cnki.jjuese.20210410.
Zhang, J.F., Xu, H., Zhou, Z., et al., 2019b. Geological characteristics of shale gas reservoir in Yichang area, western Hubei. Acta Pet. Sin. 40 (8), 887–899 (in Chinese).
Zhang, J.G., Jiang, Z.X., Liang, C., et al., 2016. Lacustrine massive mudrock in the Eocene Jiyang Depression, Bohai Bay Basin, China: Nature, origin and significance. Mar. Petrol. Geol. 77, 1042–1055. https://doi.org/10.1016/j.marpetgeo.2016.08.008.
Zhang, J.Y., Zhu, R.K., Wu, S.T., et al., 2023c. Microscopic oil occurrence in high-maturity lacustrine shales: Qingshankou Formation, Gulong Sag, Songliao Basin. Pet. Sci. 20 (5), 2726–2746. https://doi.org/10.1016/j.petsci.2023.08.026.
Zhang, J.Z., Li, X.Q., Zhang, G.W., et al., 2019a. Microstructural investigation of different nanopore types in marine–continental transitional shales: examples from the Longtan formation in Southern Sichuan Basin, south China. Mar. Petrol. Geol. 110, 912–927. https://doi.org/10.1016/j.marpetgeo.2019.09.001.
Zhang, L.H., Lu, X.C., Liu, X.D., et al., 2019d. Distribution and mobility of crude oil–brine in clay mesopores: insights from molecular dynamics simulations. Langmuir 35 (46), 14818–14832. https://doi.org/10.1021/acs.langmuir.9b02925.
Zhang, L.Y., Bao, S.Y., Li, J.Y., et al., 2015. Hydrocarbon and crude oil adsorption abilities of minerals and kerogens in lacustrine shales. Petroleum Geology & Experiment 37 (6), 776–780 (in Chinese).
Zhang, L.Y., Bao, Y.S., Li, J.Y., et al., 2014. Movability of lacustrine shale oil: A case study of Dongying Sag, Jiyang Depression, Bohai Bay Basin. Petrol. Explor. Dev. 41 (6), 703–711. https://doi.org/10.1016/S1876-3804(14)60084-7.
Zhang, L.Y., Chen, Z.H., Li, Z., et al., 2019c. Structural features and genesis of microscopic pores in lacustrine shale in an oil window: a case study of the Dongying Depression. AAPG (Am. Assoc. Pet. Geol.) Bull. 103 (8), 1889–1924. https://doi.org/10.1306/1218181522717084.
Zhang, L.Y., Liu, Q., Zhu, R.F., et al., 2009. Source rocks in Mesozoic–Cenozoic continental rift basins, east China: A case from Dongying Depression, Bohai Bay Basin. Org. Geochem. 40 (2), 229–242. https://doi.org/10.1016/j.orggeochem.2008.10.013.
Zhang, P.F., Lu, S.F., Li, J.Q., et al., 2023d. Oil occurrence mechanism in nanoporous shales: a theoretical and experimental study. Mar. Petrol. Geol. 156, 106422. https://doi.org/10.1016/j.marpetgeo.2023.106422.
Zhang, P.F., Lu, S.F., Wang, J.J., et al., 2024. Microscopic occurrence and distribution of oil and water in situ shale: Evidence from nuclear magnetic resonance. Pet. Sci. 21 (6), 3675–3691. https://doi.org/10.1016/j.petsci.2024.04.007.
Zhang, S., Liu, H.M., Chen, S.Y., et al., 2017. Classification scheme for lithofacies of fine-grained sedimentary rocks in faulted basins of eastern China: Insights from the fine-grained sedimentary rocks in Paleogene, southern Bohai Bay Basin. Acta Geol. Sin. 91 (5), 1108–1119 (in Chinese).
Zhang, S., Liu, H.M., Liu, Y.L., et al., 2020b. Main controls and geological sweet spot types in Paleogene shale oil rich areas of the Jiyang Depression, Bohai Bay basin, China. Mar. Petrol. Geol. 111, 576–587. https://doi.org/10.1016/j.marpetgeo.2019.08.054.
Zhang, S.J., Wang, T.Y., Gao, Z.R., et al., 2023e. Wettability controlling effects on the fluid occurrence and flow in shale gas reservoirs: present problems and new sights. Capillarity 9 (2), 25–31. https://doi.org/10.46690/capi.2023.11.01.
Zhang, S.L., Yan, J.P., Cai, J.G., et al., 2021. Fracture characteristics and logging identification of lacustrine shale in the Jiyang Depression, Bohai Bay Basin, Eastern China. Mar. Petrol. Geol. 132, 105192. https://doi.org/10.1016/j.marpetgeo.2021.105192.
Zhang, W., Feng, Q.H., Wang, S., et al., 2019e. Oil diffusion in shale nanopores: insight of molecular dynamics simulation. J. Mol. Liq. 290, 111183. https://doi.org/10.1016/j.molliq.2019.111183.
Zhang, X., Liu, J.Y., Hou, P.F., 2019f. A review on the formation and distribution theories of the shale oil in China. Geol. Resour. 28 (2), 165–170. https://doi.org/10.13686/j.cnki.dzyzy.2019.02.008 (in Chinese).
Zhang, Y.F., Wang, L., Zou, R., et al., 2023f. Effects of cosolvents on CO_2 displacement of shale oil and carbon storage. Petrol. Explor. Dev. 50 (6), 1509–1518. https://doi.org/10.1016/S1876-3804(24)60484-2.
Zhang, Y.M., Hou, F.H., Fang, S.X., et al., 1994. Secondary pore formation mechanism of third member of Shahejie Formation, RaoYang Depression. Oil Gas Geol. 15 (3), 208–215 (in Chinese).
Zhao, J., Yao, G., Ramisetti, S.B., et al., 2019. Molecular dynamics investigation of substrate wettability alteration and oil transport in a calcite nanopore. Fuel 239, 1149–1161. https://doi.org/10.1016/j.fuel.2018.11.089.
Zhao, R.X., Xue, H.T., Lu, S.F., et al., 2022. Multi-scale pore structure characterization of lacustrine shale and its coupling relationship with material composition: An integrated study of multiple experiments. Mar. Petrol. Geol. 140, 105648. https://doi.org/10.1016/j.marpetgeo.2022.105648.
Zhao, W.Z., Zhu, R.K., Liu, W., et al., 2023. Enrichment conditions and distribution characteristics of lacustrine medium-to-high maturityshale oil in China. Earth Sci. Front. 30 (1), 116–127. https://doi.org/10.13745/j.esf.sf.2022.8.31 (in Chinese).
Zhao, X.Z., Liu, X.P., Liu, H., et al., 2025. High-resolution astronomical records of shale strata in faulted lake basins and implications for the sedimentary process of laminated sediments. Geosci. Front. 16 (2), 101974. https://doi.org/10.1016/j.gsf.2024.101974.
Zhao, X.Z., Zhou, L.H., Pu, X.G., et al., 2020. Formation conditions and enrichment model of retained petroleum in lacustrine shale: A case study of the Paleogene in Huanghua Depression, Bohai Bay Basin, China. Petrol. Explor. Dev. 47 (5), 916–930. https://doi.org/10.1016/S1876-3804(20)60106-9.
Zheng, X.W., Zhang, B.G., Sanei, H., et al., 2019. Pore structure characteristics and its effect on shale gas adsorption and desorption behavior. Mar. Petrol. Geol. 100, 165–178. https://doi.org/10.1016/j.marpetgeo.2018.10.045.
Zhu, C.X., Jiang, F.J., Zhang, P.Y., et al., 2023. Effect of petroleum chemical fraction and residual oil content in saline lacustrine organic-rich shale: A case study from the Paleogene Dongpu Depression of North China. Pet. Sci. 20 (2), 649–669. https://doi.org/10.1016/j.petsci.2022.09.013.
Zhu, R.F., Zhang, L.Y., Li, J.Y., et al., 2015. Quantitative evaluation of residual liquid hydrocarbons in shale. Acta Pet. Sin. 36 (1), 13–18 (in Chinese).
Zhu, R.K., Li, M.Y., Yang, J.R., et al., 2022. Advances and trends of fine-grained sedimentology. Oil Gas Geol. 43 (2), 251–264 (in Chinese).
Zhu, R.K., Zou, C.N., Wu, S.T., et al., 2019a. Mechanism for generation and accumulation of continental tight oil in China. Oil Gas Geol. 40 (6), 1168–1184 (in Chinese).
Zhu, X.J., Cai, J.G., Liu, Q., et al., 2019b. Thresholds of petroleum content and pore diameter for petroleum mobility in shale. AAPG (Am. Assoc. Pet. Geol.) Bull. 103 (3), 605–617. https://doi.org/10.1306/0816181617517009.
Zhu, Y., Wu, S.W., Deng, Y.S., et al., 2024. Pore throat structures and fluid occurrences of reservoirs in Fengcheng Formation, Mahu Sag. Xinjing Pet. Geol. 45 (3), 286–295 (in Chinese).
Zolitschka, B., Francus, P., Ojala, A.E.K., et al., 2015. Varves in lake sediments — a review. Quat. Sci. Rev. 117, 1–41. https://doi.org/10.1016/j.quascirev.2015.03.019.
Zou, C.N., Ma, F., Pan, S.Q., et al., 2023. Formation and distribution potential of global shale oil and the developments of continental shale oil theory and technology in China. Earth Sci. Front. 30 (1), 128–142. https://doi.org/10.13745/j.esf.sf.2022.8.29 (in Chinese).